

# Generation and Characterization of Dual-Fluorescent Influenza Virus-Like Particles (VLPs) in Insect Cells

by

Eduardo Ramirez

A thesis

presented to the University of Waterloo

in fulfillment of the

thesis requirement for the degree of

Master of Applied Science

in

Chemical Engineering

Waterloo, Ontario, Canada, 2018

©Eduardo Ramirez 2018

## **AUTHOR'S DECLARATION**

I hereby declare that I am the sole author of this thesis. This is a true copy of the thesis, including any required final revisions, as accepted by my examiners.

I understand that my thesis may be made electronically available to the public.

## Abstract

The Baculovirus Expression Vector System (BEVS) has been widely used to produce recombinant proteins, especially for complex biopharmaceuticals. In recent years, the insect-baculovirus system has proved its value as a robust production platform. In this regard, multiple vaccines have been commercialized such as FluBlok® using this system. The work presented here aims to further explore their use on the production of influenza virus-like particles (VLPs). The goal is to successfully produce fluorescent influenza particles that behave similarly to native particles and that allow the purification of viral particles.

Four different genetic constructs were investigated for the expression of dual-fluorescent influenza VLP. Individual influenza genes were fused to different fluorescent proteins. Hemagglutinin was fused with enhanced green fluorescent protein (GFP), whereas, M1 was fused to a red fluorescent protein (RFP). The use of monomeric or multimeric RFP was studied, as well as, the fusion site to M1. HA-GFP was placed under the baculovirus p10 promoter, while M1-RFP was under the control of the baculovirus polh promoter. *Sf9* cells were used to generate baculovirus vectors that were later used to infect *Sf9* cells and produce the influenza VLPs. Flow cytometry and confocal microscopy were used to detect individual levels of influenza proteins and their localization, within the cell. A proposed downstream process consisting of a 2-step concentration procedure and a density gradient purification for influenza VLPs was evaluated by tracking HA activity and baculovirus presence. Purification of VLPs and baculovirus was achieved by using iodixanol and sucrose density gradients, an undesirable result since baculovirus is the main contaminant produced in the production process. Further sample analysis of purified fluorescent particles was performed by flow cytometry.

Our findings showed that recombinant baculovirus driving the expression of M1 fusions, with either monomeric or tetrameric RFP, in the 3' site presented red fluorescence localized at the center of the cell. The same behavior was observed when a monomeric RFP was fused at the 5' site. Further purification of fluorescent VLP constructs showed lower HA activity of fluorescent constructs when compared with a non-fluorescent VLPs. Moreover,

similar migration patterns were obtained *via* sucrose density gradient. However, the need to add more purification procedures such as ion exchange chromatography are needed to fully isolate influenza VLP particles. Lastly, a flow cytometry protocol to study purified particles was evaluated. Nano-sized fluorescent particles were detected in purified samples, which increased particle counts in samples with higher concentrations of HA activity and baculovirus. However, our analysis detected mainly coincidental events. Single particle events overlapped with signal noise, therefore an increase in the inherent fluorescent of viral particle should be explored to differentiate single particles from signal noise.

## Acknowledgements

I would like to express my gratitude first to my supervisor, Professor Marc G. Aucoin. I am thankful to have had the opportunity to work in your lab for the past two years. Your guidance and advice have shaped me as a researcher. Thanks for all the comments and support you provided.

I am grateful of have been part of the Aucoin Lab. Many thanks to Megan Logan for training me in microscopy and giving me useful insight to my experiments. Thanks to Mark Bruder for providing me with the genetic constructs to do this thesis. It has been a pleasure working with you, your input has been invaluable. Also, I am grateful to all my lab mates: Sadru Walji, Paul Brogee, Alex Pritchard-Oh, Julia Manalil, Madhuja Chakraborty, Scott Boegel and Merve Marcali, for the discussions and meaningful conversations.

Thanks to Mishi Groh and Saman Mohammadi for providing me with training and advice while running my experimental work.

Lastly, thanks to my family and friends that have been there for me. This thesis would not have been possible without your constant support and encouragement.

## **Dedication**

I would like to dedicate this work to my parents, Fabian and Carmen, who have always been a source of support and advice during these two years. Also, to my sibling, Diana, Fabian and Braulio, for giving me the strength to chase my dreams. To my aunt and grandmother, Juana and Lupita, for their encouragement and unending support. Lastly to Lucia, you are the motivation that keeps me on track of my goals.

## Table of Contents

AUTHOR'S DECLARATION .....	ii
Abstract .....	iii
Acknowledgements .....	v
Dedication .....	vi
Table of Contents .....	vii
List of Figures .....	x
List of Tables .....	xii
Chapter 1 Introduction.....	1
1.1 Purpose of the work.....	2
1.1.1 Hypothesis .....	2
1.1.2 Aims and objectives .....	3
Chapter 2 Literature Review .....	4
2.1 Influenza virus .....	4
2.1.1 Characteristics .....	4
2.1.2 Influenza morphology .....	8
2.2 Influenza vaccine: manufacturing process .....	9
2.2.1 Vaccine production.....	9
2.2.2 New influenza vaccine technologies .....	10
2.3 Insect cells .....	13
2.3.1 Baculovirus: classification and infection cycle .....	14
2.3.2 Baculovirus Expression Vector System (BEVS): production strategies .....	16
2.4 Influenza VLP production in Insect cells .....	18
2.5 Downstream processing of VLPs .....	19
2.6 Analytical techniques for characterization influenza VLPs produced in insect cells.....	21
2.6.1 Total protein concentration.....	22
2.6.2 Enzymatic assays.....	22
2.6.3 Total particle counts .....	23
2.6.4 New technologies to track and quantify VLPs .....	24
Chapter 3 Generation and Tracking of Fluorescent Influenza Proteins in Insect Cells.....	25
3.1 Chapter objective.....	25
3.2 Materials and Methods .....	26

3.2.1 Cell Culture.....	26
3.2.2 Baculovirus generation and amplification .....	26
3.2.3 Baculovirus quantification using end-point dilution assay .....	26
3.2.4 Fluorescent VLP production .....	27
3.2.5 Infection flow cytometry analysis.....	28
3.2.6 Confocal microscopy .....	28
3.3 Results.....	29
3.3.1 Tracking influenza proteins .....	30
3.3.2 Monitoring infection process and expression levels .....	32
3.4 Discussion.....	38
3.4.1 Tracking HA influenza protein .....	38
3.4.2 Monomeric vs tetrameric fusion partner for M1 .....	38
3.4.3 Evaluation of M1 fusion sites. ....	39
3.5 Conclusion .....	40
Chapter 4 Influenza VLP downstream processing.....	41
4.1 Chapter objective .....	41
4.2 Materials and Methods.....	42
4.2.1 Tangential flow filtration (TFF).....	42
4.2.2 Sucrose cushion ultracentrifugation.....	42
4.2.3 Sucrose density gradient .....	42
4.2.4 Iodixanol density gradient.....	43
4.2.5 Hemagglutination assay .....	43
4.2.6 Baculovirus quantification using flow cytometry .....	44
4.2.7 Transmission electron microscopy (TEM).....	44
4.3 Results.....	46
4.3.1 Purification of influenza VLPs by density gradient: sucrose and iodixanol. ....	49
4.3.2 Purification of fluorescent VLPs: sucrose density gradient .....	51
4.3.3 Viral particle visualization .....	54
4.4 Discussion.....	56
4.4.1 Downstream processing of fluorescent influenza particles.....	56
4.4.2 Difference on density gradients .....	56
4.4.3 Baculovirus and influenza VLPs purification .....	57

4.4.4 Conclusions .....	58
Chapter 5 Flow cytometry analysis of purified Influenza VLPs .....	59
5.1 Chapter objective.....	59
5.2 Materials and Methods .....	60
5.2.1 Data acquisition and processing .....	60
5.3 Results .....	61
5.3.1 Limit of detection and particle distribution .....	61
5.3.2 Purified VLP sample analysis.....	65
5.4 Discussion .....	70
5.4.1 Nanoscale particle detection.....	70
5.4.2 Downstream detection of VLP .....	71
5.5 Conclusion.....	72
Chapter 6 Conclusions.....	73
6.1 Generation and tracking of fluorescent influenza proteins in insect cells .....	73
6.2 Downstream processing of fluorescent VLPs .....	73
6.3 Flow cytometry analysis of purified VLPs.....	74
Chapter 7 Recommendations.....	75
References .....	77
Appendix A End Point Dilution Assay (EPDA) .....	91
Appendix B Single fluorescent VLP construct.....	92
Appendix C Flow cytometry analysis of uninfected Sf9 cells .....	93
Appendix D Calculations used for Hemagglutination Assay (HA Assay).....	94
Appendix E Specifications and calculations used for quantification of baculovirus using flow cytometry .....	95
Appendix F Green (FL1) vs red (FL3) signal plots of purified fractions.....	97

## List of Figures

- Figure 1. Influenza virus morphology
- Figure 2. Comparison of influenza and influenza VLP
- Figure 3. Baculovirus replication cycle
- Figure 4. Baculovirus morphology
- Figure 5. Generic VLP downstream processing
- Figure 6. Genetic variants for dual-fluorescent influenza VLP and non-fluorescent VLP
- Figure 7. Cell density and viability of Sf9 cells infected with recombinant baculovirus producing influenza fluorescent fusions.
- Figure 8. Confocal images of infected Sf9 cells
- Figure 9. Single Sf9 cells infected with different baculovirus constructs at 72 hpi
- Figure 10. Flow cytometry profiles for FSC and SSC during infection
- Figure 11. Analysis of the infection.
- Figure 12. Fluorescent analysis of the variant throughout the experiment
- Figure 13. Fluorescent profile analysis
- Figure 14. Influenza VLPs downstream processing and characterization
- Figure 15. HA activity and baculovirus concentration during VLP purification
- Figure 16. Purification profiles of density gradients
- Figure 17. Purified migration profiles of sucrose density gradients. Migration profile for 3' DsRed2, 3' mKate2, 5' mKate2 and M mKate2
- Figure 18. TEM imaging of purified samples
- Figure 19. Noise detection analysis
- Figure 20. Analysis of serial dilutions for 500 and 100 nm reference beads
- Figure 21. Analysis of diluted 100 nm beads.
- Figure 22. Density plots of fraction 9 of purified samples outside Noise gate.
- Figure 23. Analysis of purified fractions and reference solutions
- Figure 24. Analysis of serial dilutions of purified samples.
- Figure AB-1. Single fluorescent influenza VLP construct.

Figure AC-1. Forward Scatter (FSC) and Side Scatter (SSC) profile of uninfected Sf9 cells.

Figure AD-1 Example calculations for HA Assay.

Figure AF-1. Particle distribution of fraction 9 of purified samples.

## List of Tables

Table 1. General information influenza A virus.

Table 2. Comparison of different expression systems.

Table 3. Comparison of different recombinant expression strategies used for production of complex biologics in insect cells.

Table 4. Fluorescent events statistics.

Table 5. Physical properties of mKate2 and DsRed2 proteins.

Table 6. HA activity and baculovirus yields.

Table 7. Purification comparison among fluorescent variants.

Table 8. Comparison of density bands for influenza virus in different density gradients.

Table 9. Geometric mean and mode of red signal (FL3)

Table AE-1. Settings to analyze the sample on the FACSCalibur flow cytometer

## Nomenclature

AcMNPV	<i>Autographa californica</i> multicapsid nucleopolyhedrovirus
BEVS	Baculovirus expression vector system
BV	Budded virus
eGFP	Enhanced green fluorescent protein
FC	Flow cytometry
FSC	Forward scatter
HA	Hemagglutinin
hpi	Hours-post infection
M1	Matrix protein 1
MDCK	Madin-darby canine kidney
MOI	Multiplicity of infection
NA	Neuraminidase
NPV	Nuclear polyhedrosis virus
NSEM	Negative staining electron microscopy
ODV	Occlusion-derived virus
Pfu	Plaque forming units
polh	Polyhedrin
RBCs	Red blood cells
RFP	Red fluorescent protein
SEC	Size exclusion chromatography
Sf9	<i>Spodoptera frugiperda</i>
SRID	Single radial immunodiffusion
SSC	Side scatter
TEM	Transmission electron microscopy
VLP	Virus-like particle
WHO	World Health Organization



# Chapter 1

## Introduction

Every year biopharmaceutical companies manufacture millions of doses of influenza vaccines to protect the population against the virus. Influenza vaccine manufacturing is a process that is performed yearly due to the high rate of mutations in the virus. The rapid evolution of the virus is a major concern due to social and economic consequences that may be caused by the illness associated with virus infection (Dawood et al., 2017; Mao, Yang, Qiu, & Yang, 2012). In order to keep track of the virus mutations the World Health Organization (WHO) performs a worldwide screening to detect the circulating strains. The WHO then reports twice per year so that manufacturers can produce the most appropriate vaccine. Currently, the use of egg-based technology is still predominant for influenza vaccine manufacturing. This technology was developed during the last century and even though it has been optimized, is still labor-intensive and time-consuming. This is worrisome, especially in pandemic scenarios where accelerated manufacturing processes are needed. To meet the needs of the market and emergency cases, different manufacturing processes have been assessed as an alternative to increase vaccine production while reducing processing time (Wong & Webby, 2013).

Vaccine manufacturing using insect cells is a promising alternative, especially when used in combination with the Baculovirus Expression Vector System (BEVS) (Kollewe & Vilcinskas, 2013). This expression system has been widely used for the production of complex biopharmaceuticals since it is easy to handle, capable of post-translational modification and able to produce high protein expression via infection (Peixoto, Sousa, Silva, Carrondo, & Alves, 2007; Young et al., 2015). An example of commercially available products using this expression system is Cervarix™ (GSK), developed against human papillomavirus (HPV), and Flublok™ (Protein Science), a trivalent influenza vaccine. Furthermore, previous works have shown the capacities of insect cells to produce influenza virus-like particles (VLPs), which are particles mimicking the structure of influenza viral particles (Krammer et al., 2010; Thompson et al., 2015). Bright and collaborators (2007) showed that VLP vaccines injected to mice had sera producing higher inhibition of hemagglutination activity. Their results exhibited that

inhibit 4 isolates of a H3N2 strain were inhibited efficiently, whereas, whole inactivated virus or recombinant HA vaccines inhibit only 2 isolates.

The development of alternative methodologies for influenza vaccine production also generates the need for new analytical techniques to assess the quality, potency, and homogeneity of the final product. It has been mentioned that analytical technologies used for *in ovo* production can be implemented for new generations of vaccines (Thompson, Petiot, Lennaertz, Henry, & Kamen, 2013), however, the development of specialized techniques based on inherent features of new vaccine candidates is still needed.

Flow cytometry has been widely used as a technique for the assessment of multiple properties of cells and small particles (Gaudin & Barteneva, 2015). The technique has been previously used to characterize different baculovirus promoters driving recombinant protein production in insect cells after infection (George, Jauhar, Mackenzie, Kießlich, & Aucoin, 2015). Moreover, George & Aucoin (2015) have fused the hemagglutinin and matrix protein influenza proteins to fluorescent proteins to produce and study the assembly process of influenza VLP particles. As shown by George (2016), the latter strategy resulted in a limited amount of synthesized proteins being released from the cell. More specifically, M1 clustered in the center of the cell. Based on this work, new genetic constructs were evaluated in this thesis to further explore the assembly process of fluorescent VLPs. Here flow cytometry is used to monitor influenza VLP production in insect cells, as well as VLP purification.

## **1.1 Purpose of the work**

The main goal of this work is to characterize formation of dual-fluorescent VLPs, so that VLP can be used as a tool to develop VLP purification protocols.

### **1.1.1 Hypothesis**

Fluorescent VLPs can be used as a tool for process development; however, the yield of fluorescent VLPs is significantly reduced because M1-RFP is believed to be trapped in the nucleus. By examining different versions of fluorescent M1 fusions, it may be possible to alleviate problems in VLP formation and gain a novel tool for process development.

### **1.1.2 Aims and objectives**

This work can be broken down into two aims, each with their own objectives. The first aim is to evaluate the M1-RFP fusion, and has 3 objectives:

1. determine the effect of red fluorescent proteins fused to the M1 gene in different locations;
2. determine the effect of monomeric vs tetrameric red fluorescent proteins for M1 fusions;
3. determine indirectly protein expression of individual influenza genes based on fluorescence.

The second aim is to use flow cytometry to detect VLPs during the purification procedures. The objective for this aim is to develop a protocol that can detect nano-sized fluorescent particles without the use of particle labelling steps.

## Chapter 2

### Literature Review

#### 2.1 Influenza virus

##### 2.1.1 Characteristics

Influenza is an acute respiratory disease that causes multiple symptoms such as severe malaise, fever, dry coughing, headache, muscle and joint pain, and runny nose (WHO, 2016). According to the World Health Organization (WHO) influenza virus causes about 3 to 5 million cases of severe disease, and around 250 000 to 500 000 deaths annually (WHO, 2016). Pneumonia is the most common influenza-associated complication; nevertheless, organs other than lungs can be affected. To prevent the disease, vaccination is recommended, especially for high risk individuals (pregnant women, children, the elderly, health-care workers, and individuals with specific medical conditions).

The influenza virus belongs to the *Orthomyxoviridae* family which are negative sense, single stranded RNA viruses. There are three types of influenza viruses: A, B and C. Type A and B share similar features genetically and morphologically, but they also have differences. The former is characterized for its broad host spectrum: humans, birds, whales, pigs, and horses; while the latter has only been found in humans and seals. Lastly, type C is predominant in humans, but it has been isolated from swine as well. All types of influenza are able to infect humans, however, type A has been responsible for multiple influenza pandemics (Cheung & Poon, 2007). **Table 1** provides additional information on influenza A.

**Table 1** General information on influenza A virus. Modified from (Kiselev, 2010)

<b>Influenza A Virus</b>				
<b>Family</b>	<b>Orthomyxoviridae</b>			
<b>Type of genome</b>	<b>Negative-sense, single-stranded RNA</b>			
<b>Structure and length of genome</b>	<b>Segment</b>	<b>Size of gene (bp)</b>	<b>Encoded protein</b>	<b>Function</b>
	I	2341	PB2	Component of vRNA polymerase: It is an important protein for generating the cap structure for viral mRNA
	II	2341	PB1	Component of vRNA polymerase: Elongation of RNA synthesis
			PB1-F2	Involved in apoptosis and causes significant delay in the clearance of influenza virus by the host immune system
	III	2233	PA	Component of vRNA polymerase: endonuclease.
	IV	1778	HA	Responsible for the binding of viral particles to sialic acid containing receptors on the cell surface.
	V	1565	NP	Encapsulates the viral RNA genome. NP also helps to stabilize the viral genome and regulates the synthesis and replicative transcription.
	VI	1413	NA	Cleaves the cellular sialic acid residues that link the newly formed virions to the host cell membrane.
	VII	1027	M1	Major component of the virion. It helps assemble viral proteins and drives viral budding.
			M2	Small transmembrane protein (ion channel) responsible for the pumping protons into viral particles from the endosome.
VIII	890	NS1	Regulates a viral gene expression involved in RNA splicing and translation.	
		NS2 (NEP)	Responsible for export of nascent ribonucleoprotein from nucleus to the cytoplasm	
<b>Subtype of influenza A virus (Characterized by the type of HA and NA surface glycoproteins)</b>	-HA includes 18 different types (H1-H18) (Tong et al., 2013) -NA includes 10 different types (N1-N11) (Tong et al., 2013)		Subtypes that have been documented to infect humans (H1N1, H2N2, H3N2, H5N1, H7N7, and H9N2) (Subbarao & Katz, 2000)	
<b>Mutations</b>	Antigenic drift		Minor mutation caused by the lack of proofreading mechanism of the viral RNA polymerase	
	Antigenic shift		Genetic reassortment of at least two different influenza viruses that infect the same cell.	

Influenza virus contains eight viral RNA segments encoding 11 genes, a mixture of structural and non-structural proteins (see **Figure 1**). The genes that belong to the former group are mainly involved in structural roles and include hemagglutinin (HA), neuraminidase (NA), nucleoprotein (NP), matrix protein 1 and 2 (M1 and M2). HA, NA and M2 are surface proteins that are embedded in the lipid envelope derived from the host cell. HA is a homotrimeric glycoprotein responsible for cell attachment and cell entry via interaction with the sialic acid located on the cell membrane (Nicholls, Lai, & Garcia, 2012). Moreover, HA is synthesized as a precursor, HA0, which possess two subunits, HA1 and HA2, that are exposed as a result of cleaving HA0 by endogenous proteins (Gamblin & Skehel, 2010). The other main surface glycoprotein is NA, a homotetrameric protein which has a major role in the release of viral progeny by dissociating receptors on the protein membrane. This is possible by hydrolyzing the sialic acid from the glycoproteins (Gamblin & Skehel, 2010). Lastly, M2 is a homotetrameric ion channel located within the viral envelope which allows the acidification of the interior of the particle, causing conformational changes during the infection cycle. In addition, M1 is the major structural component located underneath the lipid envelop, playing a major role on virus morphology (Bourmakina & García-Sastre, 2003). Non-structural proteins consist of polymerase subunits (PB1, PB2 and PA), and the non-structural proteins (NS1 and NS2), participate on viral replication processes.

Influenza A virus has subtypes based on antigenic variations of surface glycoproteins: hemagglutinin (HA) and neuraminidase (NA). Currently, 18 HA and 11 NA subtypes have been identified (Tong et al., 2013). Most of the variants circulate in non-human hosts such as bats, birds, swine and other mammals (Short et al., 2015). Only the subtypes A/H1N1, A/H2N2 and A/H3N2 are known to spread commonly in humans (Petrova & Russell, 2017); however, cases of zoonotic transmission have been documented (de Wit et al., 2010; Kandeel et al., 2010; RahimiRad, Alizadeh, Alizadeh, & Hosseini, 2016), increasing the possibility of a pandemic strain, creating a major health concern.

# INFLUENZA A

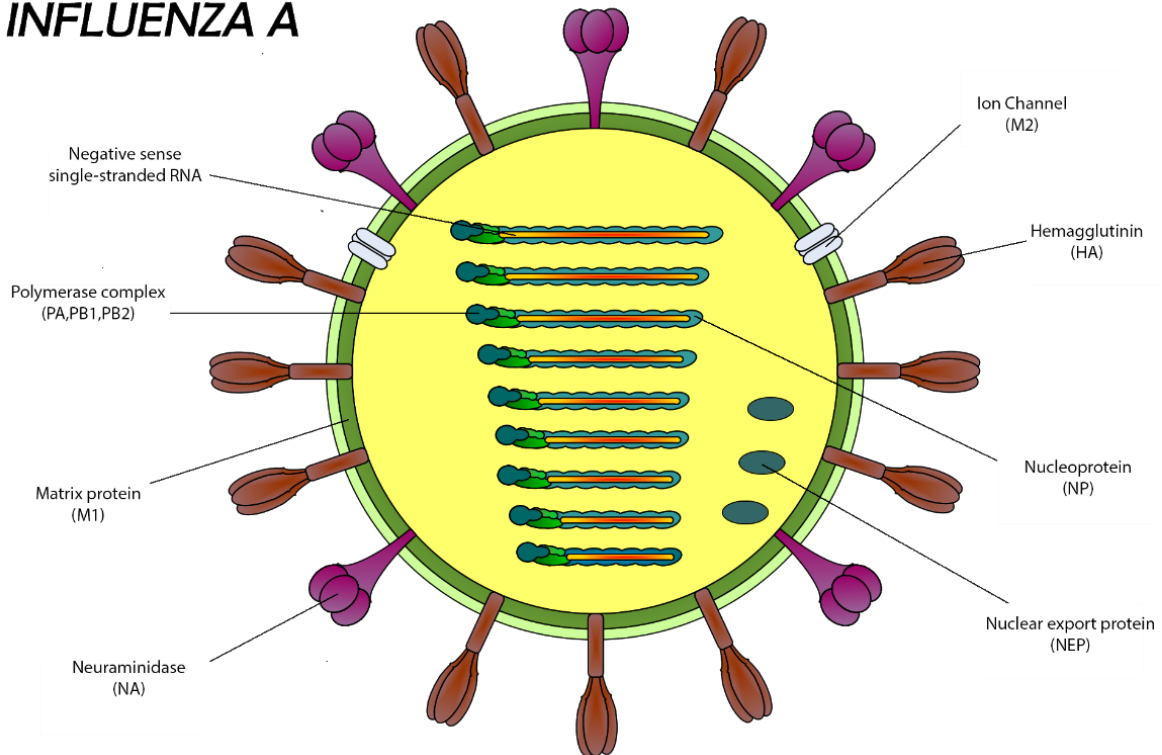


**Figure 1** Influenza virus morphology

Influenza possess a high evolution rate due to two evolutionary characteristics of the virus: its ability to undergo antigenic drift and antigenic shift. The former refers to minor nucleotide mutations that occur because the viral RNA polymerase lacks a proofreading mechanism. Surface glycoproteins show the highest rate of nucleotide substitution, happening approximately  $6.7 \times 10^3$  times per year for HA and  $3.2 \times 10^3$  times per year for NA (Smith & Palese, 1989). This causes small changes to the surface proteins leading to an ineffectiveness of previously acquired immune protection. Antigenic shift relates to a phenomenon called genetic reassortment, a process involving the exchange of genomic segments of two or more viruses. This process occurs when multiple viruses infect the same cell and their genetic material is combined during the replication cycle (Landolt & Olsen, 2007).

### **2.1.2 Influenza morphology**

Influenza virus A is a pleomorphic, enveloped virus with multiple shapes from spherical to filamentous (Calder, Wasilewski, Berriman, & Rosenthal, 2010), ranging from 80 to 120 nm. Viral morphology is influenced by replication cycles, viral factors and host factors. One factor that determines their morphology is the number of replication cycles. Chu, Dawson, & Elford (2018) found that fresh samples from patients contain a substantial presence of filamentous virus. The morphology changes to mostly spherical shape after multiple passages in eggs or tissue cultures (Choppin, Murphy, & Tamm, 1960). Moreover, morphology is determined also by genetic factors that are specific for each strain. Bourmakina & García-Sastre (2003) used reverse genetics to study the genetic factors influencing filamentous morphology in primary virus isolates. The experiment showed how transferring the M segment, coding M1 and M2 of the influenza A/Udorn/72 (H3N2), a filamentous strain, into influenza A/WSN/33 (H1N1) virus, a spherical strain, changes the phenotype, from spherical to filamentous. Further analysis showed the critical role of M1 in the morphology of influenza A virus. Similar results were found by Elleman & Barclay (2004).

## 2.2 Influenza vaccine: manufacturing process

### 2.2.1 Vaccine production

Every year a surveillance network headed by the WHO screens for new variations of influenza virus in humans and animals, especially in birds and pigs. Samples from patients with influenza-like symptoms are sent and analyzed by one of the National Influenza Centers spread worldwide. Once the virus is isolated, it is sent for characterization to the Collaborating Centers for Influenza Reference where the strain is identified and released as the recommended vaccine formulation for manufactures. This information is available twice per year in February and September, and informs on two influenza type A strains and one type B strain circulating worldwide (Gerdil, 2003). Once this information is released a new A type hybrid strain is generated by coinfecting an egg with one of the suggested strains and a high-growth strain which possesses an accepted safety profile, e.g. A/Puerto Rico/8/1934. This hybrid must express the HA and NA from the desired strain while retaining an ability to be propagated. Subsequently, the new sample is sequenced and confirmed before scale-up and manufacturing.

The predominant technology used to manufacture influenza vaccine is *in ovo* production. This technology was developed during the 1940s (Goodpasture, Woodruff, & Buddingh, 1932; Woodruff & Goodpasture, 1931) and is a standardized and established process. There are three types of products that are made using this technology: whole-virus, split-virus and subunits vaccines. In all the cases the raw material is the allantonic fluid recovered from the eggs previously used to propagate the virus. Whole-virus vaccines are produced by chemically inactivating the virus and purifying the sample to remove protein contaminants. Split-virus vaccines are prepared by using a detergent treatment to dissociate the viral lipid membrane exposing viral proteins and subviral elements (Duxbury, Hampson, & Sievers, 1968). Lastly, subunit vaccines use purified hemagglutinin and neuraminidase from the lipid complex, along with non-protective elements (Bachmayer, Liehl, & Schmidt, 1976; Brady & Furminger, 1976a, 1976b). Even though egg-based technology has been used for over 60 years and improvements have been done to the purification process and high-yield reassortant strains, there are significant drawbacks that must be addressed. The long manufacturing process and the limited manufacturing capacity due to the availability of high

quality eggs are the main concerns, especially when considering a pandemic scenario (Ulmer, Valley, & Rappuoli, 2006).

### **2.2.2 New influenza vaccine technologies**

The development of alternative processes to produce influenza vaccine has been discussed extensively (Houser & Subbarao, 2015; Krammer & Palese, 2015). The main objective is to establish a process to overcome the drawbacks of egg-based technology. Many approaches have been studied, offering different benefits. Some alternatives are discussed briefly in the following sections.

#### **2.2.2.1 Cell culture**

Cell-based production technologies possess greater scalability compared with egg-based technology. Moreover, advantages such as faster production cycles, process control, and avoidance of egg components, that could cause allergic reactions, are possible (Milian & Kamen, 2015). Some of the mammalian cell lines that have been proposed as candidates for influenza vaccine production are PER.C6® (Koudstaal et al., 2009; Pau et al., 2001), monkey kidney cells (Vero) (Kistner et al., 1998; Youil et al., 2004), Madin Darbin Canine Kidney (MDCK) (Youil et al., 2004) and human embryonic kidney 293 cell line (HEK- 293) (Le Ru et al., 2010). Furthermore, replication optimization of influenza A virus has been done by screening random mutations on the PR8 influenza strain to obtain a high yield strain for MDCK and Vero cells (Ping et al., 2015). Some of the commercially available seasonal trivalent vaccines using this approach are Optaflu® (Novartis, licensed in EU), Flucelvax® (Novartis, licensed in US), and Preflucel® (Baxter, licensed in EU). Furthermore, monovalent versions have also been produced Celtura® (Novartis) and Celvapan® (Baxter). Moreover, the use of cell culture is not limited to mammalian cell lines, FluBlok® is a recombinant trivalent HA vaccine produced in insect cells using the baculovirus expression system. Unlike the mammalian cell lines replicating the influenza virus, FluBlok® relies on the expression and purification of the HA protein.

### **2.2.2.2 Universal vaccine**

The search for a ‘universal vaccine’ capable of protecting a population against a broader spectrum of strains instead of a narrow group is on-going. The idea relies on the capacity to understand virus evolution using deep-gene-sequencing and structural biology. These studies have the ability to characterize viral changes more efficiently and to comprehend how these mutations affect function, antigenicity and immunogenicity of specific proteins, HA for example (Erbelding et al., 2018). On this matter, some researchers have studied the stalk domain of the HA, a more conserved domain compared to the globular head of the protein, as candidate for a universal vaccine. In 2010, Steel and collaborators showed that sera from mice vaccinated with the stalk domain of HA, generated from the complete HA2 polypeptide and sections from HA1 involved in the stalk region, and lacking the globular head, possessed greater ELISA activity against heterologous strains compared with mice vaccinated with full length HA. More improvements have been developed since then, mainly focusing on increasing the spectrum of protection by creating chimeric HA proteins from different HA groups (Krammer & Palese, 2013; I Margine et al., 2013) .

### **2.2.2.3 Virus-like particles (VLPs)**

VLPs are nanoscale particles that resemble a native virus structure but does not contain genomic material, thus disabling viral replication. In addition, increased immune response is expected since viral attenuation or inactivation is not required, processes than can modify protein epitopes and decrease the resemblance between native and vaccine virus (Roldão, Mellado, Castilho, Carrondo, & Alves, 2010). VLP production is achieved by expressing one or more structural viral proteins (see **Figure 2**). Several genetic constructions have been used to produce influenza VLPs, usually a combination of structural proteins involving M1 and at least one surface protein. Pushko and collaborators (2005) showed the production of a VLP containing M1, NA and HA using insect cells. Functional influenza VLPs, similar in size to native virus, were released to the media and displaying hemagglutinin and neuraminidase activity were obtained. Further experiments revealed that VLPs were able to elicit serum antibodies and inhibit viral replication in mice. Another experiment performed by Wu et al. (2010) showed the production of influenza VLPs in Vero cells by expressing the proteins M1,

NA, HA and M2 . These particles were also able to elicit an immune response, fully protecting mice against lethal infection. Influenza VLPs expressed in insect cells have shown a broader immune response compared to whole inactivated virus or recombinant HA vaccines (Bright et al., 2007). Bright and collaborators (2007) showed that mice vaccinated with H3N2 influenza VLPs produced in insect cells, had sera that inhibited hemagglutination for 4 different influenza isolates. On the other hand, mice vaccinated with either whole inactivated virus vaccines or recombinant HA vaccines were less effective eliciting hemagglutination inhibition.

Moreover, the expression system of choice plays an important role on VLP production. Different production methodologies are needed according to each system, changing upstream and downstream processing. Different production platforms have been used to achieve functional influenza particles such as HEK293 (Thompson et al., 2015), insect cells (*Sf9* and *Sf21*) (Krammer et al., 2010; G. E. Smith et al., 2013; Thompson et al., 2015), *Nicotiana benthamiana* (Makarkov et al., 2017; Pillet et al., 2016) and Vero cells (Pushko et al., 2005).

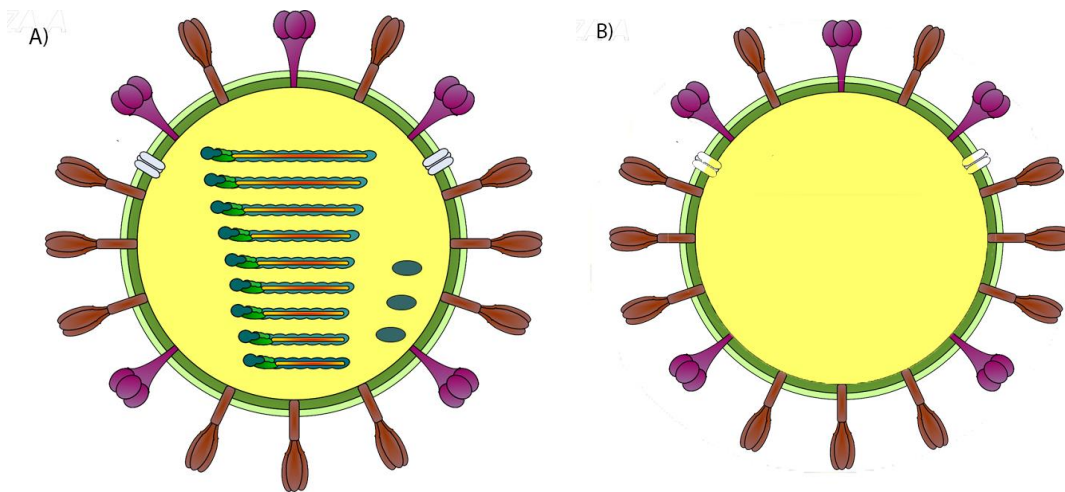


**Figure 2.** Comparison of influenza and influenza VLP. A) Influenza virion and B) influenza VLP assembled by HA, NA, M1 and M2 influenza proteins

## 2.3 Insect cells

Insect cell technology is a versatile platform to produce recombinant proteins. Insect cells have the ability to produce complex proteins requiring post-translational modifications, are easy to manipulate, and can produce high yields via viral infection (Kollewe & Vilcinskas, 2013). **Table 2** compares insect cells with other expression systems commonly used. As eukaryotic cells, post-translational modifications are possible, allowing in most cases the proper processing with respect to disulfide linkage, phosphorylation, fatty acid acylation and glycosylation (Becker-Pauly & Stöcker, 2011). Nevertheless, the glycosylation processing differs from other species. Glycosylation reactions taking place in the endoplasmic reticulum are highly conserved among eukaryotes, while the reaction in the Golgi complex are species specific and cell type specific. Insect cells have less complex *N*- and *O*- glycosylation, causing shorter sugars to be attached to the protein (Callewaert, 2009).

**Table 2** Comparison of different expression systems. Modified from  
(Van Oers, Pijlman, & Vlak, 2015)

Property	Transgenic insect cells	Baculovirus vectors in insect cells	Mammalian cells (Transient)	Bacteria cells ( <i>E. coli</i> )	Yeast ( <i>Pichia pastoris</i> )
Post-translational modifications	++	++	+++	-	+
Homogeneity of N-glycans	++	++	+	Not relevant	-
Biological activity	++	++	+++	+	++
Immunogenicity	+++	+++	+++	+	++
Production levels	+	++	+	+++	+++
Safety concerns	++	++	+	+++	+++
Downstream processing efforts	++	+	++	++	++

*Sf9* cells (derived from *Spodoptera frugiperda*) and High Five™ (derived from BTI-TN5B1-4) are the most studied insect cell lines for the production of complex biologics (Krammer et al., 2010). Three main approaches are used to produce recombinant proteins in insect cells: transient expression (Chang et al, 2018; Shen, Hacker, Baldi, & Wurm, 2013), generation of stable cell lines (Pfeifer, 1998) and viral infection using a baculovirus expression vector (BEV) (J.-P. Yang, 2016). A comparison of these approaches is shown in **Table 3**. These approaches are not mutually exclusive; there are reports showing production of complex biologics, e.g. VLPs, using a stable cell line coupled with baculovirus infection (Sequeira et al., 2017).

**Table 3.** Comparison of different recombinant expression strategies used for production of complex biologics in insect cells.

Baculovirus Expression Vector System (BEVS)		Transient expression		Stable Cell line	
Advantages	Disadvantages	Advantages	Disadvantages	Advantages	Disadvantages
-Commercial kits available -High Expression of protein -Easy baculovirus manipulation	-Protease activity after lysis -Complex purification and polishing steps	-Non-lytic process	-Low yields compared with BEVS -Non-continuous production	-Continuous protein expression	-Time-consuming -Variation due to random integration

### 2.3.1 Baculovirus: classification and infection cycle

The *Baculoviridae* is a family of viruses capable of infecting lepidopteran cells. Their genetic information is contained in a circular, doubled stranded DNA genome between 80-180 kb. The morphology of budded virus is an oval-like shaped enveloped particle with a diameter sizing from 30-60 nm and approximated width of 250-300 nm. Based on morphology the family is divided in two groups: nuclear polyhedrosis viruses (NPVs) and granulosis viruses. One of the commonly used NPVs in research and industry is the model organism *Autographa californica* multicapsid nucleopolyhedrovirus (AcMNPV) (Theilmann *et al*, 2005).

The lytic infection cycle of AcMNPV is divided into four temporal phases: immediate early, delayed-early, late and very late (**Figure 3**). The early phase of infection starts when the virus enters in the cell via endocytosis (Dong et al., 2010). Once in the nucleus, the virion releases their genetic material, initiating DNA transcription. During the early stages RNA is produced by host RNA polymerase II. Following the early phase, virus transcription transitions from using the host RNA polymerase II to using a viral polymerase leading to transcription of late and very late genes. The late phase of infection takes place starting at 6 hours post infection, whereas the expression of very late genes is active 20 hours post infection (Theilmann *et al*, 2005).

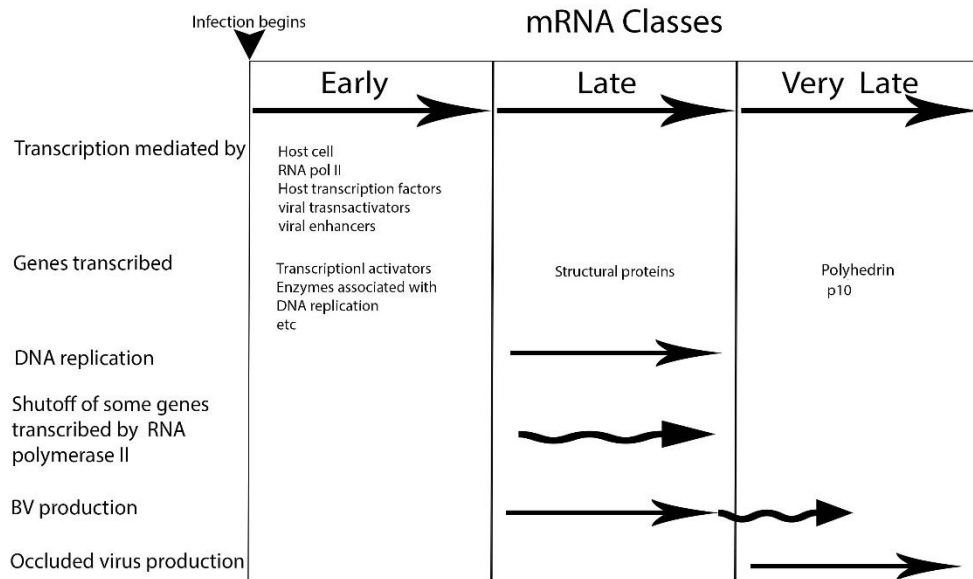


**Figure 3** Baculovirus replication cycle. Winding arrows emphasize the overlap events on the baculovirus replication cycle. Modified from Rohrmann (1992).

As a result of the infection, two types of virions are produced: budded virus (BV) and occlusion-derived virus (ODV). Even though they share the same genetic information, they differ in structural proteins, in morphology (**Figure 4**), cellular site maturation, time of maturation, source of viral envelopes, antigenicity and infectivity (Kelly *et al*, 2007). The former is produced by budding out the cell during early stages of the infection and allow cell to cell infection (Volkman & Summers, 1977). The latter is produced during late stages of

infection, primarily in the nucleus and is surrounded with polyhedral proteins. This protein layer increases particle stability outside the host insect. Typically, BV are used to infect insect cell lines for commercial and research purposes, genetic constructs normally choose promoters that are active during the late phase of infection, when ODV are formed. Polyhedrin and p10 are structural proteins that are produced in large amounts during the late phase of infection.

This is due to the high level of gene expression structural proteins (polyhedrin and p10) occurring during the late phase of infection. Moreover, ODV are capable of infecting midgut epithelial cells up to 10,000- fold more efficiently than BVs, while BVs are able to infect cell cultures 1,000-fold more efficient compared with ODVs (Volkman, Summers, & Hsieh, 1976; Volkman & Summers, 1977). Therefore, the biotechnology industry mainly uses BV in their processes instead of ODV.

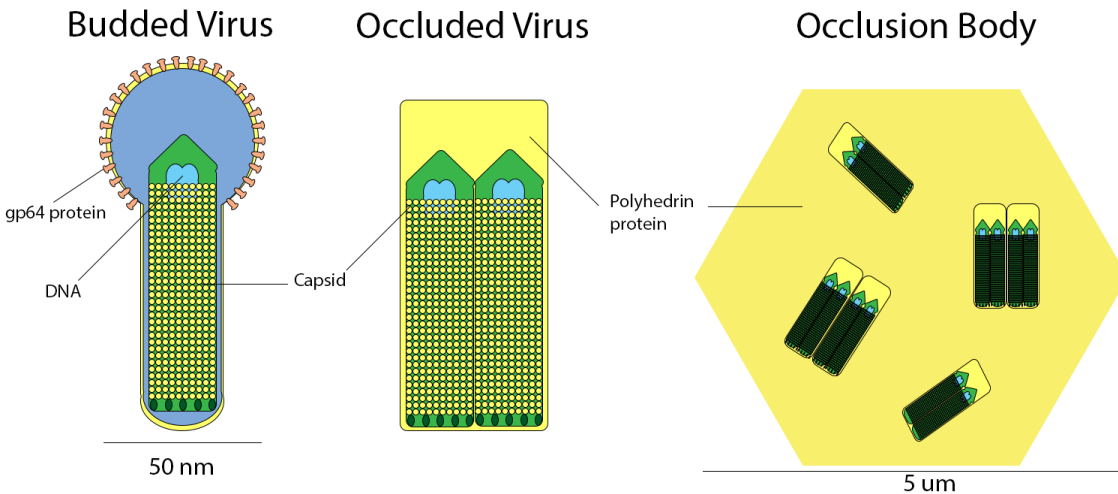


**Figure 4** Baculovirus morphology.

### 2.3.2 Baculovirus Expression Vector System (BEVS): production strategies

Baculovirus Expression Vector System (BEVS) is a platform that involves the use of a plasmid, a baculovirus vector and an insect host cell line (Hitchman et al. 2011). The technology is based on the baculovirus capacity to use the host protein processing machinery to express a protein of interest. This methodology allows easy manipulation, large DNA carrying capacity and production of high viral titers (Airenne et al, 2013). The first BEVS

developed by Smith and collaborators (1983) was designed to express human beta interferon integrating the gene under the control of the polyhedrin promoter, active during the very late stage of the process. Further experiments performed by Licari and Bailey (1991) showed the importance of multiplicity of infection (MOI) and time of infection (TOI) during expression of  $\beta$ -galactosidase under the control of the polyhedrin promoter using *Sf9* cells. MOI is a parameter that relates the number of plaque forming units (PFU) added to a specific amount of cells at the time of infection. Their results showed that increasing the MOI while infecting cells during the late exponential phase of growth leads to a logarithmic relationship between final  $\beta$ -galactosidase production and MOI. In contrast, if the infection takes place in the early exponential phase, the concentration of final product is reduced if the MOI is greater than 1. The complexity of the system demonstrates that recombinant protein production in insect cells is not trivial.

Moreover, insect cell technology is known for their capacity to produce complex and multimeric proteins, which in some cases involves the expression of more than one gene at a time. Strategies to address these requirements are co-infection or co-expression. The former involves the use of multiple recombinant baculovirus, each one carrying a single gene (monocistronic) to infect a cell culture, while the latter relies on a single recombinant baculovirus carrying multiple genes (polycistronic). Combinatorial experiments using co-infection strategies with poli- and monocistronic baculoviruses have shown that the ratio of each recombinant baculovirus added affects the yield of complex biologics (Aucoin, Perrier, & Kamen, 2006). Usually, promoters such as *p10* and *polh*, activated during the very late stage of infection, are chosen when designing genetic constructs to drive gene expression, this choice is due to previous experience obtaining high yield while using them, nevertheless, studies have shown the potential of alternative promoters activated during early, intermediate and late stages of infection (George et al., 2015; Lin & Jarvis, 2013; Martínez-Solís, Gómez-Sebastián, Escribano, Jakubowska, & Herrero, 2016). Lin and Jarvis (2013) have shown that late and very late promoters, *p6.9* and *polh*, produce higher levels of RNA but lower protein levels compared with immediate early and delayed early promoters, *ie1* and *39K*, when expressing a secreted

alkaline phosphatase. The previous evidence reinforces the need of more complex experiments to fully understand the dynamics of this platform.

## **2.4 Influenza VLP production in Insect cells**

The capacities of the insect platform to produce VLPs has been demonstrated, especially using BEVS. Co-expression (Latham & Galarza, 2001; Irina Margine, Martinez-Gil, Chou, & Krammer, 2012) and co-infection (Krammer & Palese, 2015; Thompson et al., 2015) strategies have shown to be able to properly produce VLPs. Furthermore, productivity assessments have been performed showcasing higher productivity from insect cells compared with other expression systems. Thompson and collaborators (2015) compared influenza VLP production using BEVS with *Sf9* cells and using baculovirus transduction of HEK293 cells. A co-infection strategy was used with *Sf9* cells relying on three recombinant baculovirus, each one expressing either HA, NA or M1 at a MOI of 3. The results showed that the insect cell system produced 35 times higher concentration of VLPs compared to HEK 293 cells. However, baculovirus contamination was one of the main drawbacks of the insect platform. Krammer and collaborators (2010) performed a study comparing two different insect cell lines, *Sf9* and BTI-TN5B1-4, to produce influenza VLPs. Cell cultures were co-infected with two recombinant baculovirus expressing either HA or M1 at a MOI of 10. The findings revealed that influenza VLP process in BTI-TN5B1-4 decreased the baculovirus contamination while increasing hemagglutination activity. More recently, Sequeira and collaborators (2017) have shown a modular system using a stable High Five™ cell line and baculovirus to produce influenza VLPs expressing multiple subtypes of HAs. The study involved the expression of two HA molecules by the stable cell line, whereas, infection of the cell culture was performed using a baculovirus driving the expression of M1 and three HA molecules. This new approach showcased the versatility of production strategies for the insect-BEVS platform.

## 2.5 Downstream processing of VLPs

The purpose of downstream processing is to eliminate contaminants formed during the manufacturing process and to produce large volumes of concentrated product without disturbing their biological activity (Morenweiser, 2005). For influenza VLPs produced in insect cells, downstream processing is challenging. The raw product contains multiple contaminants such as cell debris, host protein, baculovirus and baculovirus DNA (Krammer et al., 2010). Baculovirus is a by-product considered the main contaminant during the process. This can be a concern because baculovirus has been shown to have the capacity to transduce human cells (Chuang et al., 2009; Kenoutis et al., 2006; Kukkonen et al., 2003) and induce cytokine expression causing a strong immune response (Abe et al., 2003; Hu, 2008). Avoiding adverse effects is critical for manufacturing companies, which is why there is a need to develop scalable and robust purification procedures.

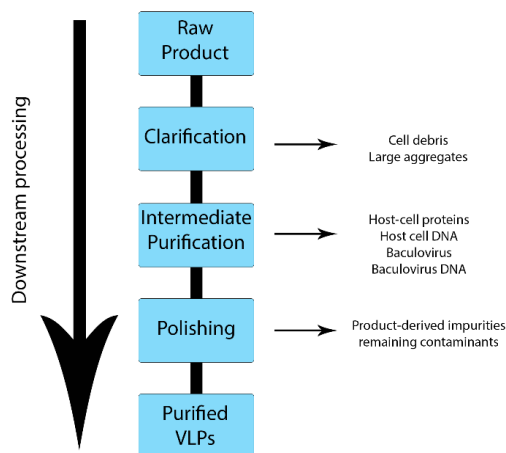


**Figure 5.** Generic VLP downstream processing.

Purification of influenza VLPs requires several steps to reach the purity, potency and morphological criteria. **Figure 5** shows an overview of downstream processing for VLPs. The first purification step is clarification: a solid-liquid separation. Given that influenza VLPs are released to the media, cell lysis is not required, diminishing purification complexity. Centrifugation and filtration are processes commonly used to separate cell debris. For a long time, batch or continuous centrifugation was the process of choice; however, in recent years

membrane processes have gained interest since they are easy to scale up and provide more control over operating shear stress (Ladd & Jürgen, 2015). During this step, cells and cell debris are removed from the bulk media. The next step is to concentrate VLPs while reducing working volume. Tangential flow filtration (TFF) has been used to concentrate VLPs in different occasions using membranes with different cut-offs ranging from 750-500 kDa (Negrete, Pai, & Shiloach, 2014; Peixoto et al., 2007). Recently, Carvalho and collaborators (2016) used TFF to concentrate influenza VLPs produced in High Five™ cells using a 300 kDa membrane cut off.

Further purification can be achieved by different methods depending on the scale of the process. At laboratory scale, ultracentrifugation and density gradients are techniques that allow VLP purification. In combination, the aforementioned techniques can be considered a two-step process. First concentrating the viral samples by ultracentrifugation, with or without a cushion, to remove low density particles. Then, viral particle purification based on density once the virus is submitted to a density gradient high-speed centrifugation. This process has been widely used to purify influenza VLPs (Thompson et al., 2015), nevertheless baculovirus contamination is still one of the main issues with this technique since baculovirus share similar density compared to influenza (Krammer et al., 2010). Moreover, ultracentrifugation steps are non-scalable, tedious and labor-intensive (Vicente, Roldão, Peixoto, Carrondo, & Alves, 2011). In contrast, large scale processing is moving towards chromatography steps. In this regard, ion exchange chromatography is one of the techniques that has shown great results as an intermediate purification step (Sofia et al., 2017). An example was shown by Carvalho et al. (2016). In their research they used a Sartobind Q MA 75 anion exchange membrane to perform negative mode chromatography as an intermediate purification step for influenza VLPs purification. Similarly, the company GE Healthcare Life Sciences (2011) have shown that the ion exchange column Capto Q is able to isolate influenza VLPs while decreasing baculovirus presence and baculovirus DNA.

Finally, a polishing step is needed to completely isolate the particle of interest. In this process, VLPs are transferred to the final formulation buffer while reaching the desired concentration to optimal dosage. Polishing of VLPs mostly involves size exclusion

chromatography (SEC) (Carvalho et al., 2016), ultrafiltration/diafiltration (Hanh et al., 2013) and sterile filtration.

## **2.6 Analytical techniques for characterization influenza VLPs produced in insect cells.**

Analytical techniques are used to obtain specific information during production processes and allow the assessment of product quality. There is no universal technique that provides all the quality information of a single molecule, thus, multiple methodologies are needed to fully characterize a specific product. Influenza vaccines have been commercially available since the last century, consequently there is already a workflow to characterize the virus when isolated directly from patients or animals, and during vaccine manufacturing. This *prior* knowledge has been transferred to evaluate new vaccine candidates facilitating quality control procedures, since no modifications were needed. In this section traditional and new analytical approaches used to characterize influenza VLP particles will be reviewed.

Methodologies can be divided into three different classes: indirect quantification based on total protein, enzymatic activity, and total particle quantification. The first class provides information related to protein content and protein features. Colorimetric techniques such as Pierce BCA Protein Assay (Thermo Science, Rockford, USA) , used to determine protein content, and western blots are protocols that belong to this classification. Commercial kits to quantify total protein are not commonly used to assess VLP production due to their non-specific nature, whereas, western blot is frequently used as a more specific technique to detect expressed proteins. The second group relies on the enzymatic activity of the antigen on the VLP surface. Depending on the VLP design, HA or/and NA properties can be used to quantify viral particles indirectly. Lastly, total particle counts of VLPs is a methodology that has shown great results to detect VLPs in semi-pure samples. Techniques to visualize the particles from a pure or semi-pure sample such as transmission electron microscopy (TEM) are part of this group.

## **2.6.1 Total protein concentration**

### **2.6.1.1 Western blot**

Western blot is a technique that allow the detection of specific proteins in a sample. The procedure involves protein separation based on molecular weight through sodium dodecyl sulfate–polyacrylamide gel electrophoresis (SDS-PAGE). The separated proteins are then transferred to a membrane, which is incubated with labeled antibodies targeting the protein of interest. After developing the membrane, the presence of the target protein is seen as a band in the membrane. This technique has been used extensively to detect the presence of HA and M1 in influenza VLP samples (Krammer et al., 2010; Thompson et al., 2015). This is the only technique that can detect the presence of M1 protein.

## **2.6.2 Enzymatic assays**

### **2.6.2.1 Hemagglutination assay**

Hemagglutination assay (HA Assay) is a technique that was developed in the 1940s to indirectly quantify agglutination properties of the HA molecule (Hirst, 1942). The methodology is based on serial dilutions of a viral sample combined with red blood cells (RBCs). This technique has been widely used in literature to quantify influenza VLPs, however, there are some issues with reproducibility of results due to blood source, blood concentration, and decay of hemagglutination activity (HA activity) over time (Thompson et al., 2013). Nevertheless, there are reports showing false positives of this technique when used for HA quantification in the insect-baculovirus system (Yang et al., 2007). Due to the budding nature of the baculovirus, it has been shown that baculovirus particles are able to display the HA molecules on their membrane (Yang et al., 2007).

### **2.6.2.2 Neuraminidase activity**

Like the HA Assay, NA enzymatic activity can be used to indirectly evaluate the concentration of VLPs. Multiple commercial kits are available, however, variability among different kits have been reported (Nayak & Reichl, 2004). A comparison among three different techniques to measure neuraminidase activity from influenza VLPs produced in MDCK cells was performed by Nayak and Reichl (2004). The activity was evaluated by thiobarbituric acid (TBA), a fluorometric method using Amplex Red as a fluorogen (FL-AR), and FL-MU-

NANA. Their results showed that FL-MU-NANA is more robust, with lower limits of detections and lower background noise. The A-star influenza neuraminidase inhibitor resistance detection kit, which was used by Quan and collaborators (2012) to evaluate M1-NA VLPs produced in insect cells, is also possible.

### **2.6.2.3 Single radial immunodiffusion (SRID) assay**

The single radial immunodiffusion (SRID) assay is the only approved test by the WHO to evaluate the potency of an influenza vaccine. The technique measures the radial diffusion of a viral antigen in an agarose matrix containing antigen-specific antibodies. In contrast to the HA assay, this technique measures the amount of HA protein rather than its activity. This technique has been previously used to evaluate the production process of influenza VLPs in HEK and insect cells (Thompson et al., 2015). However, this protocol lacks robustness. The drawbacks of this technique include: the presence of non-aqueous components which can interfere with HA diffusion, long processing times, low sensitivity, a need of updated version of the HA antigen, as well as, their antibodies, and aggregation of HA protein at high concentrations (Thompson et al., 2013).

### **2.6.3 Total particle counts**

#### **2.6.3.1 Transmission electron microscopy (TEM)**

Transmission electron microscopy (TEM) is considered the *gold standard* when quantification of viruses is needed. This technique relies on visual counting of virions along with latex particles of known concentration to determine total viral particle concentration (Malenovska, 2013). Size distribution data can also be acquired by TEM, however, the process is labor-intensive due to visual counting performed for the assay. Thompson and collaborators (2015) have used this technique to quantify production of influenza VLPs and baculovirus contamination from HEK and insect cell platforms. The main drawbacks of the previous methodologies are the need of a concentrated and pure, or semi pure, sample before imaging, and a skilled operator doing the counting. These factors can impact the particle quantification dramatically.

#### **2.6.4 New technologies to track and quantify VLPs**

Ion exchange-high performance liquid chromatography (IEX-HPLC) has been used by Transfiguracion and collaborators (2015) to quantify influenza VLPs produced in HEK cells. The technique, calibrated with a sample of known titer, allows the quantification of viral sample by calculating the area of the peak produced when the VLPs are eluted. The new methodology was compared with standard techniques such as TEM, virus counter (ViroCyt) and TCID50 assay, showing similar titers.

Another technique that has been proposed is nanoparticle tracking analysis (NTA). NTA is a new technique developed to visualize particles in suspension by a focused laser beam. This technique tracks the Brownian motion of each single particle, frame by frame, to obtain the particle hydrodynamic diameter. The concentration of particles is acquired once the particles are counted and related to the sample volume. More specific details are described by Steppert and collaborators (2017). This method has been used to quantify total enveloped virus-like particles and compared with other non-traditional methods such as size-exclusion HPLC with UV detection (SE-UV), and detection with multi-angle light scattering (SE-MALS). The results showed that NTA overestimated the particle counts, especially with crude samples, by counting cell debris rather than VLP particles. In this regard, both SE-UV and SE-MALS can quantify particles only after purification steps are performed. In addition, SE-UV needs a standard curve to calculate counts properly. On the other hand, SE-MALS does not require a pre-made calibration curve since the particle number is calculated based on the differential scattering intensity of the particles.

## **Chapter 3**

# **Generation and Tracking of Fluorescent Influenza Proteins in Insect Cells**

### **3.1 Chapter objective**

The use of fluorescent proteins to study influenza VLPs has previously been shown as a tool to monitor protein localization within the cell, mainly focusing on HA (Young et al., 2015). Expression of influenza proteins fused with fluorescent proteins can be used as a tool to understand assembly and tracking of influenza VLPs in insect cells. Previously, George & Aucoin (2015) have shown the expression of influenza genes fused to fluorescent proteins in insect cells. In their work, enhanced green fluorescent protein (GFP) was fused to HA and DsRed2, a red fluorescent protein, was fused at the 3' site of the M1 protein. Their findings showed green expression exclusively in the cell membrane, whereas, red fluorescence was detected first near the center of the cell before reaching the cell membrane. Moreover, George (2016) results also showed that only a limited amount of synthesized proteins was released as influenza VLPs.

To further explore the use of fluorescent influenza fusions, multiple genetic designs were tested to understand the effect of fluorescent proteins fused to influenza proteins. The effect of red multimeric or monomeric fluorescent protein was evaluated by comparing DsRed2 with mKate2, the former being an obligated tetrameric protein while the latter being a monomeric protein. The assessment was done while both red fluorescent proteins (RFPs) were fused at the 3' end. In addition, mKate2 was fused in different sites of the M1 gene to identify the optimal fusion site. Here, flow cytometry and confocal microscopy are used to monitor the expression and localization of fluorescent influenza protein fusions in the insect-baculovirus system. The goal of this chapter was to determine if alternative M1 fusions could be used to change the localization of the M1 fusion in the cell.

## **3.2 Materials and Methods**

### **3.2.1 Cell Culture**

*Spodoptera frugiperda* clonal isolate 9 (*Sf9*) cells were maintained in SF-900™ III serum-free media (GIBCO, Carlsbad, CA, USA) at 27°C on an orbital shaker (VBR, Champaign, Illinois, USA) rotating at 130 revolutions per minute (rpm). Cell density was maintained between  $0.5 \times 10^6$  to  $4 \times 10^6$  cells/mL in 125mL capped glass Erlenmeyer flasks having a working volume of 30 mL. Cell viability of the cell culture was measured using trypan blue staining and was maintained above 95%. Cell counts and viability were examined using Countess™ II (Thermo Fisher)

### **3.2.2 Baculovirus generation and amplification**

P2<sup>1</sup> stocks were generated by infecting *Sf9* cells at a density of  $1.5 \times 10^6$  cells/mL in a 30 mL culture with a MOI of 0.1 using P1 stock. Baculovirus was harvested once the viability was below 70%. The infected culture was collected and centrifuged at 800 xg for 10 min, then filtered through a 0.2 µm membrane (VWR International, Mississauga, ON, Canada). Baculovirus stocks were stored at 4°C. The second passage virus stocks (P2) were quantified using end-point dilution assay (EPDA) and flow cytometry.

### **3.2.3 Baculovirus quantification using end-point dilution assay**

Baculovirus titers were calculated by end point dilution assay. Exponential growth phase *Sf9* cells were diluted to a concentration of  $2 \times 10^5$  cell/mL by adding SF-900™ III serum-free media (GIBCO, Carlsbad, CA, USA). 100 µL of cell suspension was seeded in each well of a 96-well plate, allowing to attach for 1 hour. Virus stocks were diluted with SF-900™ III serum-free media, from  $10^{-2}$  to  $10^{-10}$ . 10 µL of dilution was added to the plated cells (each virus dilution being added to 12 wells). The 96-well plate was placed in a sealed plastic box containing a wet paper towel and incubated at 27 °C for 5-7 days. After incubation, the plate

---

<sup>1</sup> Recombinant baculovirus is generated by transfecting insect cells with a baculovirus genome containing the gene of interest. After 72 hrs, budded virus is released to the media and harvested, this is known as P0 virus stock. To increase viral concentration a insect cell culture is infected using a low MOI to generate the P1 virus stock.

was examined under a fluorescence microscope, and wells were scored as infected or non-infected based on fluorescence. Titer was calculated as detailed in **Appendix A**.

### 3.2.4 Fluorescent VLP production

To produce fluorescent VLPs, 100 mL of *Sf9* cells at a density of  $1.5 \times 10^6$  cells/mL were infected at a MOI of 5. Genetic constructs used for this study are shown in **Figure 6**. Recombinant baculovirus encoding these genetic constructions were generated by Mark Bruder in the Aucoin Lab. The infection was monitored by determining cell density and viability every 24 hours. The supernatant was harvested once the viability was around 70%, approximately 72 hours post-infection. The cell culture was centrifuged for 15 min at 800xg at room temperature. Supernatant was recovered and filtered using a 0.2  $\mu$ m filter and stored at 4°C, whereas the cell pellet was stored at -80°C until more experiments were performed.

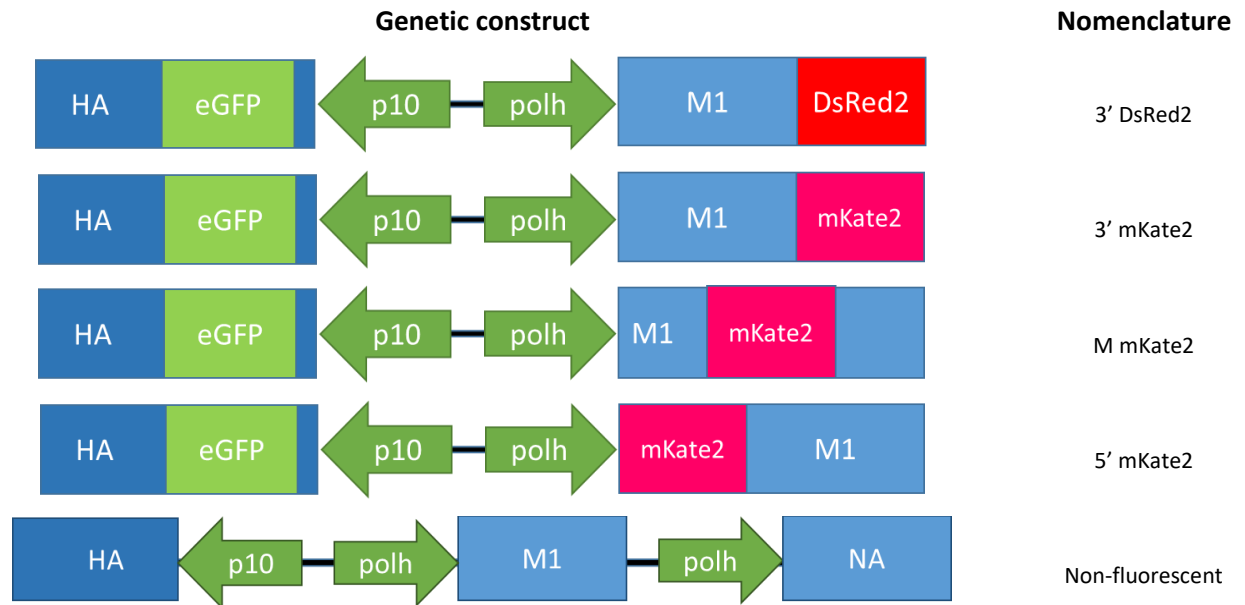


**Figure 6** Genetic variants for dual-fluorescent influenza VLP and non-fluorescent VLP. Recombinant baculovirus containing influenza constructs were generated by Mark Bruder in the Aucoin Lab.

### **3.2.5 Infection flow cytometry analysis**

To track the progress of infection, a sample of infected cell culture was analyzed using flow cytometry every 24 hours. To prepare the sample, 1 mL of infected culture was centrifuged at 100xg for 10 minutes and the supernatant was discarded. The cell pellet was resuspended using 1mL of 2% paraformaldehyde and placed in the dark at room temperature for 30 minutes. The sample was then transferred to a cytometer tube and diluted by adding 4 mL of PBS. The sample was analyzed using a BD FACSCalibur (BD Biosciences, Mississauga, ON, Canada) at a flow rate of 60  $\mu$ L/min to capture 10,000 events per sample. The results were acquired using CellQuest Pro (BD Biosciences, Mississauga, ON, Canada) and analyzed with FlowJo (Treestar Inc., Ashland, OR, United States) software. FL1 detector (emission 530 nm, bandpass 30nm) was used to detect green fluorescence, while FL3 detector (emission 670 nm, longpass) was used to detect red fluorescence. Relative particle size was analyzed by forward scatter (FSC) with a voltage of E1 and gain of 6.55. Granularity was evaluated by side scatter (SSC) setting the voltage at 300 and a gain of 1. Both, FSC and SSC, were set on a linear scale. In contrast, FL1 (voltage:258) and FL3 (voltage:304) used a logarithmic scale to acquire the data. The previous settings were maintained for all infection experiments.

### **3.2.6 Confocal microscopy**

Confocal microscopy was performed to analyze protein location inside the cell. A sample of 1 mL of infected cell culture was centrifuged at 100xg for 5 min. The supernatant was discarded, and the pellet was washed with in 1mL of PBS. The sample was pelleted and fixed for 15 minutes in the dark by adding 1mL of 4% paraformaldehyde. The sample was washed with 1mL of PBS and stained with 4',6-diamidino-2-phenylindole (DAPI) for 5 minutes in the dark. Finally, the sample was pelleted and resuspended in 10uL of PBS. A drop of stained sample was placed on a 76.2  $\times$  25.4  $\times$  1 mm microscope slide and a cover slip was placed on top of the drop. The cover slip was sealed using paraffin wax and a cotton swab. Imaging was conducted on a Zeiss LSM 510 confocal microscope (Zeiss Canada, Toronto, ON, Canada) using a lens of 63x magnification.

### 3.3 Results

With the aim of assessing bicistronic recombinant baculovirus driving the expression of fluorescent influenza fusion proteins, *Sf9* cultures were infected with a MOI of 5 and the cell density and viability were monitored every 24 hours (**Figure 7**). Cells were analyzed every 24 hours using flow cytometry and confocal microscopy to track green and red fluorescent signals.

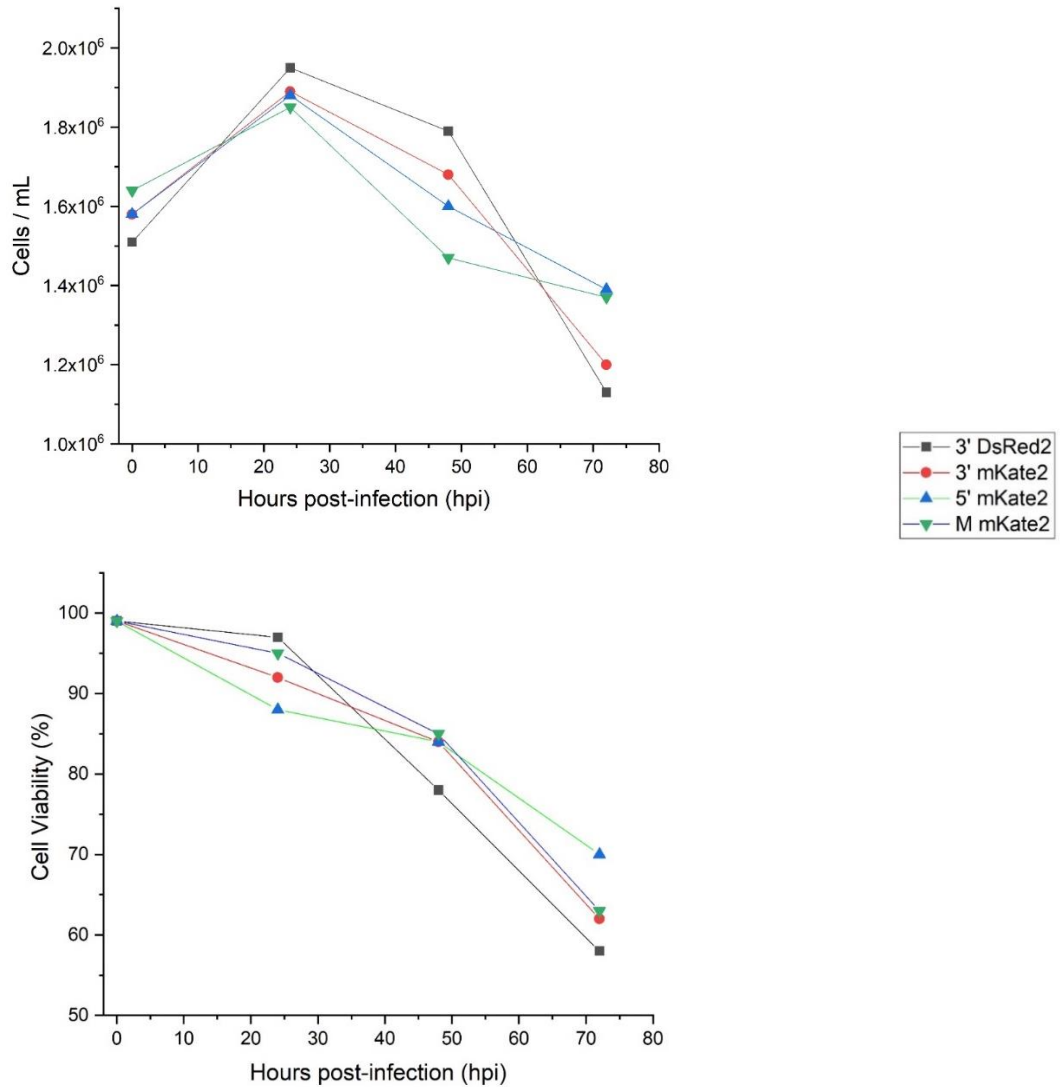


**Figure 7.** Cell density and viability of *Sf9* cells infected with recombinant baculovirus producing influenza fluorescent fusions.

### 3.3.1 Tracking influenza proteins

Protein localization was monitored by confocal microscopy every 24 hours (**Figure 8**). Confocal images for each variant showed green fluorescence situated at the cell membrane for all the variants after 24 hours post infection (hpi). Green fluorescent protein (GFP) localization did not change between 24 and 72 hpi. Infection using a baculovirus harboring a HA-GFP and a native M1 was used as an additional control (**Appendix B**). No changes in green fluorescent localization was observed. On the other hand, red fluorescence was detected at 24 hpi only for mKate2 variants, whereas, for the DsRed2 variant, red fluorescence was only detected after 48 hpi. RFP localization differed depending on the fusion site chosen. Both constructs with red fluorescent fusions at the 3'-terminus, either monomeric or tetrameric, displayed a concentrated expression of RFP at the nucleus. This feature was maintained during for the all-time points examined. The 5' mKate2 variant behaved similarly, concentrating RFP at the nucleus, but it appeared not as clustered as the counterpart located at the 3-terminus constructs. Lastly, M mKate2 variant showed a uniform distribution of red fluorescence throughout cells. Furthermore, a closer analysis on individual cells showed the presence of red fluorescent clusters at the cell membrane (**Figure 9**). This observation demonstrated that M1-RFP fusions have the capacity to reach the cell membrane, but possibly only when M1 is disrupted.

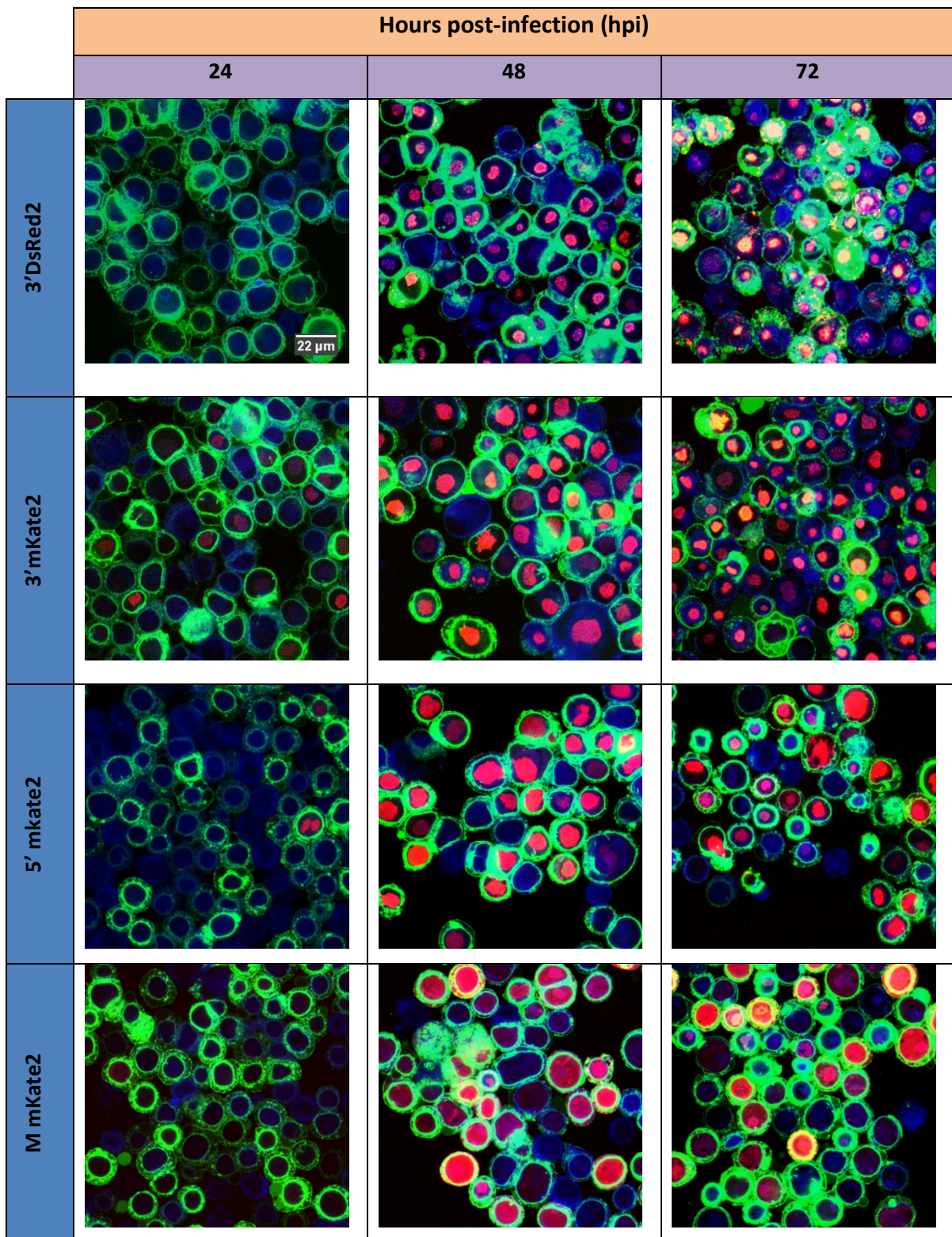


**Figure 8** Confocal images of infected Sf9 cell. Confocal microscopy was performed every 24 hours for each variant. Samples were fixed and stained with DAPI to recognize the cell nuclei, and imaged using a 63x magnification.

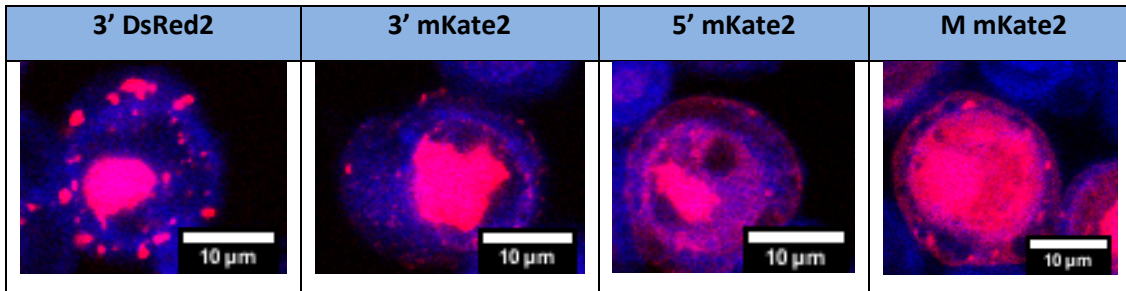
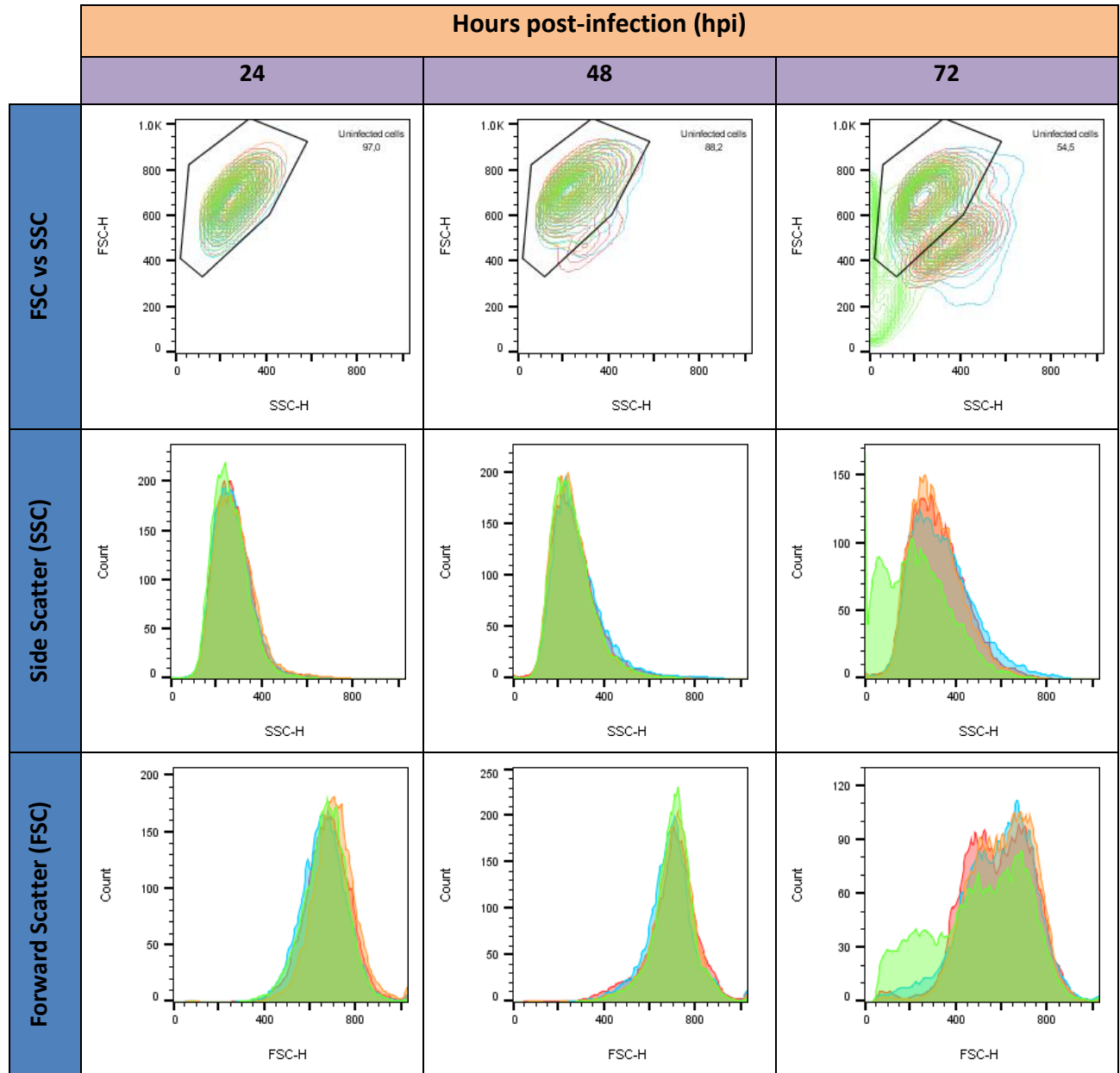


**Figure 9** Single *Sf9* cells infected with different baculovirus constructs at 72 hpi. The images only show the localization of red fluorescence inside the cells.

### 3.3.2 Monitoring infection process and expression levels

Flow cytometry was used to assess the changes in forward scatter (FSC), side scatter (SSC) and fluorescence intensity of *Sf9* cells once the cells were infected with recombinant baculovirus that allow the expression of the fluorescent influenza fusion proteins. A total of 10,000 events were acquired for each sample every 24 hours. FSC and SSC were used to evaluate the lytic process of the BEVS systems (**Figure 10**). Uninfected *Sf9* cells were used to determine the profile of healthy cells, and this population was gated as a control (**Appendix C**). The gate was applied to the profiles acquired from each culture every 24 hours. FSC vs SSC plots show the formation of a new population at 48 hpi, being more distinguishable at 72 hpi (**Figure 11 A**) shows the decrease of events inside the uninfected gate for all the variants during the infection process. Furthermore, single channel analysis was performed to determine the changes in SSC and FSC for gated events during the infection process. **Figure 11 B** and **11 C** shows an increase in mean value of SCC after 24 hpi which was maintained for 72 hours. The mean FSC value decreased at 24 hpi, except for 3' mKate2 variant which increased at 48 hpi. SSC histograms, **Figure 10**, for all the variants displayed a comparable tendency with only one peak for during the expression of fluorescent influenza fusions. Conversely, FSC profiles exhibit a single peak during the first 48 hours of infection, however, a new distinguishable peak appeared after 72 hpi.



■ 3' DsRed2   
 ■ 3' mKate2   
 ■ M mKate2   
 ■ 5' mKate2

**Figure 10** Flow Cytometry profiles for FSC and SSC during infection.

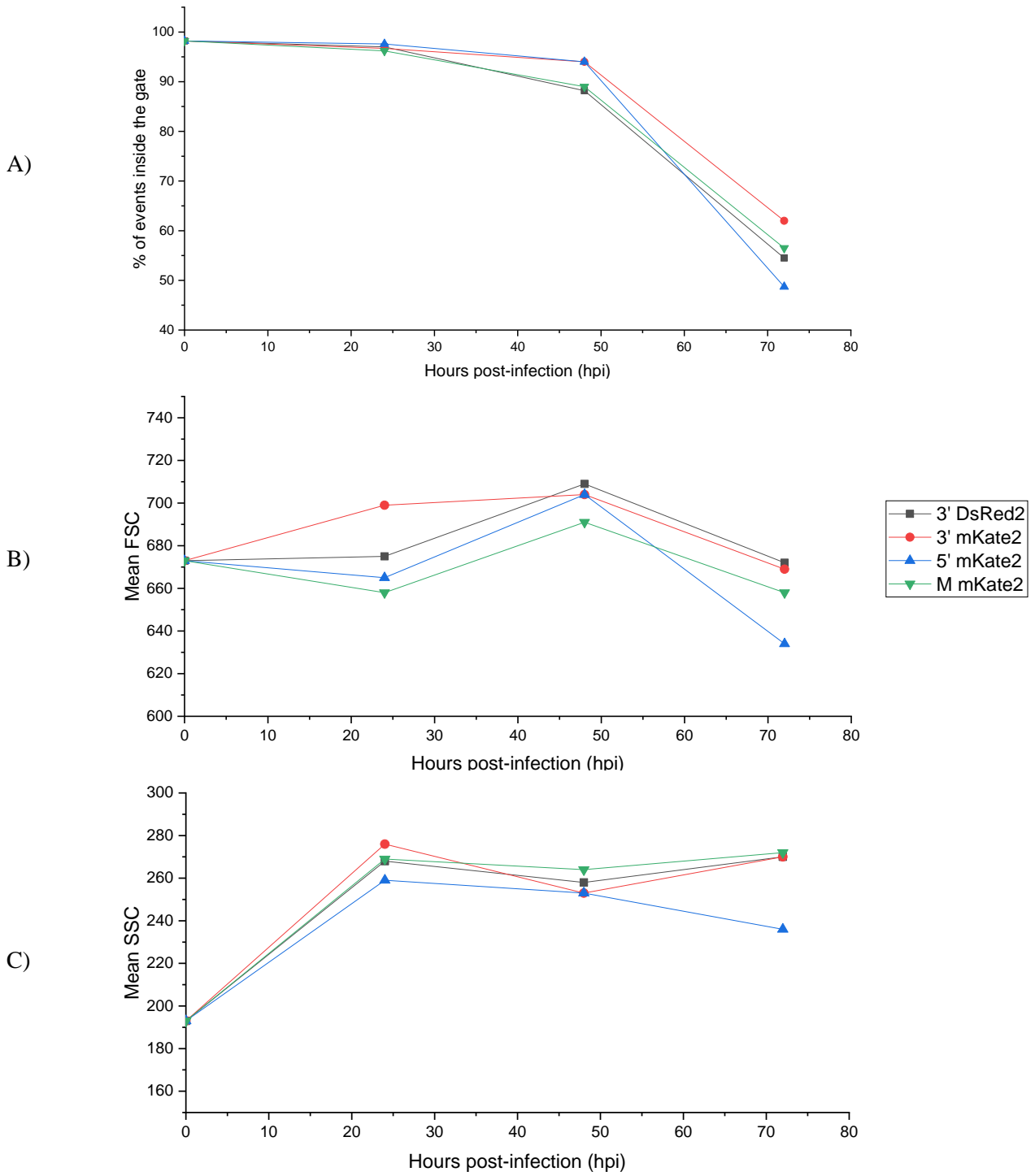


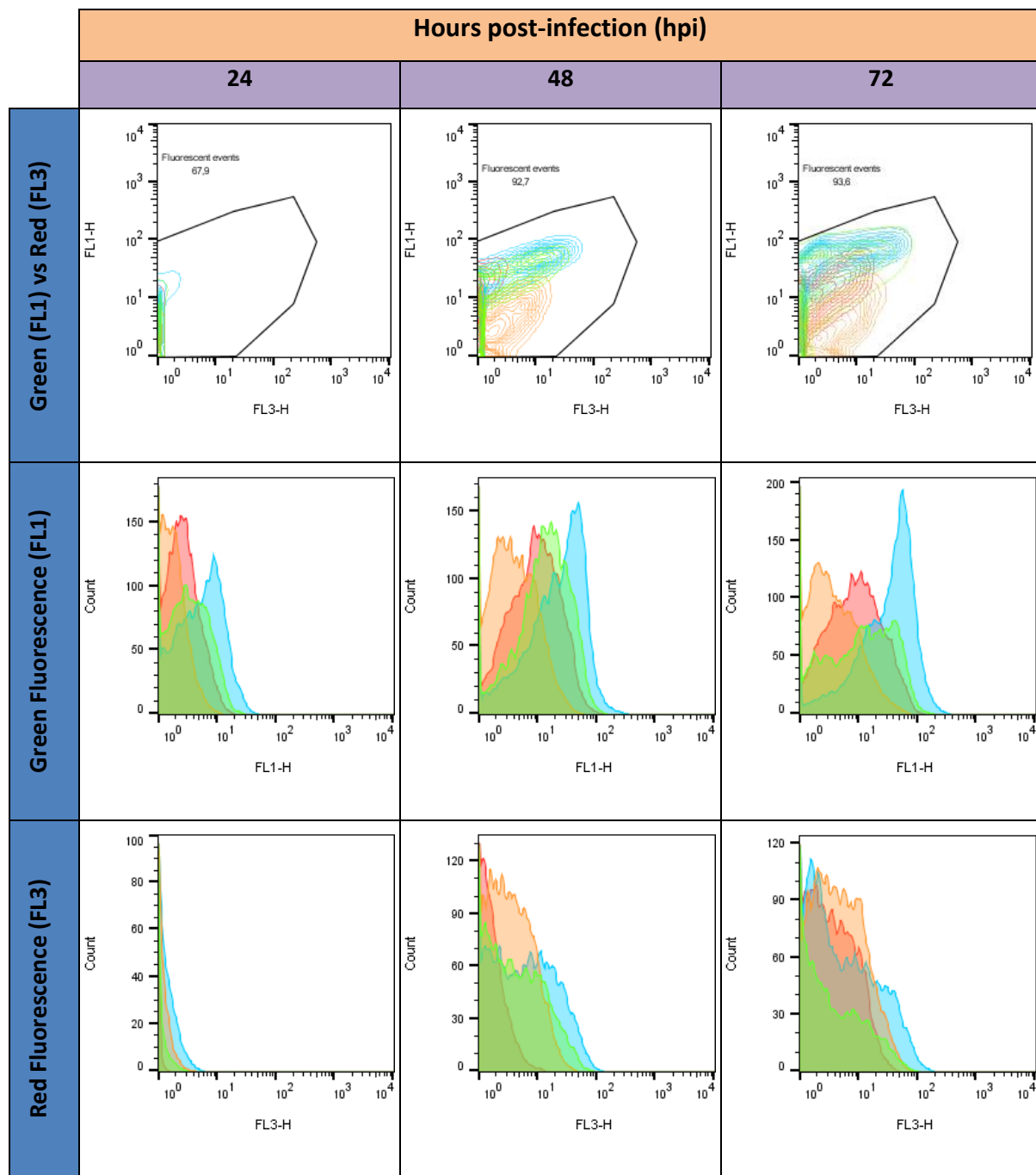
**Figure 11** Analysis of infections. A) Events localized inside the uninfected gate. B) Mean FSC value of events inside the uninfected gate and c) Mean SSC value of events inside the uninfected gate

Fluorescence expression levels were monitored during infection using flow cytometry. The FL1 channel was used to determine GFP expression levels, whereas, FL3 was used for RFP. A gate containing all the fluorescent events was created to analyze the data. **Figure 12** shows the different expression profiles acquired for each fluorescent variant, as well as, single channel profiles of gated events. These results provide indirect expression levels of HA and M1 synthesis. Moreover, geometric mean fluorescent values for GFP and RFP were determined based on gated events (**Figure 13**). Low RFP signal was detected at 24 hours, increasing at 48 hpi. Only 5' mKate2 presented a decay in RFP at 72 hpi. From these results, M mKate2 displayed the highest GFP and RFP mean values, nevertheless, analysis of GFP histograms (**Figure 12**) demonstrate that 3' DsRed2 reaches higher intensity levels even though mean relative fluorescence is lower. **Table 4** shows the statistics of fluorescent events for each variant, showing the variability of data acquired during the experiment.

Additionally, to study the expression levels of individual genes a normalized ratio of GFP and RFP intensities was calculated for all the variant, (**Figure 13 C**). The results showed that in all cases GFP is produced in higher levels when compared with RFP. The mKate2 variants showed increase in RFP signal after only 24 hpi, whereas, 3'DsRed2 variant showed a drop in the ratio after 72 hpi demonstrating increased RFP levels.

**Table 4** Fluorescent events statistics at 72 hours post-infection.

	Green Fluorescence				Red Fluorescence			
	Mode	Geometric Mean	Mean	Standard deviation	Mode	Geometric Mean	Mean	Standard deviation
<i>3' DsRed2</i>	11.1	8.79	14.4	15.6	1	2.56	4.21	5.06
<i>3' mKate2</i>	2.21	4.08	6.35	7.81	1	4.62	7.75	8.96
<i>5' mKate2</i>	39.2	11.5	21.3	23.2	1	2.12	4.74	9.31
<i>M mKate2</i>	56.2	30.6	46.2	38	1	4.23	10.9	18.2
<i>Uninfected cells</i>	1.15	1.14	1.14	n/a	1	1.01	1.01	n/a



■ 3' DsRed2   
 ■ 3' mKate2   
 ■ M mKate2   
 ■ 5' mKate2

**Figure 12** Fluorescent analysis of the variant throughout the experiment. A) GFP vs RFP profiles showing the gated events. B) Single GFP channel distribution of gated events. C) Single RFP channel distribution of gated events.

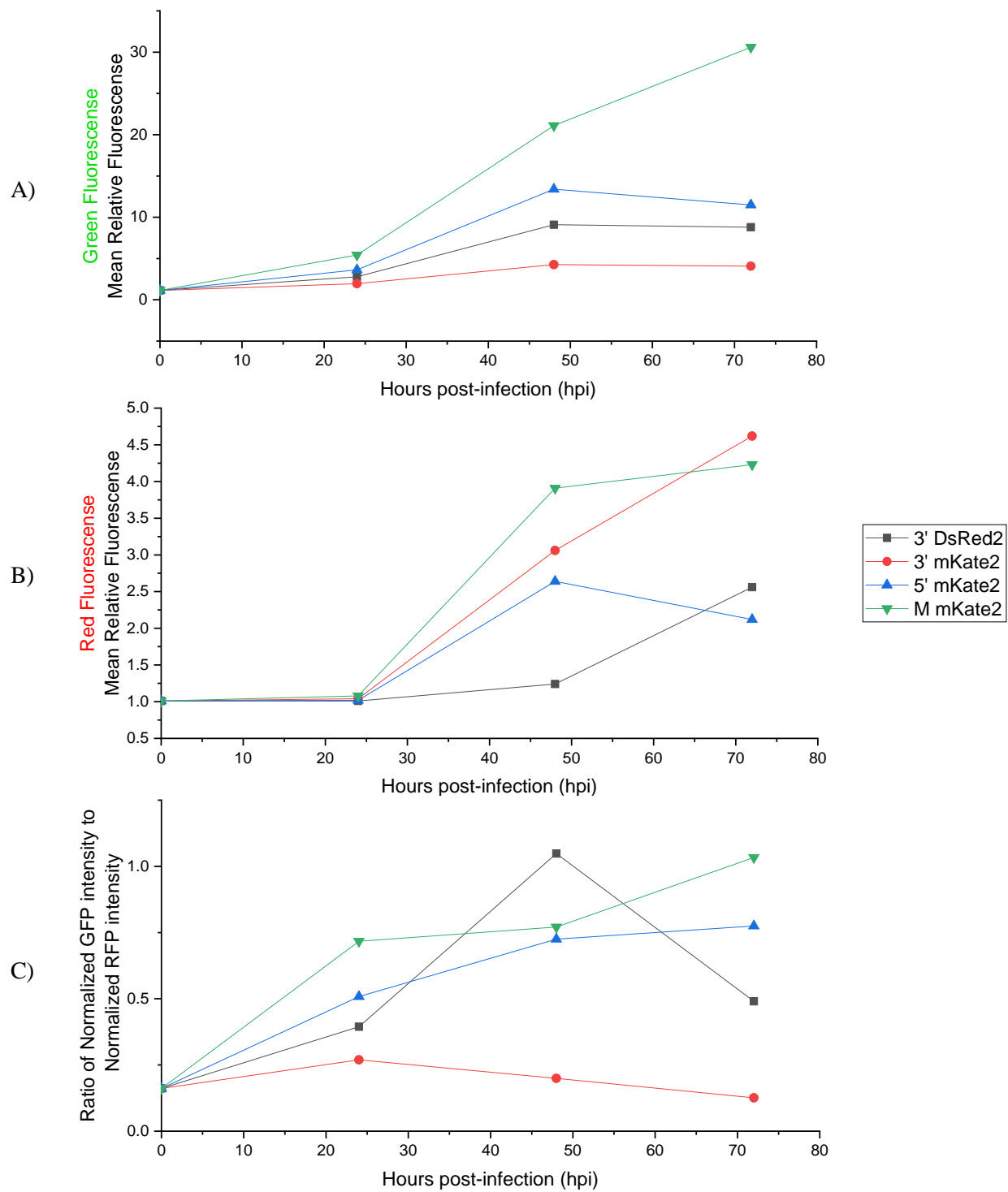


**Figure 13** Fluorescent profile analysis. A) Geometric mean Green, and. B) Geometric mean Red fluorescence values. C) Ratio of normalized GFP/RFP intensity levels.

### 3.4 Discussion

This work shows the individual tracking of influenza proteins using different fusion partners as a tool to monitor protein expression and localization within the cell. The use of fluorescent proteins allows the study of temporal and spatial expression of genes by measuring fluorescence in live cells. These properties can also be used to study localization, dynamics of viral particles and expression levels (Piatkevich & Verkhusha, 2011).

#### 3.4.1 Tracking HA influenza protein

Confocal microscopy was used to study the expression and localization of fluorescence. Expression of HA-GFP was localized at the cell membrane in all cases, which is consistent with the work of George & Aucoin (2015). This behavior is expected since influenza is an enveloped virus and HA inherently reaches the membrane in order to bud out of the cell (Szewczyk, Bieńkowska-Szewczyk, & Król, 2014). Previous studies using immunofluorescence corroborates our findings showing that HA is localized at the cell membrane when influenza VLP expression in *Sf9* cells is performed (Latham & Galarza, 2001). Moreover, expression of HA fused with GFP at the C-terminus in other systems have been reported as a strategy to understand VLP formation (Young et al., 2015). However, the quenching effects of a trimeric HA-GFP molecule is unknown, and the possibility of quenching due to proximity of GFP proteins could affect the fluorescent intensity of the particle.

#### 3.4.2 Monomeric vs tetrameric fusion partner for M1

One of the goals of this experiment was to evaluate the use of monomeric and tetrameric RFPs as fusion partner of the M1 protein. To this end, 3' DsRed2 and 3' mKate2 were tested and their expression analyzed. According to confocal images (**Figure 8**), the DsRed2 variant does not show RFP signal at 24 hpi, nevertheless, this fact does not mean that DsRed2 is not been produced during this period of time. The absence of early red fluorescence from the 3' DsRed2 variant may be due to a longer maturation process (**Table 5**). Another explanation could be the attenuation of fluorescent intensity due to fusion design. Additionally, **Figure 13 C** show a higher ratio level of expression for 3' DsRed2 at 48 hpi, decreasing to lower levels when compared with mKate2 variants at 72 hpi. This phenomenon may be caused

by the chromophore maturation of DsRed2. This protein has been engineered from DsRed and has enhanced fluorescence, better solubility and faster maturation (Bevis & Glick, 2002). Even though there is no published evidence of DsRed2 undergoing a green fluorescence intermediate, it is known that DsRed does (Baird, Zacharias, & Tsien, 2000). The data from this experiment suggest that DsRed2 preserves this green intermediate phase, which is not an ideal feature since it could disguise the signal from HA-GFP.

Furthermore, confocal imaging (**Figure 8**) showed that M1 fusions, with DsRed2 or mKate2 at the 3'-terminus, exhibited a high concentration of RFP signal on the nucleus. Similar results have been reported by George (2016) and, George & Aucoin (2015). High concentration of red expression inside the cells is a sign of low M1 exportation to the membrane. These observations support the results presented by Chen, Leser, Morita, & Lamb (2007) and Venereo-Sanchez et al. (2016) where higher expression levels of M1 were found in the cell pellet rather than in the supernatant when influenza VLPs were produced.

**Table 5.** Physical properties of mKate2 and DsRed2 proteins.

Protein	Oligomeric state	Max. Excitation (nm)	Max. Emission (nm)	Quantum Yield	Half-time maturation (hours)	Reference
DsRed2	Tetrameric	561	587	0.68	6.5	(Bevis & Glick, 2002)
mKate2	Monomeric	588	633	0.40	> 0.33	(Shcherbo <i>et al.</i> , 2009)

### 3.4.3 Evaluation of M1 fusion sites.

It is known that M1 plays a critical role in the formation of influenza particles and VLPs, however, it has not received as much attention as HA, limiting the information available involving their structure or their oligomerization. A complete crystal structure of this molecule has not been published and most of the studies focus on truncated forms of the N-terminus (Safo et al., 2014). Due to this, an evaluation of different fusion sites on the molecule were tested by adding the mKate2 gene on the 3'-terminus, 5'-terminus or in the middle of the M1 protein. The results from confocal microscopy showed that red fluorescence from 3' mKate2

fusion seems to cluster near the center of the cell. Similarly, 5' mKate2 variant was in the center of the cell, but it looks more spread. In contrast, when mkate2 is placed in the middle of M1 gene RFP expression is changed and is observed evenly throughout the cell. This was comparable to a baculovirus construct expressing only RFP is used, as shown by George & Aucoin (2015).

Moreover, individual expression levels of genes were analyzed by using the fluorescent signal as an indirect measurement (**Figure 13**). In addition, different normalized ratios of expression were obtained for all the M1 variants. The results showed ratio of expression over 0.75 for the 5' mKate2 and, 1 for the M mKate2, indicating similar expression levels of RFP and GFP. In contrast, the 3' variant performed with lower ratio levels indicating that RFP had higher expression than GFP, an indication of higher level of M1-RFP expression. The previous data suggest that the 5'- and 3'-terminus of M1 can be used as fusion site for fluorescent protein, without disrupting the M1 protein. Nevertheless, more experiments are needed to fully understand the difference on expression levels when M1 fusion proteins are designed.

### **3.5 Conclusion**

In this work, the characterization of four different recombinant baculovirus driving the expression of HA and M1 fused to a fluorescent protein was performed. Our results showed M1 influenza proteins fused to a RFP, either a tetrameric or monomeric, in the 3' site displayed red fluorescence concentrated near the center of the cell nucleus. Moreover, alternative M1 fusion placing mKate2 in the 5' site also presented high RFP levels near the center of the cell, but not as clustered as the 3' mKate2 fusion. In contrast, this behavior is disrupted when mKate2 is placed in the middle of the M1 gene. Lastly, the difference on ratio of expression levels of GFP and RFP were calculated, demonstrating expression differences among the recombinant baculovirus.

## **Chapter 4**

### **Influenza VLP downstream processing**

#### **4.1 Chapter objective**

Downstream processing has the objective to purify a specific molecule from a complex sample. Inherent properties of the targeted molecule need to be understood to improve purification processes and contaminants removal. Different approaches have been done in the past to obtain purified influenza particle, nevertheless, specific downstream procedures are needed when working with the BEVS. Baculovirus is considered the main contaminant while using the BEVS platform since it has similar physical features when compared with the influenza virus. At laboratory scale density gradients are preferred, whereas, chromatographic steps are more common for larger scales. Here we test the capacities of sucrose and iodixanol density gradient to purify VLPs. This chapter is dedicated to the study of downstream processing used on influenza VLP produced using BEVS. The goal of this chapter was to determine if VLPs are formed from the expression of M1-fusions and HA-fusions.

## **4.2 Materials and Methods**

### **4.2.1 Tangential flow filtration (TFF)**

Infected cell cultures were harvested after 72 hours post-infection or when the viability was around 70 %. A Stirred Ultrafiltration Cell Model 8050 (Millipore Sigma, Toronto, ON, Canada) was used to concentrate influenza VLPs from clarified and filtered (0.2µm filter) cell cultures. An Ultracel ultrafiltration disc with a cut-off of 10 kDa (Millipore Sigma, Toronto, ON, Canada) was employed to concentrate samples by a factor of 10. Samples were stirred at 200 rpm under nitrogen at a pressure of 75 psi. Once the desired volume was reached, the cell was depressurized, and the sample was stirred for 5 minutes to release all the particles trap on the membrane. The sample was stored at 4 °C until next purification step was performed

### **4.2.2 Sucrose cushion ultracentrifugation**

TFF concentrated samples were further concentrated by centrifugation using a 25% sucrose cushion. This step concentrates, and semi purifies VLP particles by removing low density particles. Concentrated VLP samples were layered over 1.5 mL of 25% sucrose solution in chilled 1x NTC buffer (1 M NaCl, 0.2 M Tris-HCl pH 7.4, 50 mM CaCl<sub>2</sub>). A Beckman Coulter Optima XPN-100 ultracentrifuge (Beckman Coulter, Mississauga, ON, Canada) was used to centrifuge the samples at 26,000 rpm (115, 900 rcf) at 4°C for 2 hours using a SW41 Ti Rotor (Beckman Coulter, Mississauga, ON, Canada). The supernatants were discarded and VLP pellets were resuspended using pre chilled 1x NTC buffer. Samples were shaken at 250 rpm on ice for 30 minutes and pipetted up and down for 10 min. Samples were stored at 4°C until next the experiment was performed.

### **4.2.3 Sucrose density gradient**

Sucrose density gradients were prepared in a 14x89 pollyallomer centrifuge tubes (Beckman Coulter, Mississauga, ON, Canada). The gradient consisted of 6 steps: 10, 20, 30, 40, 50, 60% sucrose solutions in 1x NTC buffer. 1.5mL of each step was layered using a pipette. The resuspended virus pellet was layered at the top of the gradient, above 10% solution, and centrifuged. The sample was spun using a SW41 Ti Rotor (Beckman Coulter, Mississauga,

ON, Canada) in a Beckman Coulter Optima XPN-100 ultracentrifuge (Beckman Coulter, Mississauga, ON, Canada) at 33,000 rpm (186, 700 rcf) for 16 hours and 4°C. 1 mL fractions were collected by puncturing the side of the tube. Fractions were weighed, and their density calculated. Fractions were stored at 4°C prior to further analysis.

#### **4.2.4 Iodixanol density gradient**

Iodixanol density gradients were prepared in a 14x89 pollyallomer centrifuge tubes (Beckman Coulter, Mississauga, ON, Canada). The gradient consisted of 6 steps, 10, 20, 30, 40, 50, 60% iodixanol solutions in 1x NTC buffer. 1.5mL of each step was layered using a pipette. The resuspended virus pellet was layered at the top of the gradient, above 10% solution, and centrifuged. The sample was spun using a SW41 Ti Rotor (Beckman Coulter, Mississauga, ON, Canada) in a Beckman Coulter Optima XPN-100 ultracentrifuge (Beckman Coulter, Mississauga, ON, Canada) at 35,000 rpm (210,100 rcf) for 2.5 hours at 4°C. 1mL fractions were collected by puncturing the side of the tube. Fractions were weighed, and density calculated. Fractions were stored at 4°C prior to further analysis.

#### **4.2.5 Hemagglutination assay**

The presence of influenza VLPs was indirectly determined by the hemagglutination assay (Hirst, 1942). Briefly, 50 µL of PBS was added to each well of a round bottom 96-well plate, 50 µL of sample was added to the first well. Following mixing, serial dilutions were done by adding 50 µL of the previous dilution to produce a row of wells sequentially diluted. 50 µL of 50% chicken red blood cells (Rockland Immunochemicals Inc. Limerick, PA, USA) in PBS was mixed with each dilution. The suspension was allowed to sit at room temperature for 2 hours before reading the results. To have hemagglutination the suspension should lack aggregation of red blood cells at the bottom of the well. The result of the experiment was noted as the number of hemagglutination units (HAU)/50 µL, being the reciprocal of the highest dilution in which complete hemagglutination activity was present. In order to have HAU/mL the result was multiplied by 20. Hemagglutination units were calculated as detailed in **Appendix D**.

#### **4.2.6 Baculovirus quantification using flow cytometry**

The protocol used was adopted from Shen, et al. (2002). Briefly, serial dilutions of viral samples were prepared ranging from  $10^{-1}$  to  $10^{-4}$ . The samples were fixed with a 2% paraformaldehyde solution for 1h at 4 °C, to obtain a final concentration of 0.02%. The fixed samples were then submitted to a freeze-thaw cycle by incubating the samples for 30 min at -80 °C. The samples were permeabilized for 5 min with a solution of 10% Triton X-100 diluted in PBS (final concentration of 0.1 % (v/v) was reached). After permeabilization, the samples were stained with a diluted solution ( $5 \times 10^{-3}$ ) of the commercial SYBR® Green I Nucleic Acid Gel Stain 10000x (Thermo Fisher, Mississauga, ON, Canada). The stained samples were transferred to a 20-well VWR® Digital Dry Block Heater (VWR International, Mississauga, ON, Canada) and incubated in the dark for 10 min at 80 °C. After the incubation, the samples were ice-cooled and transferred to 5mL polystyrene tube (Bioscience Technology, Mississauga, ON, Canada) for flow cytometry analysis.

Quantification of baculovirus was done with a BD FACSCalibur flow cytometer equipped with a 15 mW argon-ion laser emitting at 488 nm. Green fluorescence of baculovirus particles was detected using a 530nm band-pass filter. The discriminator was set on the green fluorescence (FL1), and the voltage of photomultiplier was adjusted to discriminate between the green fluorescence of viral particles and background. Settings and equations can be found in **Appendix E**. Each sample was analyzed three times for 30 seconds at medium flow rate (35µL/min). Data were stored and further processed using FlowJo® software (Treestar Inc., Ashland, OR, United States). Calibration was done using 3 µm (nominal diameter) polystyrene fluorospheres Flow-Set™ (Beckman Coulter, Mississauga, ON, Canada) with a nominal concentration of  $1 \times 10^6$  fluorospheres/mL.

#### **4.2.7 Transmission electron microscopy (TEM)**

Electron microscopy was conducted using a Philip CM10 transmission electron microscope (TEM). 5 µL of sample was placed onto a sheet of parafilm and a 200 mesh formvar-carbon-coated copper grid (Ted Pella Inc, Redding, CA, USA) was placed upside down onto the sample drop for 20 minutes. Excess of fluid was removed with filter paper, and the grid was placed into a drop of 2% paraformaldehyde in PBS buffer for 5 minutes. The

sample was rinsed twice with dH<sub>2</sub>O. The excess fluid was wicked away with filter paper. For the staining process, the grid was placed into a drop of 1% aqueous phosphotungstic acid (PTA) pH balanced to pH 7.3 using NaOH solution. After 30 seconds, the sample was removed from the drop, and PTA was wicked away with filter paper. The sample was dried overnight prior to TEM imaging

### 4.3 Results

The main goal of downstream processing is to concentrate and purify a desired product. The chosen procedures are critical to obtain maximal yield and to remove impurities present in the starting material. Supernatants recovered from the infections performed in the previous chapter were submitted to the purification process shown in **Figure 14**. After influenza VLP generation, the samples were clarified by centrifugation and filtration using a 0.2 µm polyethersulfone (PES) filter. Sample concentration was performed by a two-step process. First, clarified samples were concentrated by TFF using a 10 kDa cut-off. Further sample concentration was achieved by a 20% sucrose cushion ultracentrifugation. To evaluate each step of the process, HA activity and baculovirus quantitation was used. Moreover, supernatant from a culture infected with a baculovirus carrying native M1, NA and HA genes was also purified using the same procedures to evaluate difference in VLPs, baculovirus concentrations and yields.

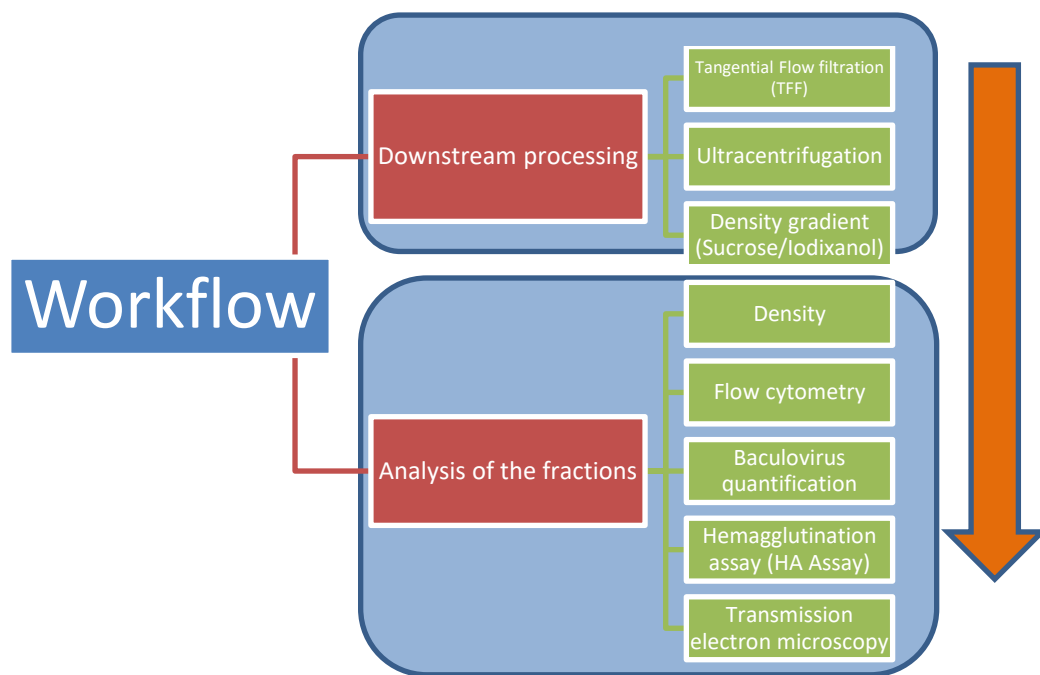


**Figure 14.** Influenza VLPs downstream processing and characterization.

**Figure 15** shows baculovirus concentration and HA activity during downstream processing. Baculovirus was detected during all the stages for all the samples, whereas, HA activity was not detected during the early purification processes for some of the fluorescent constructs. For HA activity, the 3' DsRed2 construct was the only one that was detected throughout the purification process. Moreover, 3' and 5' mKate2 variants were detected after TFF concentration, and, lastly, M mKate2 was detected after sucrose cushion concentration. The need for sample concentration was probably due to the low VLP production caused by the fluorescent partners interfering in the assembly process. **Table 6** shows the yield for each purification step for baculovirus and VLPs based on HA activity. Baculovirus purification yields for TFF fluctuated from 25 to 50 % among the samples. 5' mKate2 had the highest yield. A range from 8 to 20% was obtained after 20% sucrose cushion purification step for baculovirus. In contrast, HA yields were only calculated for 3' DsRed2 and the non-fluorescent variant since only these samples were above the detection limit in the entire process. The non-fluorescent variant obtained higher HA yields compared with 3' DsRed2.

**Table 6.** HA activity and baculovirus yields. Samples from different purification stages were tested for HA activity and baculovirus. The yields were calculated using the clarified supernatant as a 100 % recovery

% Yield HA					
Purification Step	3' DsRed2	3' mKate2	5' mKate2	M mKate2	Non-fluorescent
Clarification	100	100	100	100	100
Tangential Flow Filtration	24	-	-	-	48
Sucrose cushion	16	-	-	-	24
% Yield Baculovirus					
Purification Step	3' DsRed2	3' mKate2	5' mKate2	M mKate2	Non-fluorescent
Clarification	100.00	100.00	100.00	100.00	100.00
Tangential Flow Filtration	24.90	39.04	49.05	45.88	40.49
Sucrose cushion	11.11	14.31	14.55	7.82	19.55

-Yields were not possible to calculate since HA concentration was below detection limits

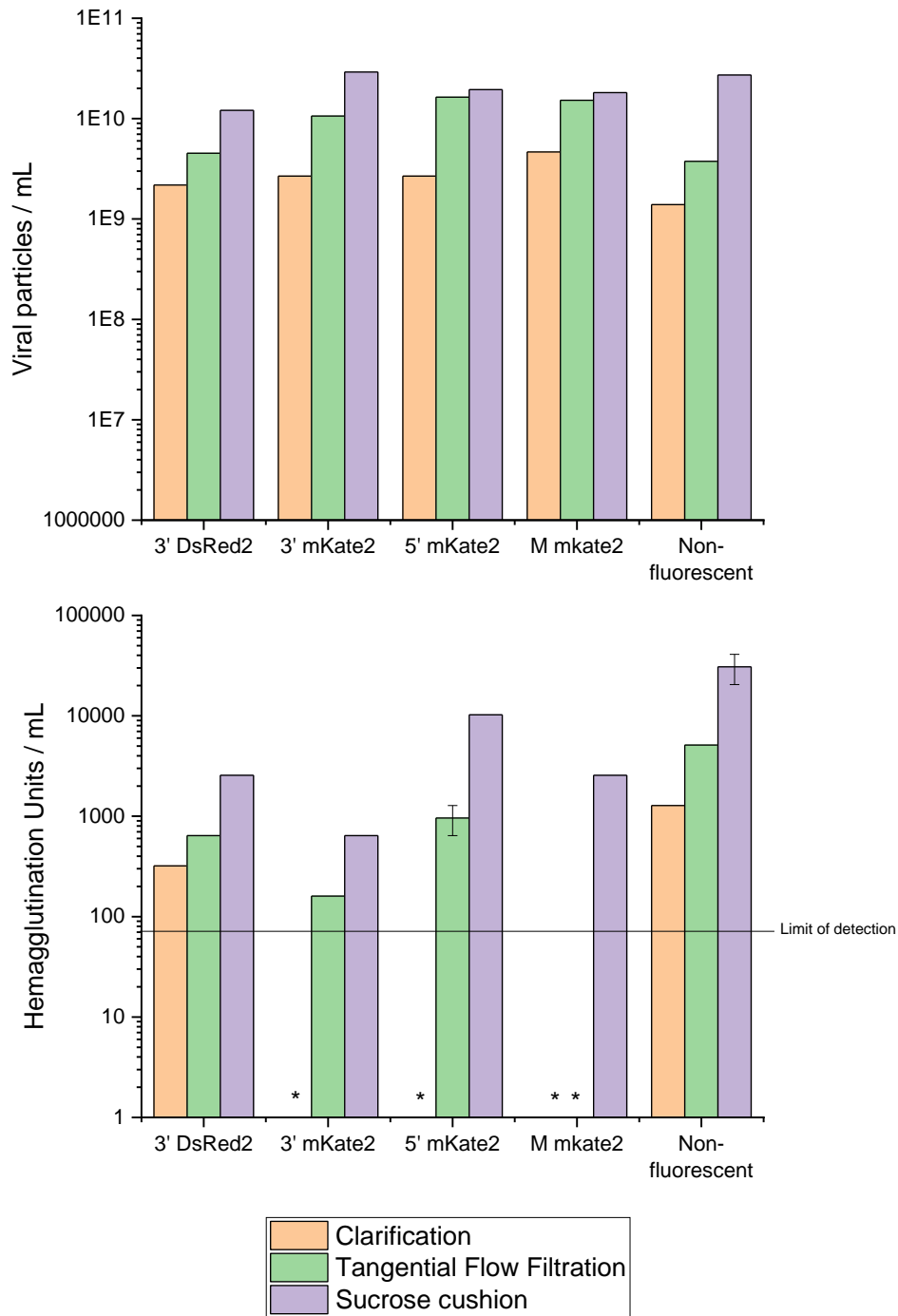


**Figure 15.** HA activity and baculovirus concentration during VLP purification. Samples from different purification stages were tested for the presence of 1) baculovirus using a genome staining procedure, and 2) hemagglutination via HA assay. \*Samples below detection limit of the experiment (80 HAU/mL)

#### 4.3.1 Purification of influenza VLPs by density gradient: sucrose and iodixanol.

Two density gradients were evaluated to purify influenza VLPs. Iodixanol is an iso-osmotic medium capable of self-generated gradients that has been reported to have little to no effect on biological samples (Ford, Graham, & Rickwood, 1994). Iodixanol has been recently used to purify adeno-associated virus (AAV) reducing processing time when compared to CsCl gradients (Strobel, Miller, Rist, & Lamla, 2015). Moreover, iodixanol has been used to purify influenza VLPs produced by insect cells (Thompson et al., 2015). On the other hand, a sucrose density gradient is a hyperosmotic environment and is a traditional technique to purify influenza VLPs (Krammer et al., 2010). To test the capacities of each gradient, a non-fluorescent VLP was used to track the migration pattern of influenza VLPs and baculovirus on each gradient. The results are shown in **Figure 16**. The two gradients showed a different migration pattern for HA activity and baculovirus. For the sucrose gradient, HA activity and baculovirus were detected from fraction 4 to 12, the highest peak for both was detected at fraction 9. Conversely, the iodixanol gradient displayed a different migration pattern, having higher concentrations in earlier samples. HA activity was detected from fractions 2 to 9, having higher concentrations in fractions 4 and 5 with equal levels. Baculovirus was found from fractions 1 to 9, and in fraction 12. Baculovirus was not detected for fractions 10 and 11. The highest baculovirus peak was detected in fraction 4. Furthermore, the density values where the HA activity and baculovirus were detected differs between the gradients. For the sucrose gradient, the density of the samples where HA and baculovirus were detected showed values from 1.09 to 1.24 mg/mL, the peak being at 1.17 mg/mL. In contrast, iodixanol fractions containing HA activity possess a density from 1.01 to 1.20 mg/mL, with higher concentrations gathering at 1.06 to 1.09 mg/mL. Baculovirus was found in densities of 0.99 to 1.20 mg/mL, and at 1.27 mg/mL. The highest concentration of baculovirus was detected at 1.06 mg/mL. These results demonstrate that density gradients do not possess the resolution capacity to properly purify VLPs and baculovirus.

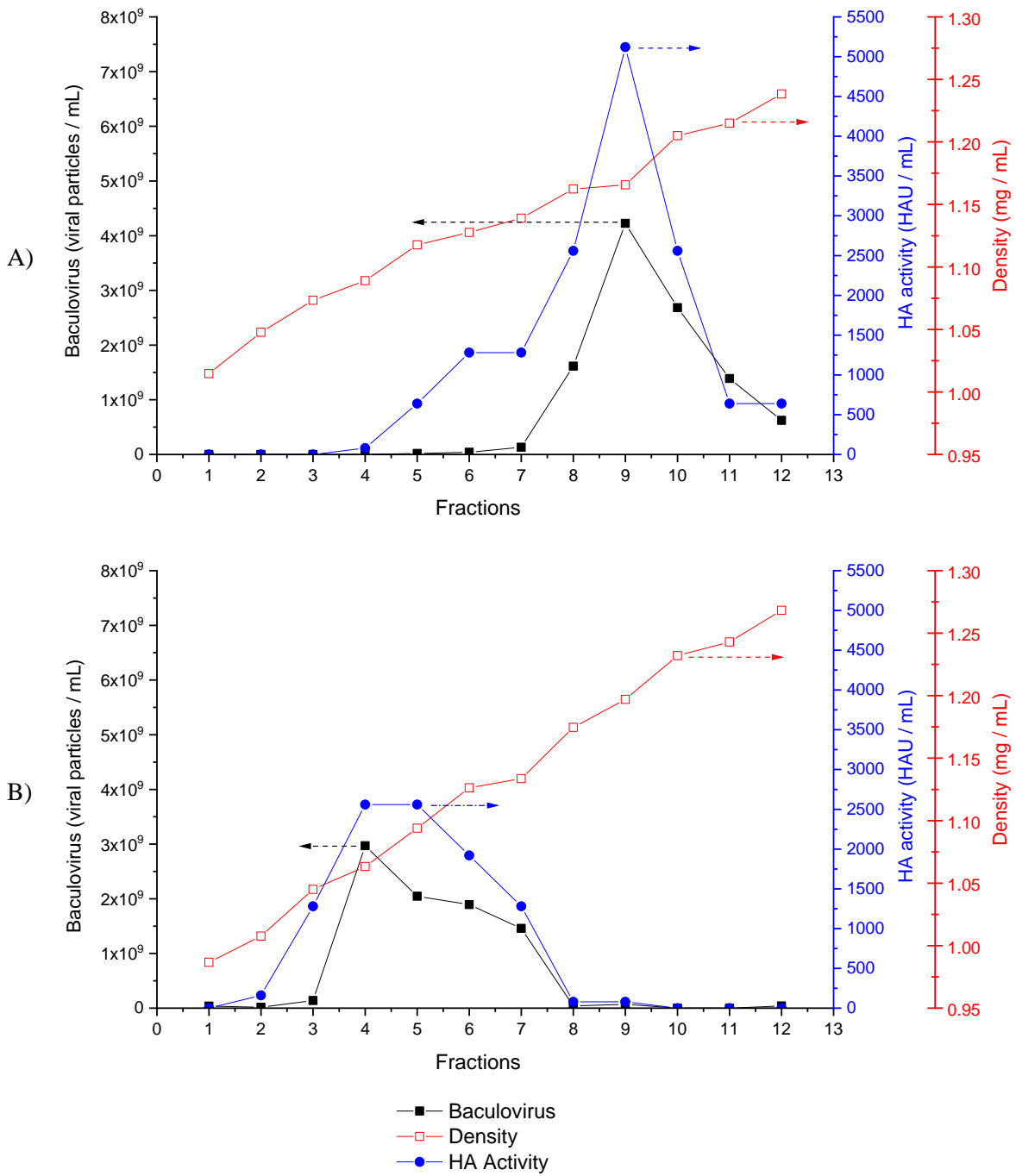


**Figure 16** Purification profiles of density gradients. A concentrated sample of influenza VLPs was split and centrifuged in different density gradients. Profile migration pattern for A) sucrose gradient and B) iodixanol gradient

#### 4.3.2 Purification of fluorescent VLPs: sucrose density gradient

Purification of fluorescent influenza VLPs was performed via sucrose density gradient. Fractions of 1 mL were collected and analyzed for HA activity, baculovirus and through TEM imaging. **Figure 17** show the different migration profiles obtained from each sample. Moreover, **Table 7** shows detailed information of the profiles acquired. The results show lower HA activity levels for “fluorescent” VLP fractions when compared to non-fluorescent VLP values. Overall, the non-fluorescent VLP construct had an HA activity 16 to 36 times higher compared with the fluorescent constructs. Conversely, baculovirus concentrations were similar for all the samples in the highest peak (**Table 7**). Profile HA activity and baculovirus distribution, based on fraction density was also analyzed. Density migration patterns presented in **Table 7** exhibit similar density ranges for HA and baculovirus for all the samples. Furthermore, higher concentration of HA activity was found at the same fraction, or close to the fraction containing higher baculovirus concentrations. It is still debatable if the changes in density values are due to new properties of the fluorescent influenza particles or due to sampling variability.

**Table 7.** Purification comparison among fluorescent variants. Concentrated samples of fluorescent influenza VLP variants were purified via sucrose density gradient. The results can be shown below.

<b>HA activity</b>			
<b>Sample</b>	<b>Density range/ highest peak (mg/mL)</b>	<b>Highest peak (Fraction)</b>	<b>HA activity (HAU/mL)</b>
<b>3' DsRed2</b>	(1.18 - 1.21) 1.21	9	160
<b>3' mKate2</b>	(1.16 - 1.18) 1.18	9	160
<b>5' mKate2</b>	(1.13 - 1.18) 1.15-1.18	9	320
<b>M mKate2</b>	(1.19) 1.19	9	160
<b>Non-fluorescent VLP</b>	(1.09 - 1.24) 1.17	9	5120
<b>Baculovirus</b>			
<b>Sample</b>	<b>Density range/ highest peak (mg/mL)</b>	<b>Highest peak (Fraction)</b>	<b>Viral particles at highest peak (viral particles/mL)</b>
<b>3' DsRed2</b>	(1.15- 1.20) 1.18	8	2.00E+09
<b>3' mKate2</b>	(1.02 - 1.05/1.12 - 1.18) 1.16	8	7.56E+09
<b>5' mKate2</b>	(1.00 – 1.23) 1.18	9	3.78E+09
<b>M mKate2</b>	(1.02 – 1.23) 1.19	9	1.25E+09
<b>Non-fluorescent VLP</b>	(1.12-1.24) 1.17	9	4.23E+09

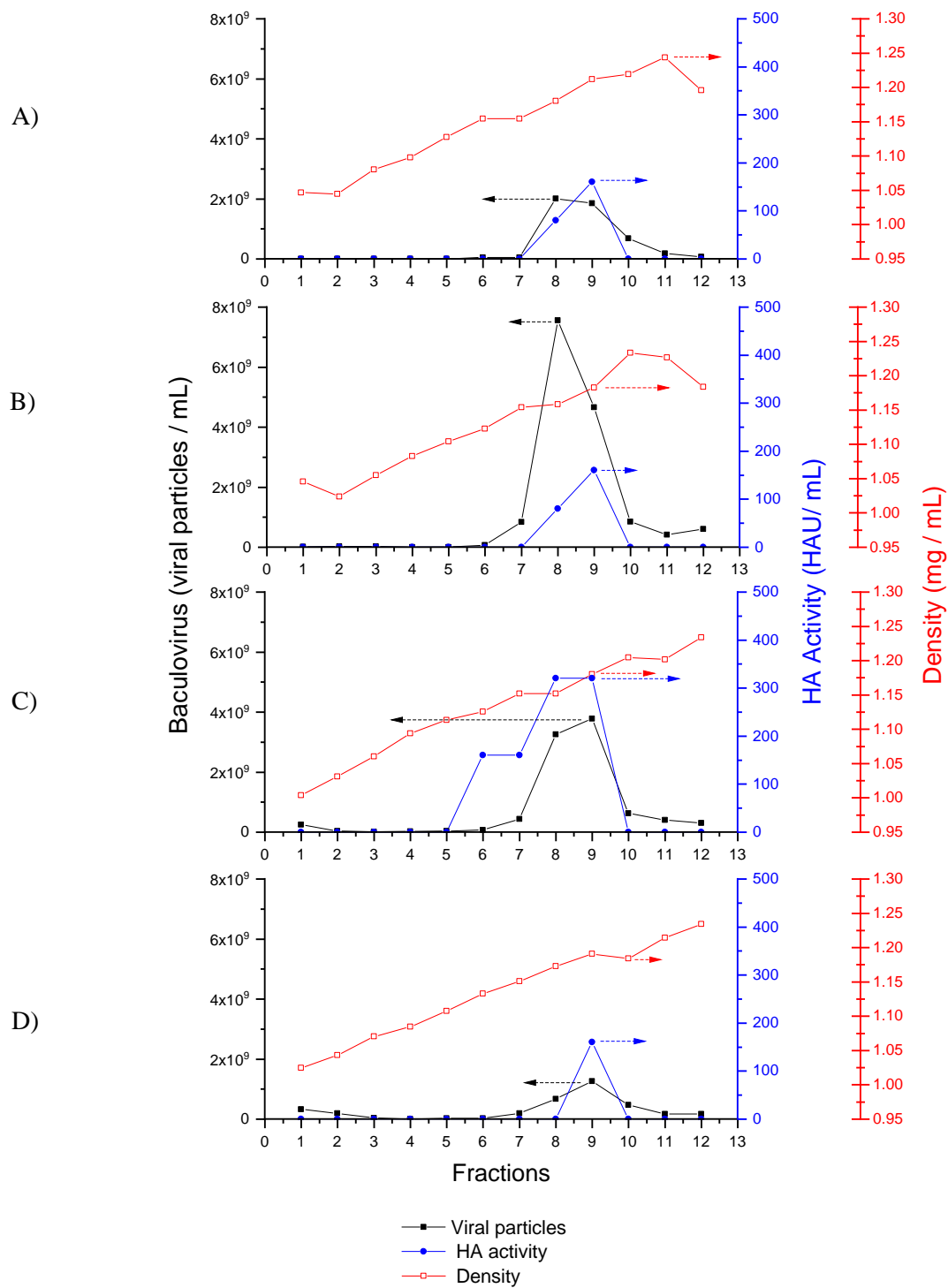


**Figure 17** Purified migration profiles of sucrose density gradients. Migration profile for A)3' DsRed2, B)3' mKate2, C) 5' mKate2 and D) M mKate2

### 4.3.3 Viral particle visualization

To obtain visual confirmation of viral particles, TEM imaging was performed on purified samples. For each genetic variant, the fraction with the highest HA activity was used for TEM imaging. **Figure 18** shows images of the purified fractions after sucrose gradient. Baculovirus was detected in all the purified samples imaged. Influenza VLPs were only observed on the non-fluorescent variant (**Figure 18 E**). These results are in accordance with our other findings and confirm the low presence of “fluorescent” influenza VLPs. Furthermore, lack of visual confirmation could also indicate absence of VLP particles. It is possible that the genetic modifications performed to influenza genes disrupt the VLP assembly process.

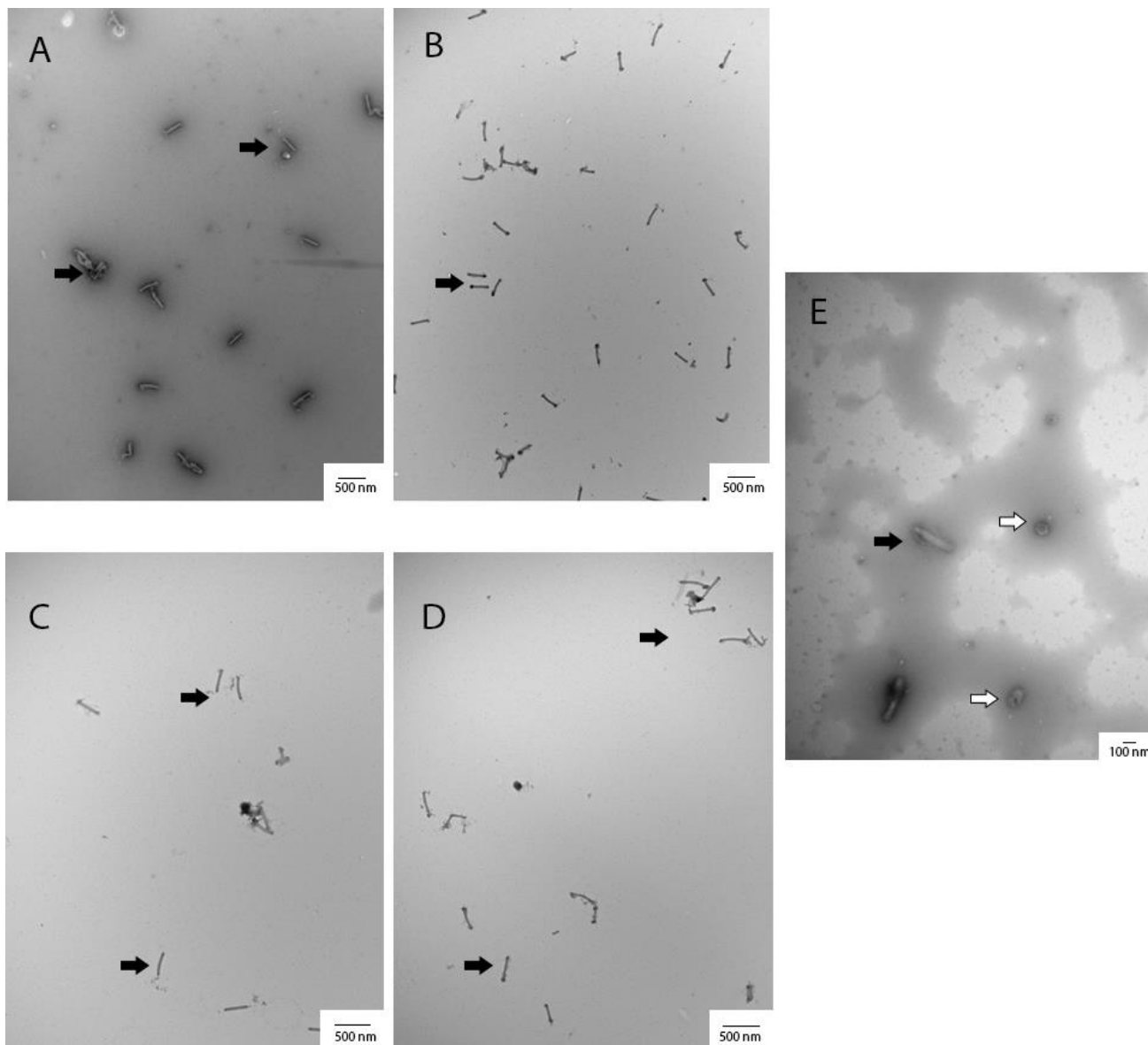


**Figure 18.** TEM imaging of purified samples. A) 3' DsRed2 fraction 8. B) 3' mKate2 fraction 8. C) M mKate2 fraction 9. D) 5' mKate2 fraction 9 and E) non-fluorescent fraction 9. Black arrows point at baculovirus, white arrows point at influenza VLPs

## 4.4 Discussion

### 4.4.1 Downstream processing of fluorescent influenza particles

In this chapter, isolation of influenza like particles derived from influenza-fusion proteins was attempted. A series of downstream processing steps were performed and samples along the way were analyzed to estimate process yields for influenza VLPs and baculovirus. The results gathered during concentration steps indicated lower HA concentrations for fluorescent variants, while preserving comparable baculovirus concentration when compared to non-fluorescent constructs (**Figure 15**). A decrease in HA concentration could be caused by the fusion of the fluorescent partner on the influenza genes, either HA or M1. In the past it has been shown that adding eGFP at the C terminus of the HA0 proteins sequence of H5 does not disrupt VLP formation when expressed in *Nicotiana benthamiana* (Young et al., 2015). Nevertheless, there is a lack of information related to the effects of designing M1 fusions. It is known that M1 mutations are able to cause morphological changes (Burleigh, Calder, Skehel, & Steinhauer, 2005; Elleman & Barclay, 2004), but no reports have been made related to M1 fusions on either 3'- or 5'- terminus, and how these changes could affect viral assembly. Since M1 is the most abundant protein in the influenza virus, it is believed that M1 fusions may cause low VLP formation by partially disrupting the viral assembly process.

### 4.4.2 Difference on density gradients

The use of density gradients to purify influenza virions has been a technique used for the past century, and it has proven the capacity to isolate influenza particles from complex samples such as allantoic fluid from eggs. In addition, different density gradients have been used to isolate influenza particles such as cesium chloride (Barry, 1960) as well as sucrose (Sengbusch, 1971). In this work sucrose and iodixanol density gradients were compared as a purification step for influenza VLPs. **Figure 16** shows a different migration pattern for each gradient, resulting in purification at different density values. Difference in density band for influenza virus has been previously documented when different reagents are used to prepare the density gradient (**Table 8**). The change in density may be due to inherent properties of the gradients, sucrose being hyperosmotic, whereas, iodixanol is iso-osmotic. Moreover, slight

variability in viral density bands when using the same density gradient could be the result of different handling and recovery techniques.

**Table 8.** Comparison of density band for influenza virus in different density gradients.

Density gradient	Density band (mg/mL)	Reference
Cesium chloride	1.25	(Barry, 1960)
Sucrose	1.17 - 1.18	(Sengbusch, 1971)
Iodixanol	1.06 - 1.09	From this chapter

#### 4.4.3 Baculovirus and influenza VLPs purification

One of the main concerns when producing influenza VLPs using the BEVS is the generation of baculovirus as a side product of the platform. Due to intrinsic similarities between baculovirus and influenza, such as similar size and the composition of their lipid membrane, specialized purification steps are needed to separate these two viruses. As seen in **Figures 17** and **18**, purified fractions from density gradient containing high HA activity possess a high baculovirus content. The lack of resolution power from density gradients is a major issue when quantification of influenza particles is required. Previous studies have shown that baculovirus is able to display HA molecules on their membrane (Yang et al., 2007). This phenomenon is triggered by the enveloped nature of both viruses and may cause noise for HA quantification. Given that the HA assay is an indirect quantification of VLPs based on HA activity, high levels of baculovirus displaying HA on their surface is not desired. In order to separate baculovirus and influenza VLPs other methodologies are needed. Other purification procedures including multiple chromatographic steps have been shown in the literature (Morenweiser, 2005; Peixoto et al., 2007). Influenza VLPs in insect cells have been purified by ion exchange chromatography (IEX) and size-exclusion chromatography (SEC) (Carvalho et al., 2016). It has been shown that IEX is able to reduce baculovirus content in an influenza VLP sample (GE Healthcare Life Sciences, 2011).

#### **4.4.4 Conclusions**

In this chapter a proposed downstream process to purify fluorescent influenza VLPs was studied. Bioprocessing characterization of 4 fluorescent influenza VLPs is shown. Each purification step of the process was evaluated by quantifying HA activity and baculovirus presence. Furthermore, migration patterns of influenza VLPs and baculovirus particles were characterized for sucrose and iodixanol density gradient. Our results show that the aforementioned methodologies lack enough resolution to separate baculovirus and influenza VLPs. To improve the bioprocess shown in this chapter, additional chromatographic steps are recommended. The use of size exclusion and ion exchange chromatography are two procedures that have showed to reduce baculovirus contamination. Furthermore, the development of specific methods to identify the presence of VLPs are needed.

## **Chapter 5**

### **Flow cytometry analysis of purified Influenza VLPs**

#### **5.1 Chapter objective**

Flow cytometry is a technique that offers the analysis of multiple factors of single particles. It is known that the detection limit of a conventional flow cytometer is around 300-500 nm (Steen, 2004). Nevertheless, there have been studies showing the study of different nano-sized biological molecules (>100 nm) such as vesicles (Morales-Kastresana et al., 2017; van der Vlist, Nolte-'t Hoen, Stoorvogel, Arkesteijn, & Wauben, 2012) and viral particles (Brussaard, 2009; Gaudin & Barteneva, 2015). Previous studies have shown that conventional flow cytometers do not always possess enough resolution power to distinguish between noise and small particles. Moreover, it has been shown that in order to detect nano-sized biological samples additional preparation steps are needed, which may include staining the genome of a virus (Brussaard, 2009) or labeling particles with fluorescent antibodies (Hoen et al., 2012). The work presented here showcases the use of flow cytometry to try and detect nano-sized fluorescent particles. The goal was to detect fluorescent influenza virus-like particles based on their inherent properties without additional staining or fluorescent conjugations.

## 5.2 Materials and Methods

### 5.2.1 Data acquisition and processing

A BD FACSCalibur flow cytometer Pro (BD Biosciences, Mississauga, ON, Canada) equipped with a 15 mW argon-ion laser emitting at 488 nm was used to analyze the samples. Flow cytometry parameters were optimized by using NTC buffer and PBS as negative controls. A log scale was used to collect FSC, SSC, FL1 and FL3 signals with voltages set at E01,474, 750 and 628 respectively. Moreover, TetraSpeck™ Fluorescent Microspheres (Thermo Fisher, Mississauga, ON, Canada) 100 nm at a concentration of  $2 \times 10^{10}$  beads/mL, and 500 nm beads at concentration of  $1.6 \times 10^8$  beads/mL were used to determine particle distribution.

Fractions purified by sucrose density gradient were used in the analysis of the fluorescent properties (see **Chapter 4**). Samples were prepared as follows: 100  $\mu$ L of purified sample was diluted in 900  $\mu$ L NTC buffer before flow cytometry data acquisition. Each sample was run in duplicate at medium flow rate (35  $\mu$ L/min) for 30 seconds. In addition, serial dilutions of purified samples were performed. The results were acquired using CellQuest Pro (BD Biosciences, Mississauga, ON, Canada) and analyzed with FlowJo (Treestar Inc., Ashland, OR, United States) software.

## 5.3 Results

### 5.3.1 Limit of detection and particle distribution

Detection of nano-sized particles was performed by determining the limit of detection of the flow cytometer. Settings were optimized to reduce noise using NTC buffer and PBS filtered using a 0.2  $\mu\text{m}$  filter as negative controls (**Figure 19 A**). From this analysis a population was gated, *Noise* gate, which was noise detected in the SSC vs FL1 plot. The events outside the *Noise* gate were used to analyze nano-sized particles. Fluorescent beads of known size were used as reference. It was found that events corresponding to reference beads of 100 nm and 500 nm were detected outside *Noise* gate (**Figure 19 B**). Single channel analysis (**Figure 19 C**) showed an overlap between 100 nm and 500 nm beads on FSC signal. Additionally, SSC and FL1 had a better resolution power to distinguish particles of different sizes compared with FSC and FL3.

Serial dilutions of fluorescent beads were performed to detect the decrease in events and changes in FL1 signal (**Figure 20**). A decrease in counts for 500 nm beads was detected, while maintaining a constant geometric mean. This behavior is expected when analyzing single events, and coincidental events are not detected. On the other hand, dilution decreased the number of events for 100 nm in a non-linear fashion. Furthermore, a decrease in geometric mean was detected, and never reached a steady measurement. This is an indication of coincidental events. To further study coincidental events, single channel analysis of 100 nm using the FL1 channel was performed (**Figure 21 A**). The results showed that when diluting the sample, the population was moving towards the limits of detection of the equipment, moving inside the *Noise* gate. When events inside the *Noise* gate were evaluated an inverse relationship was detected when comparing events corresponding to noise and those of 100 nm beads (**Figure 21 B**).

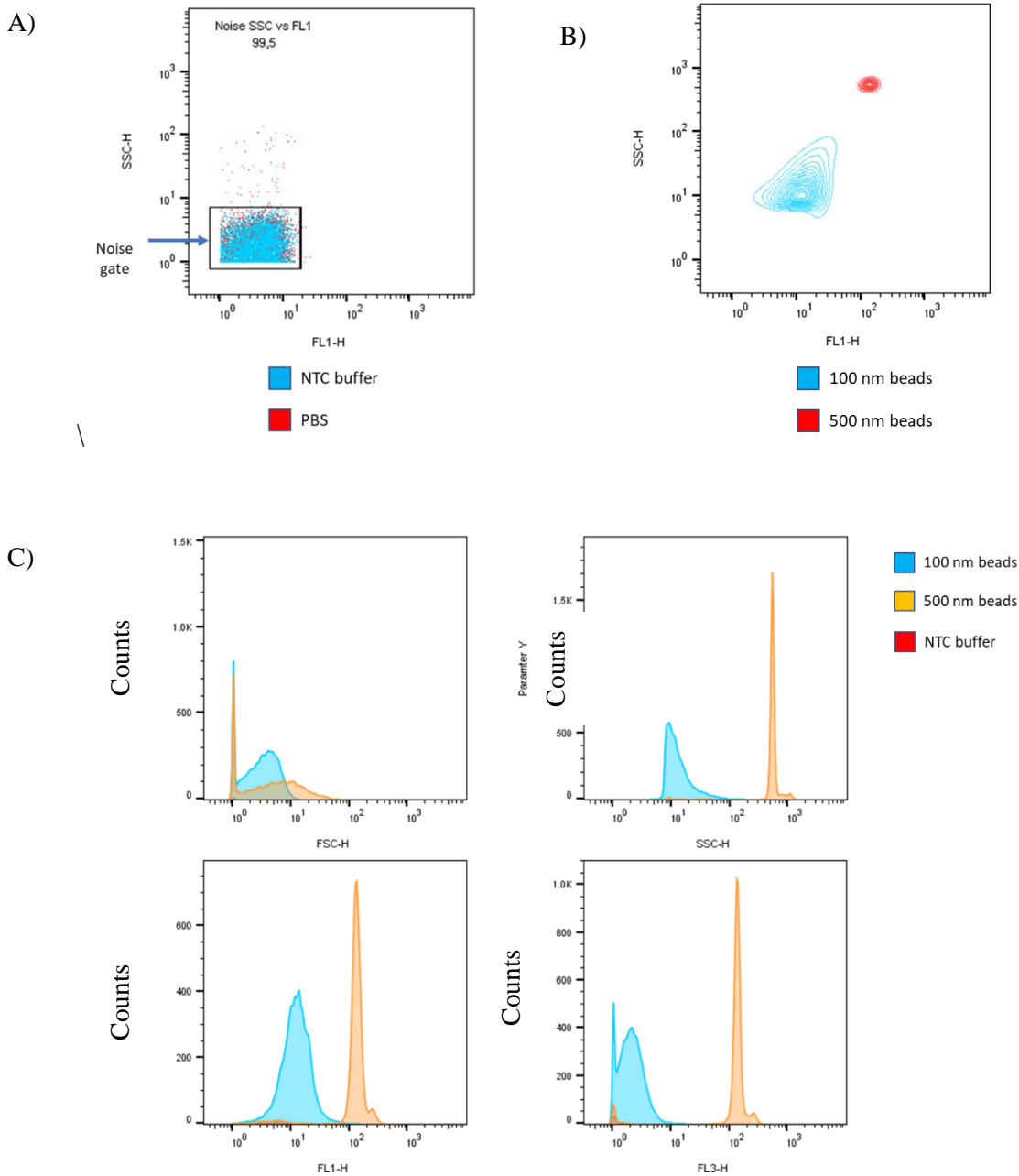


**Figure 19.** Noise detection analysis and single channel analysis of nano-sized particles. A) Noise detection analysis. NTC buffer (red events) and PBS (blue events) were used to optimized parameters and identified the *Noise gate* (noise detected in SSC vs FL1). B) SSC vs FL1 plot of nano-sized beads detected outside the *Noise gate*, countour lines represent the 5% dispersion of the data. C) Single channel analysis of nano-sized beads. The plots show the detection of events corresponding to fluorescent beads outside *Noise gate*.

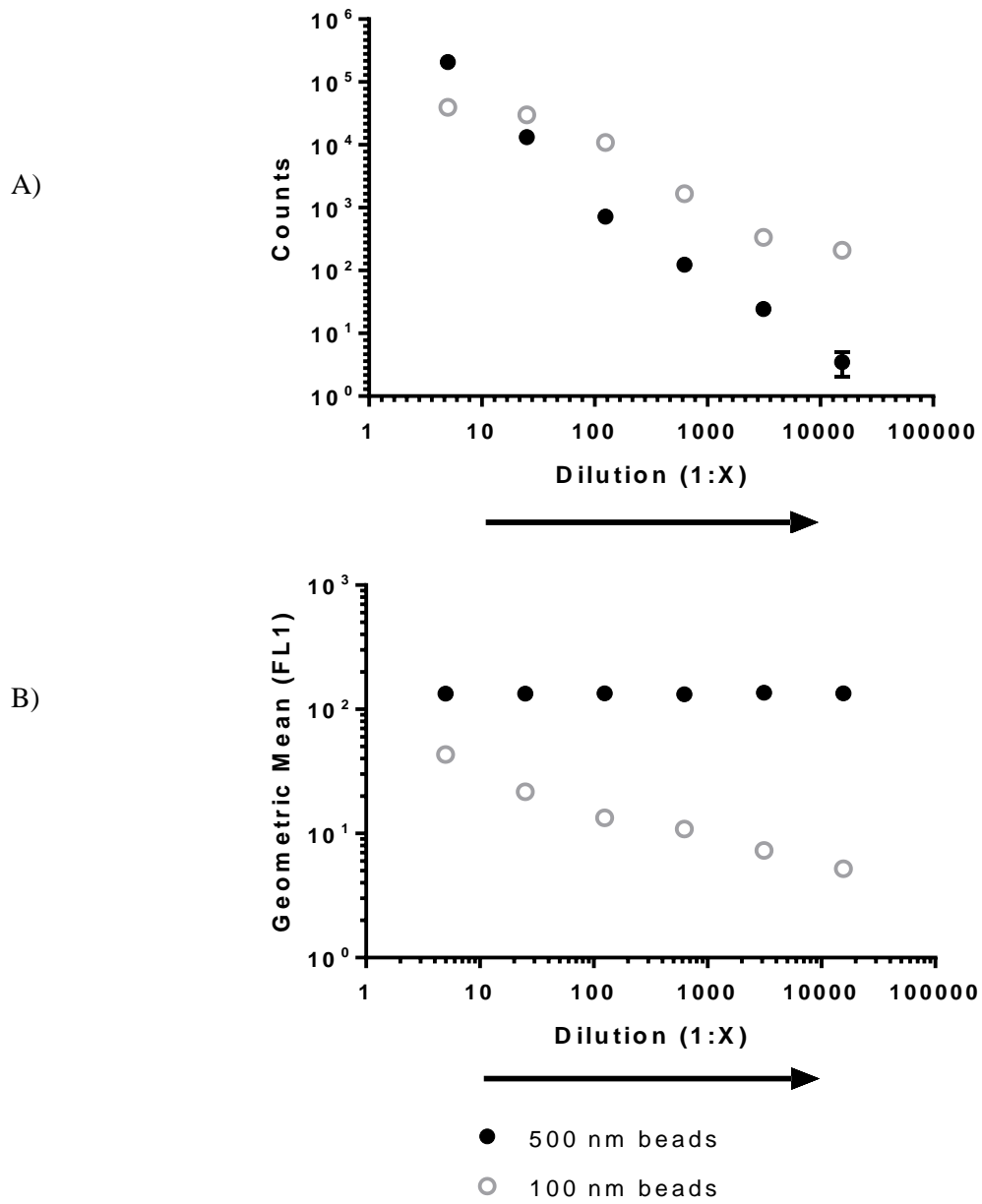


**Figure 20.** Analysis of serial dilutions for 500 and 100 nm reference beads outside *Noise* gate. A) Counts detected and B) geometric mean of serial dilutions.

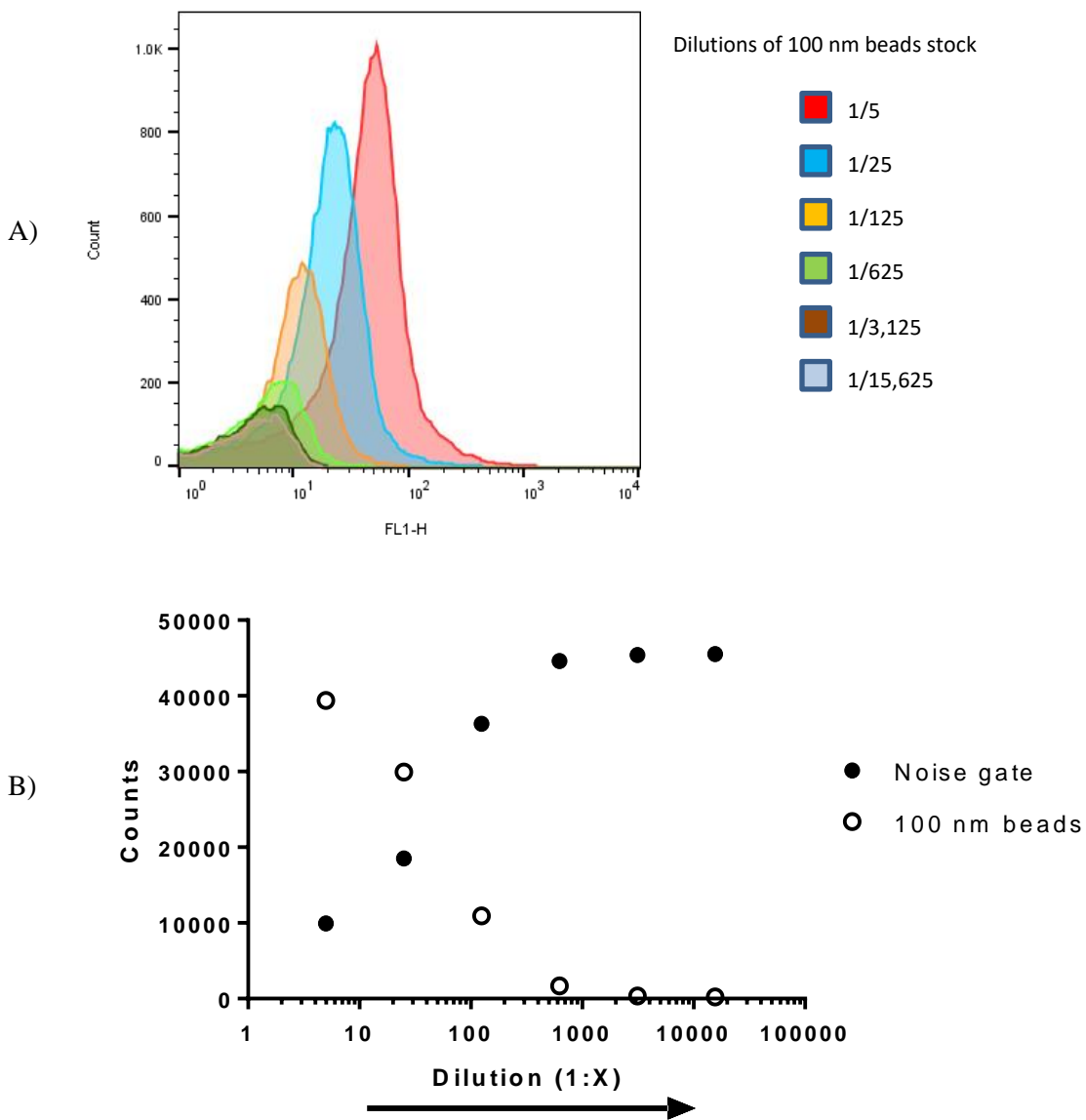


**Figure 21.** Analysis of diluted 100 nm beads. A) Single channel analysis of population corresponding to 100 nm beads outside *Noise gate*. B) Noise analysis and particle detection

Our observations showed that single particle detection was not achieved, however, with higher particle concentrations, less noise was detected. The use of this relationship was not appropriate to quantify nano-sized particle since the decrease in events could not be categorized as single events. However, this phenomenon was used as an indication to detect particle presence. The analysis of populations outside the *Noise gate* showed general features of the sample analyzed. This approach was used to further study the presence of fluorescent particles in purified VLP samples.

### 5.3.2 Purified VLP sample analysis.

Dual-fluorescent and non-fluorescent VLP samples obtained from sucrose density gradient purification were assessed by flow cytometry. **Figure 22** shows the particle distribution of purified samples outside the *Noise gate*. A new population was gated, named *Gate 1*, and used for further analysis. **Figure 23 A** shows the number of detected events inside *Gate 1* and *Noise gate* of purified fractions. An increase in events inside *Gate 1* was observed from fraction 5 to 12, with fraction 9 being the sample with the highest events detected. Similar trends were detected for all the variants, including the non-fluorescent construct. Furthermore, it was found that counts inside *Noise gate* decreased when an increase in events detected inside *Gate 1* (**Figure 23 A**). To evaluate this phenomenon, reference solutions were analyzed (**Figure 23 B**). These solutions were used during the purification process and could have an impact on particle detection. However, the results showed that reference solutions possess a reduced number of events inside *Gate 1*.

Serial dilutions were performed on fractions number 9 to study the properties of purified samples (**Figure 24**). FL1 and FL3 filter were used to study green and red fluorescence, respectively. The results showed a decrease in counts inside *Gate 1* when the samples are diluted (**Figure 24 A**). In addition, Green fluorescence signal (FL1) was used to detect the presence of HA-GFP in the samples. **Figure 24 B** shows a decrease in green signal when the samples are diluted, this trend was seen for all the fluorescent purified samples. However, the non-fluorescent VLP samples maintained a steady green signal. In addition, the presence of M1-RFP was evaluated using the red fluorescent signal (FL3). It is expected that baculovirus could possess a GFP signal, but no RFP signal, since M1 is the principal protein

involved in influenza morphology and is not needed for baculovirus replication. The results (**Figure 24 C**) showed a constant red intensity even when the samples were diluted. The same trend was observed for all the samples. Further analysis of the red signal showed that the mode of diluted samples was located at the limit of detection (**Table 4**). In addition, FL1 vs FL3 plots do not show a visual indication of differences on the red signal (**Appendix F**).

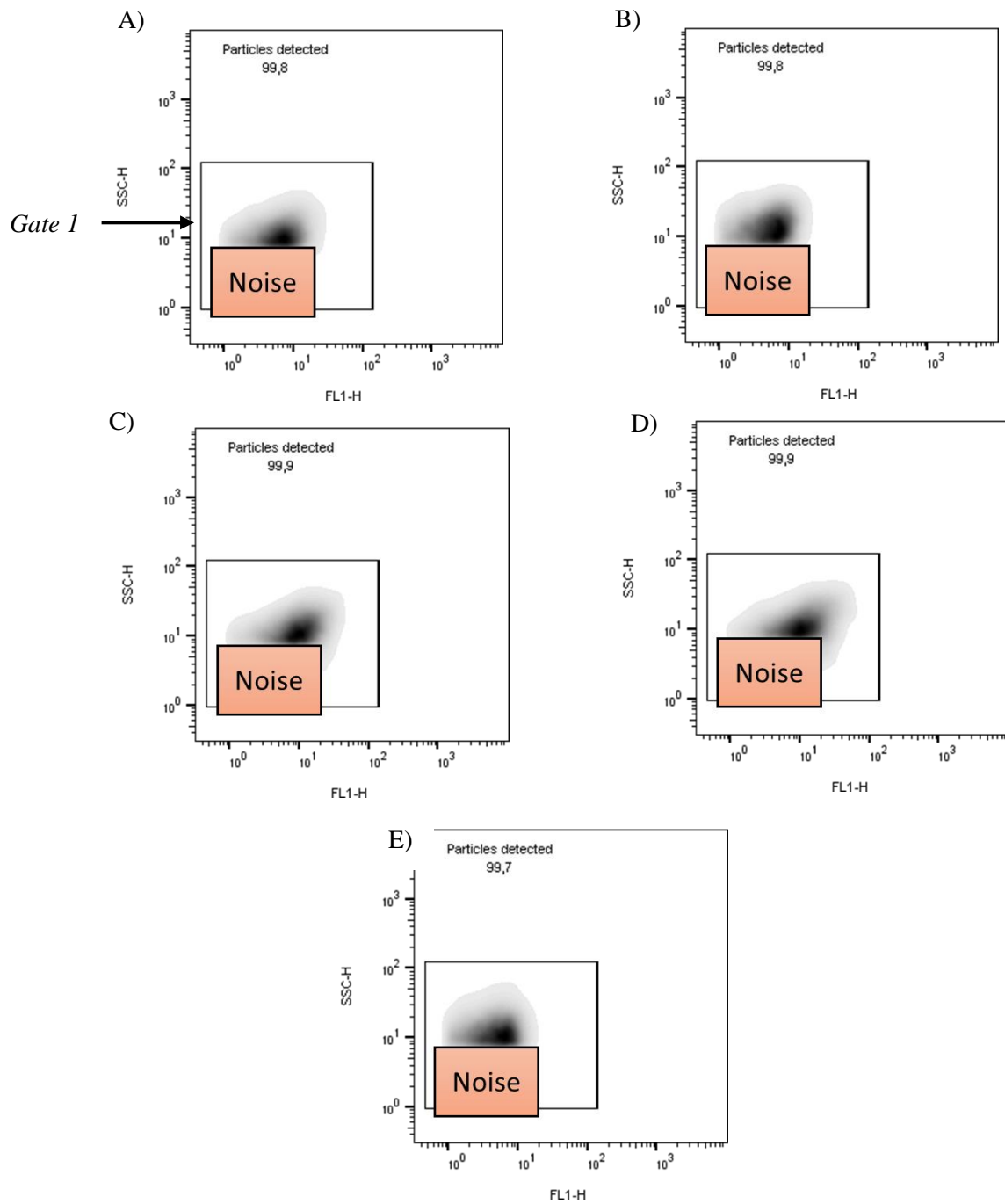
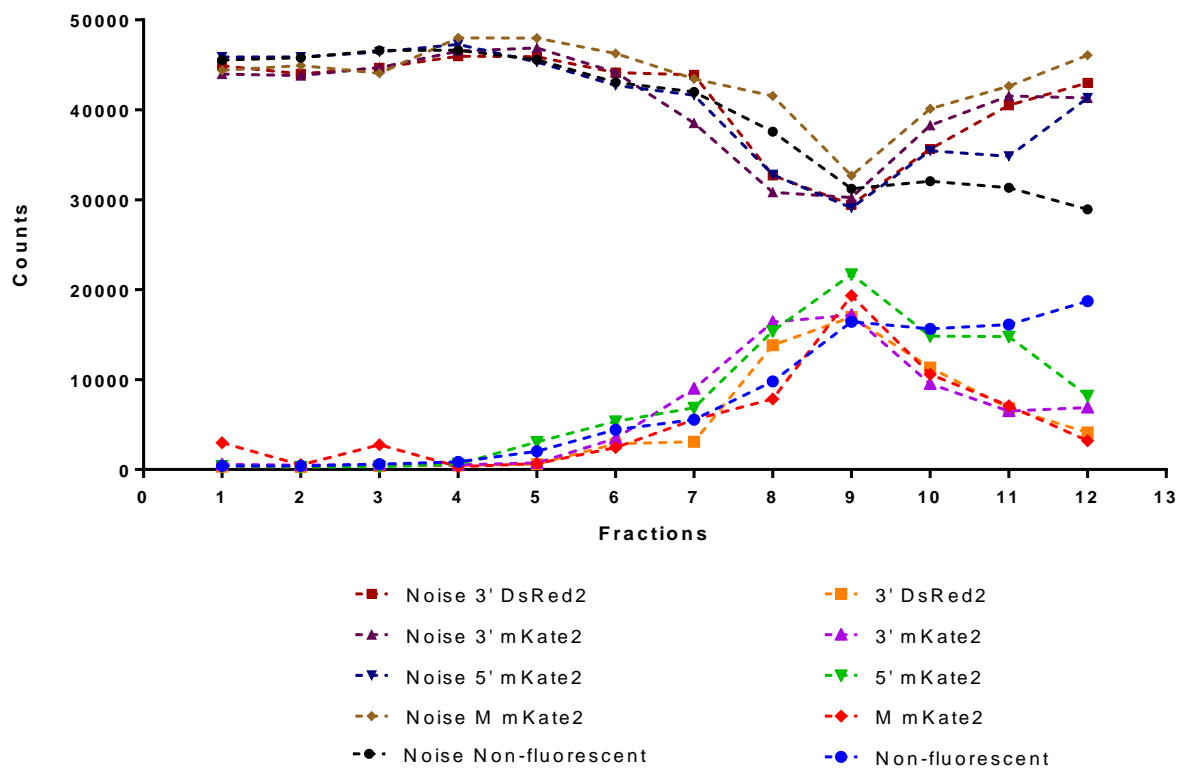


**Figure 22.** Density plots of fraction 9 of purified samples outside *Noise* gate. A) 3' DsRed2, B) 3' mKate2, C) 5' mKate2, D) M mKate2 and E) Non-fluorescent VLP.

A)



B)

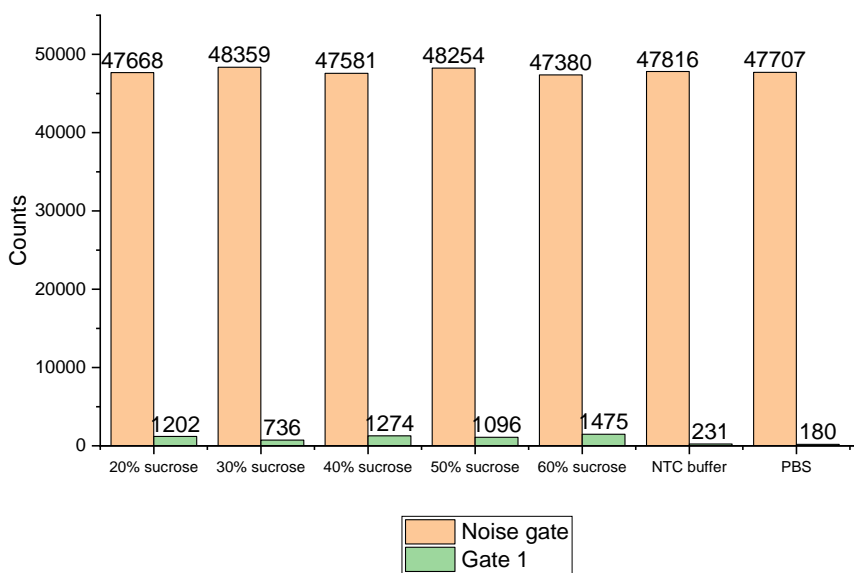


**Figure 23.** Analysis of purified fractions and reference solutions. A) Events inside *Noise* and *Gate 1* of purified samples. B) Reference solutions used during purification process.

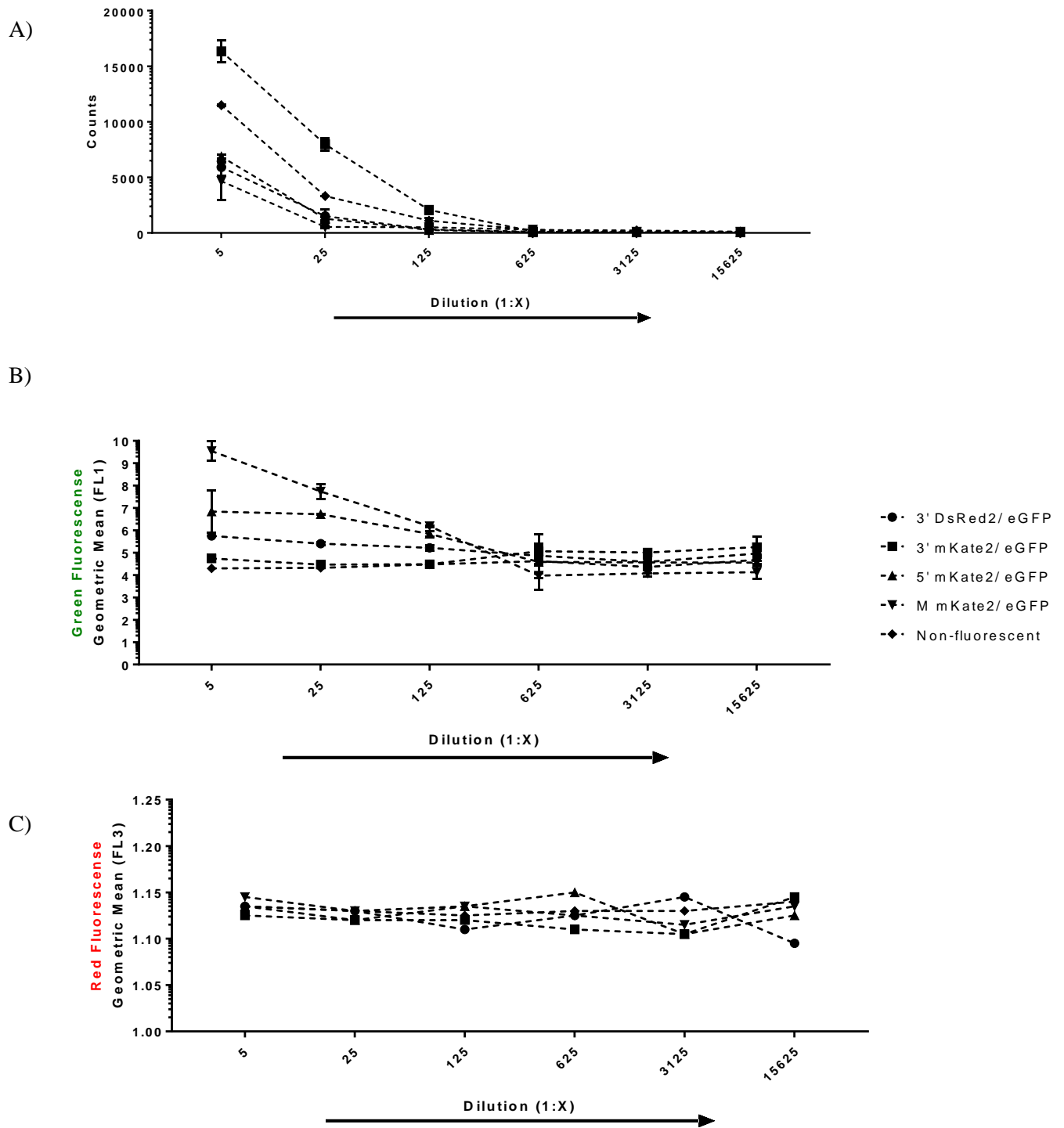


**Figure 24.** Analysis of serial dilutions of purified samples fraction9 A) Events detected, B) green geometric mean (FL1) signal, and C) red geometric mean (FL3) signal.

**Table 9.** Geometric mean and mode of red signal (FL3)

Samples	3' DsRed2	3' mKate2	5' mKate2	M mKate2	Non-fluorescent
<b>Dilution (1:X)</b>	<b>Geometric mean</b>				
5	1.14	1.13	1.14	1.15	1.14
25	1.13	1.12	1.12	1.13	1.13
125	1.11	1.12	1.14	1.14	1.13
625	1.13	1.11	1.15	1.13	1.13
3125	1.15	1.11	1.11	1.12	1.13
15625	1.10	1.15	1.13	1.14	1.14
<b>Dilution (1:X)</b>	<b>Mode</b>				
5	1.02	1.02	1.02	1.02	1.02
25	1.02	1.02	1.02	1.02	1.02
125	1.02	1.02	1.02	1.02	1.02
625	1.02	1.02	1.02	1.02	1.02
3125	1.02	1.02	1.02	1.02	1.02
15625	1.02	1.02	1.02	1.02	1.02

## 5.4 Discussion

Nanoscale detection using flow cytometry is not a trivial task since overlapping noise and particles are detected. In addition, limits of detection vary among different flow cytometers, and conventional flow cytometers lack resolution power to distinguish nanoscale populations (Bonar & Tilton, 2017). Moreover, inherent properties do not always allow appropriate particle identification due to their small size and lack of high fluorescence intensity. Generation of nanoscale biomolecules with inherent fluorescence could increase the intensity of signal detected enabling proper particle identification without further sample processing such as fluorescent labelling (van der Vlist et al., 2012).

### 5.4.1 Nanoscale particle detection.

Assessment of nano-sized particles using the FACSCalibur flow cytometer was performed using fluorescent beads of known size as controls. 500 and 100 nm beads were detected using the optimized parameters gating out signal noise (**Figure 19 B** and **C**). In our work we showed that the FSC signal of reference beads overlap, whereas SSC and FL1 allowed for better resolution of nano-sized beads (**Figure 19 C**). Similar results were found by Nolan & Stoner (2013) when 100 and 500 nm beads were used to evaluate the capacities of the BD

FACSCalibur flow cytometer. Their results showed that single channel analysis of SSC and FL2 provides better resolution when detecting small-sized particles. Serial dilutions of reference beads were used to distinguish between single events and coincidental events (**Figure 20**). It is known that high concentration of nanoscale particles causes coincidental events which can lead to poor data acquisition (Morales-Kastresana et al., 2017). Single events were detected for the 500 nm reference beads, which showed a linear decrease in number of events detected while maintaining a constant fluorescent signal. On the other hand, serial dilution of 100 nm beads exhibited a decrease in fluorescent signal, an indication of coincidental events. In addition, **Figure 21 A** shows how the single channel histogram of FL1 changed in intensity and number of counts when diluting the beads, not reaching a steady value. This behavior was an indication of fluorescent beads located inside the *Noise* gate.

#### **5.4.2 Downstream detection of VLP**

Our findings indicate that flow cytometry could be used to detect particle presence of fluorescent particles, nevertheless, there are still challenges to overcome. The first challenge is to increase the resolution to distinguish noise and nanoparticles. Our data showed that isolation of VLP particles was not achieved since two populations were expected, one for baculovirus, emitting green signal, and other for VLPs, emitting green and red signal. A possible solution could be the use of more sensitive flow cytometers equipped with a more powerful laser. Gaudin and Barteneva (2015) have shown detection of Junín virus (approximate size between 50 -300 nm) fluorescently labeled using a FACSAria II flow cytometer customized with a 488 nm, 300 mW laser. Furthermore, to properly detect VLPs and baculovirus, other modifications are needed. It has been shown that detection of small particles using the FSC channel with a different angle of scatter light is possible. The use of wide-angle (14-25 degrees) instead of conventional FSC (<15 degrees) is preferred and has proven better resolution power for nano-sized particles (Hoen et al., 2012). Hoen and collaborators (2012) have shown detection of nanosized membrane vesicles using wide-angle FSC signal in combination with fluorescent signal in a BD Influx™ flow cytometer.

Our results indicate an increase in the number of events when data processing was performed on the purified fractions (**Figure 23 A**). The increase of events corresponds to the

fractions containing HA activity and baculovirus presence, data shown in Chapter 4. The decrease in events detected inside the *Noise* gate seems to be related to higher particle concentration, as seen in **Figure 23 A**. A similar phenomena was reported by Morales-Kastresana and collaborators (2017), who showed that a reduction in noise counts is related to higher concentration of particles detected.

Additionally, serial dilutions of fractions 9 were performed to evaluate fluorescent capacities of the particles. **Figure 24** shows that a distinguishable intensity signals was detected by the green channel (FL1). However, since only one population was detected, it is still not clear if the events detected represent VLPs and /or baculovirus particles. It is uncertain if the source of green fluorescence detected are fluorescent VLPs or fluorescent HA molecules displayed on the baculovirus membrane (Yang et al., 2007). Furthermore, red fluorescent signal does not provide valuable information to distinguish populations, as seen in **Table 4**, in the system studied.

## 5.5 Conclusion

In this chapter the use of inherent fluorescence of dual-fluorescent particles in combination with flow cytometry as a tool to study purified influenza VLP samples was discussed. Particle detection was achieved by parameter optimization. Moreover, higher particles detection was obtained from samples containing higher HA concentrations and baculovirus presence. However, changes in green fluorescent signal (FL1) when samples were diluted indicated coincidental events. Furthermore, the red fluorescent signal (FL3) was low and on the limits of detection for the equipment, thus not providing any valuable information. This work provides a starting point for studying fluorescent VLP or fluorescent baculovirus.

## Chapter 6

### Conclusions

#### 6.1 Generation and tracking of fluorescent influenza proteins in insect cells

Four different recombinant baculovirus driving the expression of different genetic constructions were used to evaluate production of a dual-fluorescent VLP expression. Each genetic construct was designed to evaluate two red fluorescent protein as fusion partners of M1. DsRed2 and mKate2 were fused at the 3'-terminus of M1 and further evaluated. Our findings showed that mKate2 is able to generate a detectable red fluorescent signal after 24 hpi, whereas, DsRed2 required 48 hpi in order to be detected. In addition, DsRed2 also increased the green fluorescent signal on early infection stages since the protein undergoes a green fluorescent phase of maturation before reaching full maturation. In parallel, three different fusion sites were chosen to evaluate the effects of mKate2 fusion on M1. It was found that the 5'-terminus and 3'- terminus can be used as fusion site without disturbing RFP localized expression near the nucleus. In contrast, the fusion of mKate2 in the middle of M1 resulted in red expression all over the cell.

#### 6.2 Downstream processing of fluorescent VLPs

A laboratory-scale downstream process for fluorescent influenza VLPs was proposed and compared with a non-fluorescent influenza VLP. Samples were concentrated by TFF followed by an ultracentrifugation using a 25% sucrose cushion. Further purification was performed by density gradient. Sucrose and iodixanol density gradients were compared to purify non-fluorescent VLPs. The results show a difference between gradients with respect to where HA activity and baculovirus have their highest concentration. The highest concentration of HA activity and baculovirus was determined at 1.17 mg/mL for sucrose, whereas, for iodixanol was in a range of 1.06 to 1.09 mg/mL. Moreover, fluorescent VLP samples purified by sucrose density gradient showed similar migration patterns when compared to non-fluorescent VLPs. Based on our results, the proposed purification process does not fully purify influenza VLPs, since baculovirus is largely what is being detected.

### **6.3 Flow cytometry analysis of purified VLPs**

Flow cytometry was used to detect particles in purified samples. Parameters optimization and noise caused by the equipment was assessed using NTC buffer. Nano-sized particle detection was evaluated by running fluorescent beads of known sizes. It was found that 500 nm dilution were detected as single particle events, whereas, 100 nm dilutions present coincidental events. Moreover, purified samples were analyzed to study their fluorescent properties. Our finding showed the presence of particles with green fluorescent signal. It was found that purified samples of fluorescent constructs decreased when the samples were diluted. Moreover, non-fluorescent VLP possessed a consistent green signal

## Chapter 7

### Recommendations

The following recommendations will focus on three main problems: increase of VLP released to media, further sample purification to reduce baculovirus contamination, and enhancement of detection in flow cytometry.

The use of complementary controls to further understand the VLP assembly process are needed. A strategy will be the use of a recombinant baculovirus driving the expression of a native M1 gene. This construct could be used in co-infection experiments along with the genetic construct used in this work to further study the impact of M1 fusions on VLP assembly. Similarly, co-infections using single recombinant baculovirus carrying a single native or fluorescent influenza gene can be used to control the expression levels of each gene. Moreover, the combined expression of native M1 and fluorescently fused M1 could increase the stability of VLP formation.

To reduce baculovirus contamination, from a downstream processing point of view, additional purification steps based on differential particle features are needed. The additional processes should have enough resolution power to properly separate influenza VLPs and baculovirus. The inclusion of chromatographic steps to further purify influenza VLPs is a possible solution. It has been shown that the combination of ion exchange and size exclusion chromatography can considerably reduce baculovirus presence (Carvalho et al., 2016; GE Healthcare Life Sciences, 2011). Moreover, Opitz and collaborators (2007) have used affinity chromatography to purify influenza viruses produced in MDCK cells. Their work showed the screening of different lectins, non-immune origin proteins, as affinity ligands to target influenza viruses. Moreover, chromatographic steps are highly scalable, which is a desired feature to increase industrial production capacity if needed (Sofia et al., 2017; Vicente et al., 2011).

On the other hand, improvements in flow cytometry detection are required to fully characterize fluorescent VLP particles. One of the possible solutions could be labelling influenza VLPs and baculovirus particles with different fluorescent markers to enhance the

signal detected. As shown by Nichols and collaborators (1993) influenza virions can be labeled by binding fluorescein isothiocyanate (FITC) to the HA and NA influenza proteins. Another example is the work performed by Ilushina and collaborators (2014) where they used a lipid-based technology to label the membrane of influenza particles produced in MDCK cells. However, the purpose of labeling influenza particles has been mainly to evaluate the binding and internalization of viral particles in cell cultures, but have not been used as a quantification technique for flow cytometry

This approach has been used in the past in order to distinguish small sized populations (van der Vlist et al., 2012). Another change could be the use of a specialized flow cytometer with enhanced capacities such as a different detection angle of scattered light and/or the use of powerful laser (>40 mW). It has been shown that detection of small particles using the FSC channel is possible when a different angle for scattered light is used (Bonar & Tilton, 2017). It is known that as particle size decreases, light scatter intensity decreases in a nonlinear and angle-dependent manner (Nolan & Stoner, 2013). The use of wide angle (14-25 degrees) instead of conventional FSC (<15 degrees) is preferred and has proven better resolution power for nano-sized particles (Hoen et al., 2012). Furthermore, it has been shown that using a powerful laser (>40mW) is commonly used when small particle detection is required. Flow cytometers such as FACSAria II can be customized with a specially powerful laser (300 mW) and can be used to this end (Gaudin & Barteneva, 2015)

## References

- Abe, T., Takahashi, H., Hamazaki, H., Miyano-Kurosaki, N., Matsuura, Y., & Takaku, H. (2003). Baculovirus Induces an Innate Immune Response and Confers Protection from Lethal Influenza Virus Infection in Mice. *The Journal of Immunology*, *171*(3), 1133 LP-1139.  
<http://www.jimmunol.org/content/171/3/1133.abstract>
- Aucoin, M. G., Perrier, M., & Kamen, A. A. (2006). Production of adeno-associated viral vectors in insect cells using triple infection: Optimization of baculovirus concentration ratios. *Biotechnology and Bioengineering*, *95*(6), 1081–1092. <https://doi.org/10.1002/bit.21069>
- Bachmayer, H., Liehl, E., & Schmidt, G. (1976). Preparation and properties of a novel influenza subunit vaccine. *Postgraduate Medical Journal*, *52*(608), 360–367.  
<http://www.ncbi.nlm.nih.gov/pmc/articles/PMC2496314/>
- Baird, G. S., Zacharias, D. A., & Tsien, R. Y. (2000). Biochemistry, mutagenesis, and oligomerization of DsRed, a red fluorescent protein from coral. *Proceedings of the National Academy of Sciences*, *97*(22), 11984 LP-11989.  
<http://www.pnas.org/content/97/22/11984.abstract>
- Barry, R. D. (1960). Equilibrium sedimentation of influenza virus in caesium chloride density gradient. *Australian Journal Of Experimental Biology And Medical Science*, *38*, 499.  
<http://dx.doi.org/10.1038/icb.1960.55>
- Becker-Pauly, C., & Stöcker, W. (2011). Insect Cells for Heterologous Production of Recombinant Proteins BT - Insect Biotechnology. In A. Vilcinskas (Ed.) (pp. 197–209). Dordrecht: Springer Netherlands. [https://doi.org/10.1007/978-90-481-9641-8\\_10](https://doi.org/10.1007/978-90-481-9641-8_10)
- Bevis, B. J., & Glick, B. S. (2002). Rapidly maturing variants of the *Discosoma* red fluorescent protein (DsRed). *Nature Biotechnology*, *20*, 83+.  
<http://link.galegroup.com.proxy.lib.uwaterloo.ca/apps/doc/A190116001/AONE?u=uniwater&sid=AONE&xid=1a05b1a9>
- Bonar, M. M., & Tilton, J. C. (2017). High sensitivity detection and sorting of infectious human immunodeficiency virus (HIV-1) particles by flow virometry. *Virology*, *505*, 80–90.  
<https://doi.org/10.1016/j.virol.2017.02.016>
- Bourmakina, S. V., & García-Sastre, A. (2003). Reverse genetics studies on the filamentous

- morphology of influenza A virus. *Journal of General Virology*, 84(3), 517–527.  
<https://doi.org/10.1099/vir.0.18803-0>
- Brady, M. I., & Furminger, I. G. (1976a). A surface antigen influenza vaccine. 1. Purification of haemagglutinin and neuraminidase proteins. *The Journal of Hygiene*, 77(2), 161–172. R  
<http://www.ncbi.nlm.nih.gov/pmc/articles/PMC2129851/>
- Brady, M. I., & Furminger, I. G. (1976b). A surface antigen influenza vaccine. 2. Pyrogenicity and antigenicity. *The Journal of Hygiene*, 77(2), 173–180.  
<http://www.ncbi.nlm.nih.gov/pmc/articles/PMC2129869/>
- Bright, R. A., Carter, D. M., Daniluk, S., Toapanta, F. R., Ahmad, A., Gavrillov, V., Massare, M., Pushko, P., Mytle, N., Rower, T., Smith, G., Ross, T. M. (2007). Influenza virus-like particles elicit broader immune responses than whole virion inactivated influenza virus or recombinant hemagglutinin. *Vaccine*, 25(19), 3871–3878. <https://doi.org/10.1016/j.vaccine.2007.01.106>
- Brussaard, C. P. D. (2009). Enumeration of Bacteriophages Using Flow Cytometry BT - Bacteriophages: Methods and Protocols, Volume 1: Isolation, Characterization, and Interactions. In M. R. J. Clokie & A. M. Kropinski (Eds.) (pp. 97–111). Totowa, NJ: Humana Press.  
[https://doi.org/10.1007/978-1-60327-164-6\\_11](https://doi.org/10.1007/978-1-60327-164-6_11)
- Burleigh, L. M., Calder, L. J., Skehel, J. J., & Steinhauer, D. A. (2005). Influenza A Viruses with Mutations in the M1 Helix Six Domain Display a Wide Variety of Morphological Phenotypes. *Journal of Virology*, 79(2), 1262–1270. <http://jvi.asm.org/content/79/2/1262.abstract>
- Calder, L. J., Wasilewski, S., Berriman, J. A., & Rosenthal, P. B. (2010). Structural organization of a filamentous influenza A virus. *Proceedings of the National Academy of Sciences*, 107(23), 10685 LP-10690. <http://www.pnas.org/content/107/23/10685.abstract>
- Callewaert, P. P. J. and N. K. (2009). N-glycosylation Engineering of Biopharmaceutical Expression Systems. *Current Molecular Medicine*. <http://dx.doi.org/10.2174/156652409789105552>
- Carvalho, S. B., Freire, J. M., Moleirinho, M. G., Monteiro, F., Gaspar, D., Castanho, M. A. R. B., Carrondo, M., J., M., Alves, P., M., Bernardes, G., J., L., Peixoto, C. (2016). Bioorthogonal Strategy for Bioprocessing of Specific-Site-Functionalized Enveloped Influenza-Virus-Like Particles. *Bioconjugate Chemistry*, 27(10), 2386–2399.  
<https://doi.org/10.1021/acs.bioconjchem.6b00372>

- Chang, J.C., Lee, S. J., Kim, J. S., Wang, C.H., & Nai, Y.S. (2018). Transient Expression of Foreign Genes in Insect Cells (Sf9) for Protein Functional Assay. *JoVE*, (132), e56693. <https://doi.org/doi:10.3791/56693>
- Chen, B. J., Leser, G. P., Morita, E., & Lamb, R. A. (2007). Influenza Virus Hemagglutinin and Neuraminidase, but Not the Matrix Protein, Are Required for Assembly and Budding of Plasmid-Derived Virus-Like Particles. *Journal of Virology* , 81(13), 7111–7123. <https://doi.org/10.1128/JVI.00361-07>
- Cheung, T. K. W., & Poon, L. E. O. L. M. (2007). Biology of Influenza A Virus. *Annals of the New York Academy of Sciences*, 1102(1), 1–25. <https://doi.org/10.1196/annals.1408.001>
- Choppin, P. W., Murphy, J. S., & Tamm, I. (1960). Studies of two kinds of virus particles which comprise influenza A2 virus strains. *The Journal of Experimental Medicine*, 112(5), 945 LP-952. <http://jem.rupress.org/content/112/5/945.abstract>
- Chu, C. M., Dawson, I. M., & Elford, W. J. (2018). Filamentous forms associated with newly isolated influenza virus *The Lancet*, 253(6554), 602. [https://doi.org/10.1016/S0140-6736\(49\)91699-2](https://doi.org/10.1016/S0140-6736(49)91699-2)
- Chuang, C. K., Wong, T. H., Hwang, S. M., Chang, Y. H., Chen, G. Y., Chiu, Y. C., Huang, S. F., Hu, Y.C. (2009). Baculovirus Transduction of Mesenchymal Stem Cells: In Vitro Responses and In Vivo Immune Responses After Cell Transplantation. *Molecular Therapy: The Journal of the American Society of Gene Therapy*, 17(5), 889–896. <https://doi.org/10.1038/mt.2009.30>
- Dawood, F. S., Iuliano, A. D., Reed, C., Meltzer, M. I., Shay, D. K., Cheng, P.-Y., Bandaranayake, D., Breiman, R. F., Brooks, W. A., Buchy, P., Feikin, D. R., Fowler, K. B., Gordon, A., Hien, N. T., Horby, P., Huang, Q. S., Katz, M. A., Krishnan, A., Lal, R., Montgomery, J.,M., Mølbak, K., Pebody, R., Presanis, A. M., Razuri, H., Steens, A., Tinoco, Y. O., Wallinga, J., Yu, H., Vong, S., Bresee, J., Widdowson, M. A. (2017). Estimated global mortality associated with the first 12 months of 2009 pandemic influenza A H1N1 virus circulation: a modelling study. *The Lancet Infectious Diseases*, 12(9), 687–695. [https://doi.org/10.1016/S1473-3099\(12\)70121-4](https://doi.org/10.1016/S1473-3099(12)70121-4)
- de Wit, E., Munster, V. J., van Riel, D., Beyer, W. E. P., Rimmelzwaan, G. F., Kuiken, T., Osterhaus, A. D., Fouchier, R. A. M. (2010). Molecular Determinants of Adaptation of Highly Pathogenic Avian Influenza H7N7 Viruses to Efficient Replication in the Human Host . *Journal of Virology*, 84(3), 1597–1606. <https://doi.org/10.1128/JVI.01783-09>

- Dong, S., Wang, M., Qiu, Z., Deng, F., Vlak, J. M., Hu, Z., & Wang, H. (2010). Autographa californica Multicapsid Nucleopolyhedrovirus Efficiently Infects Sf9 Cells and Transduces Mammalian Cells via Direct Fusion with the Plasma Membrane at Low pH . *Journal of Virology*, 84(10), 5351–5359. <https://doi.org/10.1128/JVI.02517-09>
- Duxbury, A. E., Hampson, A. W., & Sievers, J. G. M. (1968). Antibody Response in Humans to Deoxycholate-Treated Influenza Virus Vaccine. *The Journal of Immunology*, 101(1), 62 LP-67. <http://www.jimmunol.org/content/101/1/62.abstract>
- Elleman, C. J., & Barclay, W. S. (2004). The M1 matrix protein controls the filamentous phenotype of influenza A virus. *Virology*, 321(1), 144–153. <https://doi.org/10.1016/j.virol.2003.12.009>
- Erbelding, E. J., Post, D. J., Stemmy, E. J., Roberts, P. C., Augustine, A. D., Ferguson, S., Paules, C. I., Graham, B. S., Fauci, A. S. (2018). A Universal Influenza Vaccine: The Strategic Plan for the National Institute of Allergy and Infectious Diseases. *The Journal of Infectious Diseases*, jiy103-jiy103. <http://dx.doi.org/10.1093/infdis/jiy103>
- Ford, T., Graham, J., & Rickwood, D. (1994). Iodixanol: A Nonionic Iso-osmotic Centrifugation Medium for the Formation of Self-Generated Gradients. *Analytical Biochemistry*, 220(2), 360–366. <https://doi.org/10.1006/abio.1994.1350>
- Gamblin, S. J., & Skehel, J. J. (2010). Influenza Hemagglutinin and Neuraminidase Membrane Glycoproteins. *The Journal of Biological Chemistry*, 285(37), 28403–28409. <https://doi.org/10.1074/jbc.R110.129809>
- Gaudin, R., & Barteneva, N. S. (2015). Sorting of small infectious virus particles by flow virometry reveals distinct infectivity profiles. *Nature Communications*, 6, 6022. <http://dx.doi.org/10.1038/ncomms7022>
- GE Healthcare Life Sciences. (2011). *Removal of DNA and baculovirus from influenza virus-like particles using Capto™ Q*. BioPharm International. <http://www.processdevelopmentforum.com/files/articles/28992441AA.pdf>
- George, S. (2016). *Use and Control of Co-Expression in the Baculovirus-Insect Cell System for the Production of Multiple Proteins and Complex Biologics*. UWSpace. <http://hdl.handle.net/10012/10660>
- George, S., & Aucoin, M. G. (2015). Characterization of Alternative Promoters to Stagger and

Control Protein Expression in the Baculovirus-Insect Cell System: From Intracellular Reporter Proteins to Fluorescent Influenza Virus-like Particles. *BMC Proceedings*, 9(9), P49.

<https://doi.org/10.1186/1753-6561-9-S9-P49>

George, S., Jauhar, A. M., Mackenzie, J., Kießlich, S., & Aucoin, M. G. (2015). Temporal characterization of protein production levels from baculovirus vectors coding for GFP and RFP genes under non-conventional promoter control. *Biotechnology and Bioengineering*, 112(9), 1822–1831. <https://doi.org/10.1002/bit.25600>

Gerdil, C. (2003). The annual production cycle for influenza vaccine. *Vaccine*, 21(16), 1776–1779. [https://doi.org/10.1016/S0264-410X\(03\)00071-9](https://doi.org/10.1016/S0264-410X(03)00071-9)

Goodpasture, E. W., Woodruff, A. M., & Buddingh, G. J. (1932). Vaccinal Infection of the Chorio-Allantoic Membrane of the Chick Embryo. *The American Journal of Pathology*, 8(3), 271–282.7. <http://www.ncbi.nlm.nih.gov/pmc/articles/PMC2062681/>

Hanh, T., Courbron, D., Hamer, M., Masoud, M., Wong, J., Taylor, K., Hatch, J., Sowers, M., Shane, E., Nathan, M., Jiang, H., Wei, Z., Higgins, J., Roh, K-H., Burd, J., Chinchilla-Olszar, D., Malou-Williams, M., Baskind, P., Smith, G. (2013). Rapid Manufacture and Release of a GMP Batch of Avian Influenza A(H7N9) Virus-Like Particle Vaccine Made Using Recombinant Baculovirus-Sf9 Insect Cell Culture Technology. *Bioprocessing Journal, Summer*, 1–10.

Hirst, G. K. (1942). The quantitative determination of influenza virus and antibodies by means of red cell agglutination. *The Journal of Experimental Medicine*, 75(1), 49–64. <http://www.ncbi.nlm.nih.gov/pmc/articles/PMC2135212/>

Hoen, E. N. M. N.-'t, van der Vlist, E. J., Aalberts, M., Mertens, H. C. H., Bosch, B. J., Bartelink, W., Mastrobattista, E. van, Gaal, E. V., Stoorvogel, W., Arkensteijn, G. J., Wauben, M. H. M. (2012). Quantitative and qualitative flow cytometric analysis of nanosized cell-derived membrane vesicles. *Nanomedicine: Nanotechnology, Biology and Medicine*, 8(5), 712–720. <https://doi.org/10.1016/j.nano.2011.09.006>

Houser, K., & Subbarao, K. (2015). Influenza Vaccines: Challenges and Solutions. *Cell Host & Microbe*, 17(3), 295–300. <https://doi.org/10.1016/j.chom.2015.02.012>

Hu, Y.-C. (2008). Baculoviral Vectors for Gene Delivery: A Review. *Current Gene Therapy*. <http://dx.doi.org/10.2174/156652308783688509>

- Ilyushina, N. A., Chernyy, E. S., Korchagina, E. Y., Gambaryan, A. S., Henry, S. M., & Bovin, N. V. (2014). Labeling of influenza viruses with synthetic fluorescent and biotin-labeled lipids. *Virologica Sinica*, 29(4), 199–210. <https://doi.org/10.1007/s12250-014-3475-1>
- Kandeel, A., Manoncourt, S., el Kareem, E. A., Ahmed, A.-N. M., El-Refaie, S., Essmat, H., Tjaden, J., de Mattos, C. C., Earhart, K. C., Marfin, A. A., El-Sayed, N. (2010). Zoonotic Transmission of Avian Influenza Virus (H5N1), Egypt, 2006–2009. *Emerging Infectious Diseases*, 16(7), 1101–1107. <https://doi.org/10.3201/eid1607.091695>
- Kenoutis, C., Efrose, R. C., Swevers, L., Lavdas, A. A., Gaitanou, M., Matsas, R., & Iatrou, K. (2006). Baculovirus-Mediated Gene Delivery into Mammalian Cells Does Not Alter Their Transcriptional and Differentiating Potential but Is Accompanied by Early Viral Gene Expression. *Journal of Virology*, 80(8), 4135–4146. <https://doi.org/10.1128/JVI.80.8.4135-4146.2006>
- Kiselev, O. I. (2010). Progress in the development of pandemic influenza vaccines and their production technologies. *Applied Biochemistry and Microbiology*, 46(9), 815–830. <https://doi.org/10.1134/S0003683810090024>
- Kistner, O., Barrett, P. N., Mundt, W., Reiter, M., Schober-Bendixen, S., & Dorner, F. (1998). Development of a mammalian cell (Vero) derived candidate influenza virus vaccine. *Vaccine*, 16(9), 960–968. [https://doi.org/10.1016/S0264-410X\(97\)00301-0](https://doi.org/10.1016/S0264-410X(97)00301-0)
- Kollewe, C., & Vilcinskas, A. (2013). Production of recombinant proteins in insect cells. *American Journal of Biochemistry and Biotechnology*, 9(3), 255–271. <https://doi.org/10.3844/ajbbsp.2013.255.271>
- Koudstaal, W., Hartgroves, L., Havenga, M., Legastelois, I., Ophorst, C., Sieuwerts, M., Zuijdgheest, D., Vogels, R., Custer, J., de Boer-Luijtz, E., de Leeuw, O., Cornelissen, L., Goudsmit, J., Barclay, W. (2009). Suitability of PER.C6® cells to generate epidemic and pandemic influenza vaccine strains by reverse genetics. *Vaccine*, 27(19), 2588–2593. <https://doi.org/10.1016/j.vaccine.2009.02.033>
- Krammer, F., & Palese, P. (2013). Influenza virus hemagglutinin stalk-based antibodies and vaccines. *Current Opinion in Virology*, 3(5), 521–530. <https://doi.org/10.1016/j.coviro.2013.07.007>
- Krammer, F., & Palese, P. (2015). Advances in the development of influenza virus vaccines. *Nat Rev*

*Drug Discov*, 14(3), 167–182. <http://dx.doi.org/10.1038/nrd4529>

- Krammer, F., Schinko, T., Palmberger, D., Tauer, C., Messner, P., & Grabherr, R. (2010). Trichoplusia ni cells (High Five™) are highly efficient for the production of influenza A virus-like particles: a comparison of two insect cell lines as production platforms for influenza vaccines. *Molecular Biotechnology*, 45(3), 226–234. <https://doi.org/10.1007/s12033-010-9268-3>
- Kukkonen, S. P., Airene, K. J., Marjomäki, V., Laitinen, O. H., Lehtolainen, P., Kankaanpää, P., Mähönen, A. J., Rätty, J. K., Nordlund, H. R., Oker-Blom, C., Kulomaa, M. S., Ylä-Herttuala, S. (2003). Baculovirus capsid display: a novel tool for transduction imaging. *Molecular Therapy*, 8(5), 853–862. <https://doi.org/10.1016/j.ymthe.2003.07.009>
- Ladd, E. C., & Jürgen, H. (2015). Next generation vaccines and vectors: Designing downstream processes for recombinant protein-based virus-like particles. *Biotechnology Journal*, 10(5), 715–727. <https://doi.org/10.1002/biot.201400392>
- Landolt, G. A., & Olsen, C. W. (2007). Up to new tricks – A review of cross-species transmission of influenza A viruses. *Animal Health Research Reviews*, 8(1), 1–21. <https://doi.org/DOI:10.1017/S1466252307001272>
- Latham, T., & Galarza, J. M. (2001). Formation of Wild-Type and Chimeric Influenza Virus-Like Particles following Simultaneous Expression of Only Four Structural Proteins. *Journal of Virology*, 75(13), 6154–6165. <https://doi.org/10.1128/JVI.75.13.6154-6165.2001>
- Le Ru, A., Jacob, D., Transfiguracion, J., Ansorge, S., Henry, O., & Kamen, A. A. (2010). Scalable production of influenza virus in HEK-293 cells for efficient vaccine manufacturing. *Vaccine*, 28(21), 3661–3671. <https://doi.org/10.1016/j.vaccine.2010.03.029>
- Licari, P., & Bailey, J. (1991). Factors influencing recombinant protein yields in an insect cell–baculovirus expression system: Multiplicity of infection and intracellular protein degradation. *Biotechnology and Bioengineering*, 37(3), 238–246. <https://doi.org/10.1002/bit.260370306>
- Lin, C.-H., & Jarvis, D. L. (2013). Utility of temporally distinct baculovirus promoters for constitutive and baculovirus-inducible transgene expression in transformed insect cells. *Journal of Biotechnology*, 165(1), 11–17. <https://doi.org/10.1016/j.jbiotec.2013.02.007>
- Makarkov, A. I., Chierzi, S., Pillet, S., Murai, K. K., Landry, N., & Ward, B. J. (2017). Plant-made virus-like particles bearing influenza hemagglutinin (HA) recapitulate early interactions of

- native influenza virions with human monocytes/macrophages. *Vaccine*, 35(35, Part B), 4629–4636. <https://doi.org/10.1016/j.vaccine.2017.07.012>
- Malenovska, H. (2013). Virus quantitation by transmission electron microscopy, TCID50, and the role of timing virus harvesting: A case study of three animal viruses. *Journal of Virological Methods*, 191(2), 136–140. <https://doi.org/10.1016/j.jviromet.2013.04.008>
- Mao, L., Yang, Y., Qiu, Y., & Yang, Y. (2012). Annual economic impacts of seasonal influenza on US counties: Spatial heterogeneity and patterns. *International Journal of Health Geographics*, 11, 16. <https://doi.org/10.1186/1476-072X-11-16>
- Margine, I., Krammer, F., Hai, R., Heaton, N. S., Tan, G. S., Andrews, S. A., Runstadler, J.A., Wilson, P. C., Albrecht, R. A., Palese, P. (2013). Hemagglutinin Stalk-Based Universal Vaccine Constructs Protect against Group 2 Influenza A Viruses. *Journal of Virology*, 87(19), 10435–10446. <https://doi.org/10.1128/JVI.01715-13>
- Margine, I., Martinez-Gil, L., Chou, Y., & Krammer, F. (2012). Residual Baculovirus in Insect Cell-Derived Influenza Virus-Like Particle Preparations Enhances Immunogenicity. *PLoS ONE*, 7(12), e51559. <https://doi.org/10.1371/journal.pone.0051559>
- Martínez-Solís, M., Gómez-Sebastián, S., Escribano, J. M., Jakubowska, A. K., & Herrero, S. (2016). A novel baculovirus-derived promoter with high activity in the baculovirus expression system. *PeerJ*, 4, e2183. <https://doi.org/10.7717/peerj.2183>
- Milian, E., & Kamen, A. A. (2015). Current and Emerging Cell Culture Manufacturing Technologies for Influenza Vaccines. *BioMed Research International*, 2015. <https://doi.org/10.1155/2015/504831>
- Morales-Kastresana, A., Telford, B., Musich, T. A., McKinnon, K., Clayborne, C., Braig, Z., Rosner, A., Demberg, T., Watson, D. C., Karpova, T. S., Freeman, G. J., DeKruyff, R., Pavlakis, G. N., Terabe, M., Robert-Guroff, M., Berzofsky, J. A., Jones, J. C. (2017). Labeling Extracellular Vesicles for Nanoscale Flow Cytometry. *Scientific Reports*, 7(1), 1878. <https://doi.org/10.1038/s41598-017-01731-2>
- Morenweiser, R. (2005). Downstream processing of viral vectors and vaccines. *Gene Therapy*, 12, S103. <http://dx.doi.org/10.1038/sj.gt.3302624>
- Nayak, D. P., & Reichl, U. (2004). Neuraminidase activity assays for monitoring MDCK cell culture

derived influenza virus. *Journal of Virological Methods*, 122(1), 9–15.

<https://doi.org/10.1016/j.jviromet.2004.07.005>

Negrete, A., Pai, A., & Shiloach, J. (2014). Use of hollow fiber tangential flow filtration for the recovery and concentration of HIV virus-like particles produced in insect cells. *Journal of Virological Methods*, 195, 240–246. <https://doi.org/10.1016/j.jviromet.2013.10.017>

Nicholls, J. M., Lai, J., & Garcia, J.-M. (2012). Investigating the Interaction Between Influenza and Sialic Acid: Making and Breaking the Link BT - Influenza Virus Sialidase - A Drug Discovery Target. In M. von Itzstein (Ed.) (pp. 31–45). Basel: Springer Basel. [https://doi.org/10.1007/978-3-7643-8927-7\\_2](https://doi.org/10.1007/978-3-7643-8927-7_2)

Nolan, J. P., & Stoner, S. A. (2013). A trigger channel threshold artifact in nanoparticle analysis. *Cytometry Part A*, 83 A(3), 301–305. <https://doi.org/10.1002/cyto.a.22255>

Opitz, L., Salaklang, J., Büttner, H., Reichl, U., & Wolff, M. W. (2007). Lectin-affinity chromatography for downstream processing of MDCK cell culture derived human influenza A viruses. *Vaccine*, 25(5), 939–947. <https://doi.org/https://doi.org/10.1016/j.vaccine.2006.08.043>

Pau, M. G., Ophorst, C., Koldijk, M. H., Schouten, G., Mehtali, M., & Uytdehaag, F. (2001). The human cell line PER.C6 provides a new manufacturing system for the production of influenza vaccines. *Vaccine*, 19(17), 2716–2721. [https://doi.org/10.1016/S0264-410X\(00\)00508-9](https://doi.org/10.1016/S0264-410X(00)00508-9)

Peixoto, C., Sousa, M. F. Q., Silva, A. C., Carrondo, M. J. T., & Alves, P. M. (2007). Downstream processing of triple layered rotavirus like particles. *Journal of Biotechnology*, 127(3), 452–461. <https://doi.org/10.1016/j.jbiotec.2006.08.002>

Petrova, V. N., & Russell, C. A. (2017). The evolution of seasonal influenza viruses. *Nature Reviews Microbiology*, 16, 47. <http://dx.doi.org/10.1038/nrmicro.2017.118>

Pfeifer, T. A. (1998). Expression of heterologous proteins in stable insect cell culture. *Current Opinion in Biotechnology*, 9(5), 518–521. [https://doi.org/10.1016/S0958-1669\(98\)80039-6](https://doi.org/10.1016/S0958-1669(98)80039-6)

Piatkevich, K. D., & Verkhusha, V. V. (2011). Chapter 17 - Guide to Red Fluorescent Proteins and Biosensors for Flow Cytometry. In Z. Darzynkiewicz, E. Holden, A. Orfao, W. Telford, & D. B. T.-M. in C. B. Wlodkovic (Eds.), *Recent Advances in Cytometry, Part A* (Vol. 102, pp. 431–461). Academic Press. <https://doi.org/10.1016/B978-0-12-374912-3.00017-1>

Pillet, S., Aubin, É., Trépanier, S., Bussière, D., Dargis, M., Poulin, J.-F., Yassine-Diab, B., Ward, B.

- J., Landry, N. (2016). A plant-derived quadrivalent virus like particle influenza vaccine induces cross-reactive antibody and T cell response in healthy adults. *Clinical Immunology*, *168*, 72–87. <https://doi.org/10.1016/j.clim.2016.03.008>
- Ping, J., Lopes, T. J. S., Nidom, C. A., Ghedin, E., Macken, C. A., Fitch, A., Imai, M., Maher, E. A., Neumann, G., Kawaoka, Y. (2015). Development of high-yield influenza A virus vaccine viruses. *Nature Communications*, *6*, 8148. <http://dx.doi.org/10.1038/ncomms9148>
- Pushko, P., Tumpey, T. M., Bu, F., Knell, J., Robinson, R., & Smith, G. (2005). Influenza virus-like particles comprised of the HA, NA, and M1 proteins of H9N2 influenza virus induce protective immune responses in BALB/c mice. *Vaccine*, *23*(50), 5751–5759. <https://doi.org/10.1016/j.vaccine.2005.07.098>
- Quan, F.-S., Kim, M.-C., Lee, B.-J., Song, J.-M., Compans, R. W., & Kang, S.-M. (2012). Influenza M1 VLPs containing neuraminidase induce heterosubtypic cross-protection. *Virology*, *430*(2), 127–135. <https://doi.org/10.1016/j.virol.2012.05.006>
- RahimiRad, S., Alizadeh, A., Alizadeh, E., & Hosseini, S. M. (2016). The avian influenza H9N2 at avian-human interface: A possible risk for the future pandemics. *Journal of Research in Medical Sciences : The Official Journal of Isfahan University of Medical Sciences*, *21*, 51. <https://doi.org/10.4103/1735-1995.187253>
- Rohrmann, G. F. (1992). Baculovirus structural proteins. *Journal of General Virology*, *73*(4), 749–761. <https://doi.org/10.1099/0022-1317-73-4-749>
- Roldão, A., Mellado, M. C. M., Castilho, L. R., Carrondo, M. J. T., & Alves, P. M. (2010). Virus-like particles in vaccine development. *Expert Review of Vaccines*, *9*(10), 1149–1176. <https://doi.org/10.1586/erv.10.115>
- Safo, M. K., Musayev, F. N., Mosier, P. D., Zhou, Q., Xie, H., & Desai, U. R. (2014). Crystal Structures of Influenza A Virus Matrix Protein M1: Variations on a Theme. *PLoS ONE*, *9*(10), e109510. <https://doi.org/10.1371/journal.pone.0109510>
- Sengbusch, P. V. (1971). Purification of influenza virus by phase separation and selective adsorption. *FEBS Letters*, *15*(1), 78–80. [https://doi.org/10.1016/0014-5793\(71\)80083-2](https://doi.org/10.1016/0014-5793(71)80083-2)
- Sequeira, D. P., Correia, R., Carrondo, M. J. T., Roldão, A., Teixeira, A. P., & Alves, P. M. (2017). Combining stable insect cell lines with baculovirus-mediated expression for multi-HA influenza

VLP production. *Vaccine*. <https://doi.org/10.1016/j.vaccine.2017.02.043>

Shcherbo, D., Murphy, C. S., Ermakova, G. V., Solovieva, E. A., Chepurnykh, T. V., Shcheglov, A. S., Pletnev, V. Z., Hazelwood, K. L., Roche, P. M., Lukyanov, S., Zaraisky, A. G., Davidson, M. W., Chudakov, D. M. (2009). Far-red fluorescent tags for protein imaging in living tissues. *The Biochemical Journal*, *418*(3), 567–574. <https://doi.org/10.1042/BJ20081949>

Shen, C. F., Meghrou, J., & Kamen, A. (2002). Quantitation of baculovirus particles by flow cytometry. *Journal of Virological Methods*, *105*(2), 321–330. [http://doi.org/10.1016/S0166-0934\(02\)00128-3](http://doi.org/10.1016/S0166-0934(02)00128-3)

Shen, X., Hacker, D. L., Baldi, L., & Wurm, F. M. (2013). Study of the improved Sf9 transient gene expression process. *BMC Proceedings*, *7*(Suppl 6), P19–P19. <https://doi.org/10.1186/1753-6561-7-S6-P19>

Short, K. R., Richard, M., Verhagen, J. H., van Riel, D., Schrauwen, E. J. A., van den Brand, J. M. A., Manz, B., Bodewes, R., Herfst, S. (2015). One health, multiple challenges: The inter-species transmission of influenza A virus. *One Health*, *1*, 1–13. <https://doi.org/10.1016/j.onehlt.2015.03.001>

Smith, F. I., & Palese, P. (1989). Variation in Influenza Virus Genes BT - The Influenza Viruses. In R. M. Krug (Ed.) (pp. 319–359). Boston, MA: Springer US. [https://doi.org/10.1007/978-1-4613-0811-9\\_7](https://doi.org/10.1007/978-1-4613-0811-9_7)

Smith, G. E., Flyer, D. C., Raghunandan, R., Liu, Y., Wei, Z., Wu, Y., Kpamegan, E., Courbron, D., Fries, L. F., Glenn, G. M. (2013). Development of influenza H7N9 virus like particle (VLP) vaccine: Homologous A/Anhui/1/2013 (H7N9) protection and heterologous A/chicken/Jalisco/CPA1/2012 (H7N3) cross-protection in vaccinated mice challenged with H7N9 virus. *Vaccine*, *31*(40), 4305–4313. <https://doi.org/10.1016/j.vaccine.2013.07.043>

Sofia, B. C., Raquel, F. A., W, W. M., Cristina, P., Paula, M. A., Udo, R., & Manuel, J. T. C. (2017). Purification of influenza virus-like particles using sulfated cellulose membrane adsorbers. *Journal of Chemical Technology & Biotechnology*, *0*(0). <https://doi.org/10.1002/jctb.5474>

Steel, J., Lowen, A. C., Wang, T. T., Yondola, M., Gao, Q., Haye, K., Garcia-Sastre, A., Palese, P. (2010). Influenza Virus Vaccine Based on the Conserved Hemagglutinin Stalk Domain. *MBio*, *1*(1). <https://doi.org/10.1128/mBio.00018-10>

- Steen, H. B. (2004). Flow cytometer for measurement of the light scattering of viral and other submicroscopic particles. *Cytometry*, *57A*(2), 94–99. <https://doi.org/10.1002/cyto.a.10115>
- Steppert, P., Burgstaller, D., Klausberger, M., Tover, A., Berger, E., & Jungbauer, A. (2017). Quantification and characterization of virus-like particles by size-exclusion chromatography and nanoparticle tracking analysis. *Journal of Chromatography A*, *1487*, 89–99. <https://doi.org/10.1016/j.chroma.2016.12.085>
- Strobel, B., Miller, F. D., Rist, W., & Lamla, T. (2015). Comparative Analysis of Cesium Chloride- and Iodixanol-Based Purification of Recombinant Adeno-Associated Viral Vectors for Preclinical Applications. *Human Gene Therapy Methods*, *26*(4), 147–157. <https://doi.org/10.1089/hgtb.2015.051>
- Subbarao, K., & Katz, J. (2000). Avian influenza viruses infecting humans. *Cellular and Molecular Life Sciences*, *57*(12), 1770–1784. <https://doi.org/10.1007/PL00000657>
- Szewczyk, B., Bieńkowska-Szewczyk, K., & Król, E. (2014). Introduction to molecular biology of influenza A viruses. *Acta Biochimica Polonica*, *61*(3), 397–401. [http://www.actabp.pl/pdf/3\\_2014/397.pdf](http://www.actabp.pl/pdf/3_2014/397.pdf)
- Thompson, C. M., Petiot, E., Lennaertz, A., Henry, O., & Kamen, A. A. (2013). Analytical technologies for influenza virus-like particle candidate vaccines: challenges and emerging approaches. *Virology Journal*, *10*(1), 141. <https://doi.org/10.1186/1743-422X-10-141>
- Thompson, C. M., Petiot, E., Mullick, A., Aucoin, M. G., Henry, O., & Kamen, A. A. (2015). Critical assessment of influenza VLP production in Sf9 and HEK293 expression systems. *BMC Biotechnology*, *15*(1), 31. <https://doi.org/10.1186/s12896-015-0152-x>
- Tong, S., Zhu, X., Li, Y., Shi, M., Zhang, J., Bourgeois, M., Yang, H., Chen, X., Recuenco, S., Gomez, J., Chen, L.-M., Johnson, A., Tao, Y., Dreyfus, C., Yu, W., McBride, R., Carney, P. J., Gibert, A. T., Chang, J., Guo, Z., Davis, C. T., Paulson, J. C., Stevens, J., Rupprecht, C. E., Holmes, E. C., Wilson, I. A., Donis, R. O. (2013). New World Bats Harbor Diverse Influenza A Viruses. *PLOS Pathogens*, *9*(10), e1003657. <https://doi.org/10.1371/journal.ppat.1003657>
- Transfiguracion, J., Manceur, A. P., Petiot, E., Thompson, C. M., & Kamen, A. A. (2015). Particle quantification of influenza viruses by high performance liquid chromatography. *Vaccine*, *33*(1), 78–84. <https://doi.org/10.1016/j.vaccine.2014.11.027>

- Ulmer, J. B., Valley, U., & Rappuoli, R. (2006). Vaccine manufacturing: challenges and solutions. *Nature Biotechnology*, *24*, 1377. <http://dx.doi.org/10.1038/nbt1261>
- van der Vlist, E. J., Nolte-'t Hoen, E. N. M., Stoorvogel, W., Arkesteijn, G. J. A., & Wauben, M. H. M. (2012). Fluorescent labeling of nano-sized vesicles released by cells and subsequent quantitative and qualitative analysis by high-resolution flow cytometry. *Nature Protocols*, *7*, 1311. <http://dx.doi.org/10.1038/nprot.2012.065>
- Van Oers, M. M., Pijlman, G. P., & Vlak, J. M. (2015). Thirty years of baculovirus-insect cell protein expression: From dark horse to mainstream technology. *Journal of General Virology*, *96*(1), 6–23. <https://doi.org/10.1099/vir.0.067108-0>
- Venereo-Sanchez, A., Gilbert, R., Simoneau, M., Caron, A., Chahal, P., Chen, W., Ansorge, S., Li, X., Henry, O., Kamen, A. (2016). Hemagglutinin and neuraminidase containing virus-like particles produced in HEK-293 suspension culture: An effective influenza vaccine candidate. *Vaccine*, *34*(29), 3371–3380. <https://doi.org/10.1016/j.vaccine.2016.04.089>
- Vicente, T., Roldão, A., Peixoto, C., Carrondo, M. J. T., & Alves, P. M. (2011). Large-scale production and purification of VLP-based vaccines. *Journal of Invertebrate Pathology*, *107*, S42–S48. <https://doi.org/10.1016/j.jip.2011.05.004>
- Volkman, L. E., & Summers, M. D. (1977). Autographa californica nuclear polyhedrosis virus: Comparative infectivity of the occluded, alkali-liberated, and nonoccluded forms. *Journal of Invertebrate Pathology*, *30*(1), 102–103. [https://doi.org/10.1016/0022-2011\(77\)90045-3](https://doi.org/10.1016/0022-2011(77)90045-3)
- Volkman, L. E., Summers, M. D., & Hsieh, C. H. (1976). Occluded and nonoccluded nuclear polyhedrosis virus grown in *Trichoplusia ni*: comparative neutralization comparative infectivity, and in vitro growth studies. *Journal of Virology*, *19*(3), 820–832. <http://jvi.asm.org/content/19/3/820.abstract>
- WHO. (2016). Influenza (Seasonal) fact sheet. <http://www.who.int/mediacentre/factsheets/fs211/en/>
- Wong, S.-S., & Webby, R. J. (2013). Traditional and New Influenza Vaccines. *Clinical Microbiology Reviews*, *26*(3), 476–492. <https://doi.org/10.1128/CMR.00097-12>
- Woodruff, A. M., & Goodpasture, E. W. (1931). The Susceptibility of the Chorio-Allantoic Membrane of Chick Embryos to Infection with the Fowl-Pox Virus. *The American Journal of Pathology*, *7*(3), 209–222.5. <http://www.ncbi.nlm.nih.gov/pmc/articles/PMC2062632/>

- Wu, C.-Y., Yeh, Y.-C., Yang, Y.-C., Chou, C., Liu, M.-T., Wu, H.-S., ... Hsiao, P.-W. (2010). Mammalian Expression of Virus-Like Particles for Advanced Mimicry of Authentic Influenza Virus. *PLOS ONE*, 5(3), e9784. <https://doi.org/10.1371/journal.pone.0009784>
- Yang, D.-G., Chung, Y.-C., Lai, Y.-K., Lai, C.-W., Liu, H.-J., & Hu, Y.-C. (2007). Avian Influenza Virus Hemagglutinin Display on Baculovirus Envelope: Cytoplasmic Domain Affects Virus Properties and Vaccine Potential. *Molecular Therapy*, 15(5), 989–996. <https://doi.org/10.1038/mt.sj.6300131>
- Yang, J.-P. (2016). Small-Scale Production of Recombinant Proteins Using the Baculovirus Expression Vector System. In D. W. Murhammer (Ed.), *Baculovirus and Insect Cell Expression Protocols* (pp. 225–239). New York, NY: Springer New York. [https://doi.org/10.1007/978-1-4939-3043-2\\_10](https://doi.org/10.1007/978-1-4939-3043-2_10)
- Youil, R., Su, Q., Toner, T. J., Szymkowiak, C., Kwan, W.-S., Rubin, B., ... DiStefano, D. (2004). Comparative study of influenza virus replication in Vero and MDCK cell lines. *Journal of Virological Methods*, 120(1), 23–31. <https://doi.org/10.1016/j.jviromet.2004.03.011>
- Young, K. R., Arthus-Cartier, G., Yam, K. K., Lavoie, P.-O., Landry, N., D'Aoust, M.-A., Vezina, L. P., Couture, M. M., Ward, B. J. (2015). Generation and characterization of a trackable plant-made influenza H5 virus-like particle (VLP) containing enhanced green fluorescent protein (eGFP). *The FASEB Journal*, 29(9), 3817–3827. <https://doi.org/10.1096/fj.15-270421>

## Appendix A

### End Point Dilution Assay (EPDA)

This technique is based on the Tissue Culture Infectious Dose 50 (TCID<sub>50</sub>). In order to calculate the titer of a baculovirus stock serial dilutions are used to infect a 96-well plate that has been previously seeded with *Sf9* cells. Then, the dilution where 50 percent of the cells are infected is determine and the following equations are used to titer the virus.

**Equation AA-1.** Proportional response calculation

$$PD = \frac{(\text{Percentage rate dilutions next greater than } 50\% - 50\%)}{(\% \text{ rate dilutions next greater than } 50\%) - (\% \text{ rate dilutions next less than } 50\%)}$$

Where PD is the proportional response

**Equation AA-2.** TCID<sub>50</sub> dose calculation

$$\text{Log}_{10}(\text{TCID}_{50}) = (\text{Log of the dilutions giving reponse greater than } 50\% - PD)$$

**Equation AA-3.** Proportional response calculation

$$\frac{pfu}{mL} = \frac{\text{TCID}_{50}}{\text{Volume of virus added}} \quad (0.69)$$

**Appendix B**  
**Single fluorescent VLP construct**

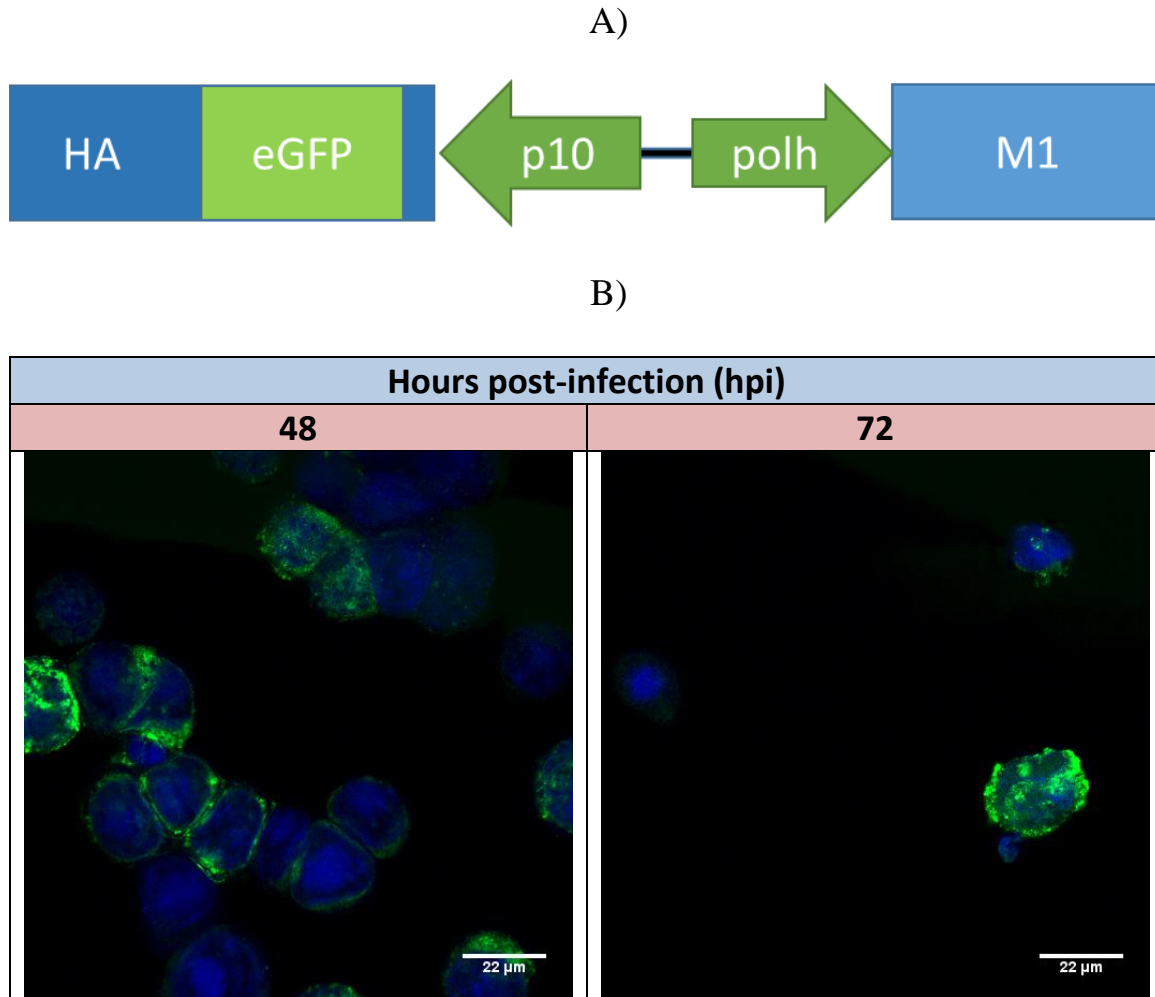


**Figure AB-1.** Single fluorescent influenza VLP construct. A) Genetic construct design of single fluorescent VLP. A 30 mL *Sf9* culture was infected with an MOI of 5. B) shows confocal microscopy images of infected *Sf9* cells at 48 and 72 hpi.

## Appendix C

### Flow cytometry analysis of uninfected Sf9 cells

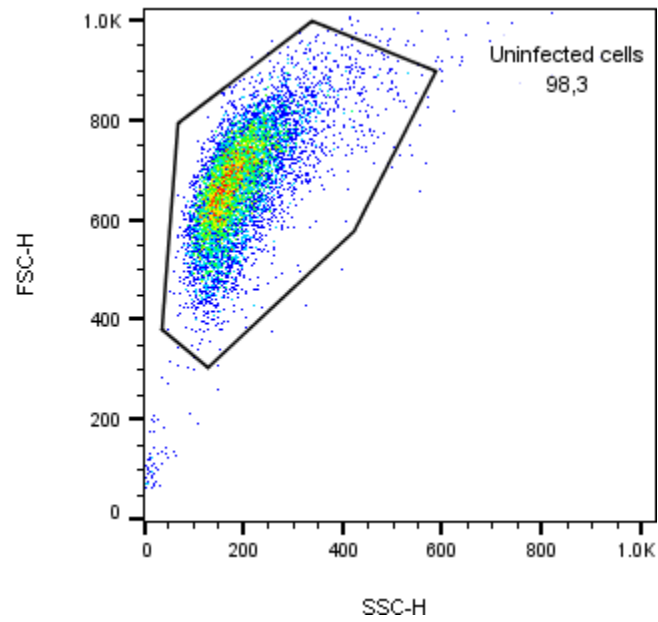


**Figure AC-1.** Forward Scatter (FSC) and Side Scatter (SSC) profile of uninfected *Sf9* cells.

## Appendix D

### Calculations used for Hemagglutination Assay (HA Assay)

This assay is based on the agglutination of red blood cells due to virus presence. The HA titer will be the reciprocal of the last dilution without aggregation, the numeric number represents the Hemagglutination Units (HAU) per 50  $\mu$ L. To have HAU/mL this number is multiplied by 20. Figures AD-1 shows an example.

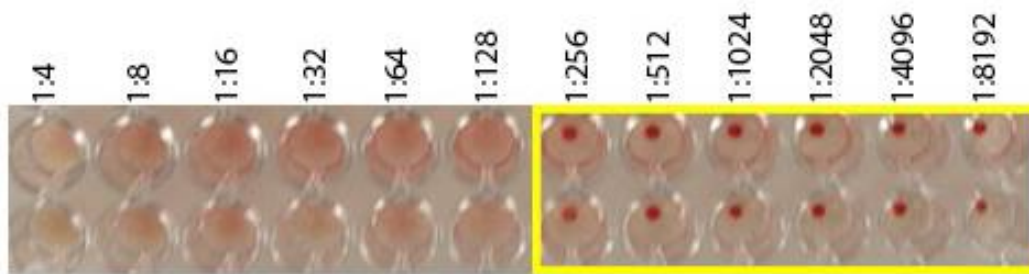


**Figure AD-1** Example calculations for HA Assay

Last agglutination achieved at 1:128. Thus, the HAU for this sample can be calculated as

$$\frac{128 \text{ HAU}}{50 \text{ uL}} \times \frac{1000 \text{ uL}}{1 \text{ mL}} = \frac{2560 \text{ HAU}}{\text{mL}}$$

## Appendix E

### Specifications and calculations used for quantification of baculovirus using flow cytometry

The settings used in the FACSCalibur equipment were:

**Table AE-1.** Settings to analyze the sample on the FACSCalibur flow cytometer

Channel	Voltage
<b>FSC Log</b>	<b>E01</b>
<b>SSC Log</b>	<b>490</b>
<b>FL1 Log</b>	<b>480</b>
No Threshold Medium flow 35µL/min Acquisition time: 30 sec	

Calculation of viral particles concentrations using the gated events

**Equation AE-1.** Viral particles concentration

$$\frac{\text{Viral particle concentration}}{\text{mL}} = C_v * D * 1000 * \frac{50000}{C_f * Vol}$$

Where

C<sub>v</sub> and C<sub>f</sub>: particles counts for viral particles and Flowset, respectively.

D: Dilution rate of the viral solution

Vol: volume (µL) of the diluted solution taken for the sample preparation

1000: final volume of the sample

50000: particle concentration of the diluted Flowset

Example of data acquired from flow cytometry and analysis

<b>Dilution rate</b>	10		
<b>Counts</b>	<b>Particles Counts (Cv)</b>	<b>Flow set Standard Count (FS)</b>	<b>Titer (viral particles/mL)</b>
1	3950	1208	1.66E+07
2	3654	1072	
3	3754	1146	
<b>Average</b>	3786	1142	

## Appendix F

### Green (FL1) vs red (FL3) signal plots of purified fractions

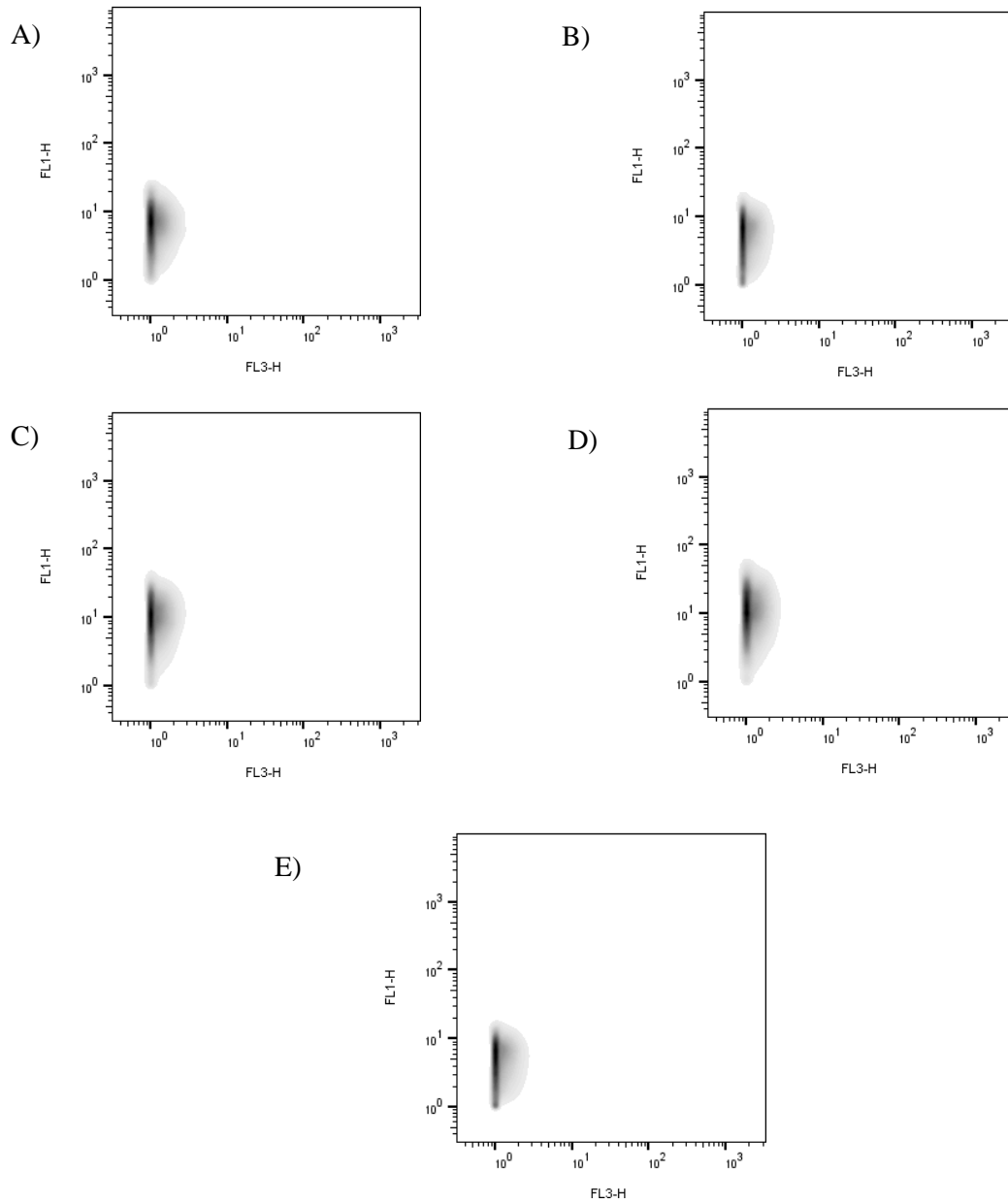


**Figure AF-1.** Particle distribution of fraction 9 of purified samples. A) 3' DsRed2, B) 3' mKate2, C) 5' mKate2, D) M mKate2 and E) Non-fluorescent VLP.